Universitat Autònoma de Barcelona

TESIS DOCTORAL

Vertically-aligned ZnO Nanostructures for excitonic Solar Cells

DEFENDED BY:

Irene González Valls

THESIS DIRECTOR:

Dra. Mónica Lira Cantú

TUTOR:

Dra. Maria Muñoz Tapia

PROGRAMA DE DOCTORAT EN CIÈNCIA DE MATERIALS

DEPTARTAMENT DE QUÍMICA

FACULTAT DE CIÈNCIES

2013

CIN2 CENTRE D'INVESTIGACIÓ EN NANOCIÈNCIA I NANOTECNOLOGIA

CSIC

Chapter 3
ZnO Nanotrees

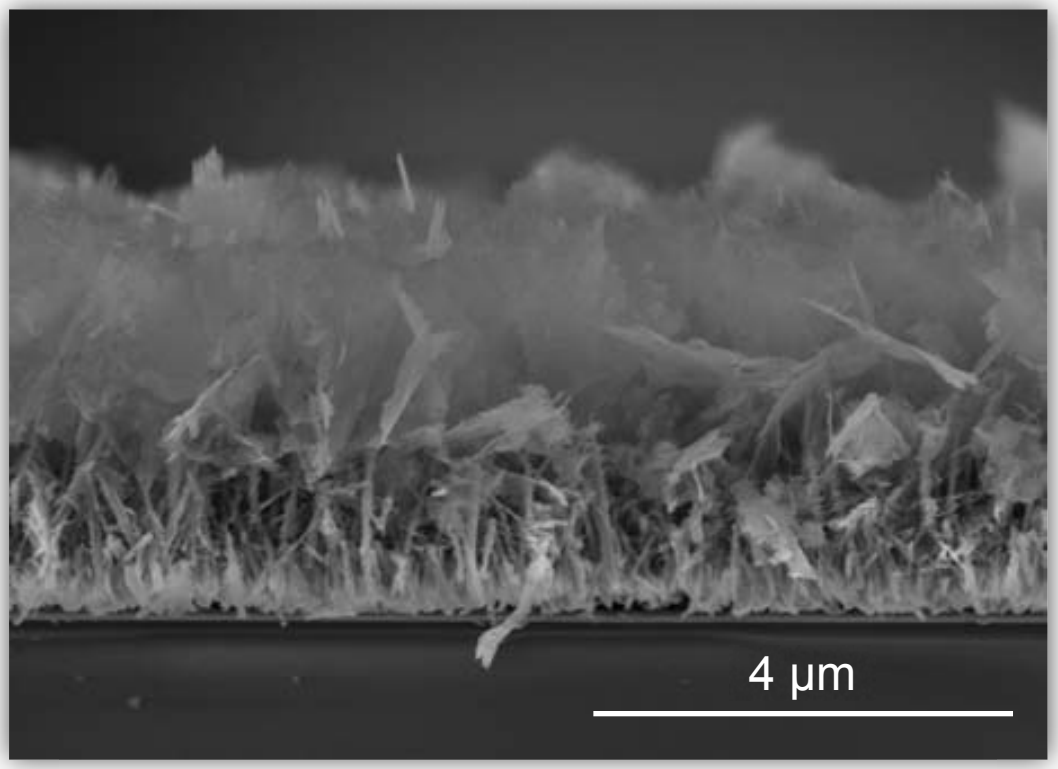

Chapter 3
ZnO Nanotrees

3.1 Introduction

As already described in past chapters of this work, the synthesis of vertically-aligned ZnO nanorods (NR) prepared by the hydrothermal synthesis method is an easy, low-cost and scalable technique.[1-5] It permits the growth of ZnO NRs on almost any substrate and on relatively large areas.[6] While there are many advantages of the technique, recent results indicate that the ZnO NRs obtained by this method shows low surface area and high amount of defects which translates in high charge recombination and low photovoltaic performance when applied in DSC.[7, 8] Recent reviews on the application of ZnO in DSC showed that the power conversion efficiencies applying bare vertically-aligned ZnO NRs have not been higher than 2.5-3.1%,[9, 10] not even when NRs with lengths up to 40 μm[11] are used.[12] This can be observed by the analysis of Table 2.1 in Chapter 2, where we enlisted the photovoltaic response of DSC applying vertically aligned ZnO NRs (the NR length is also included). Although it is difficult to arrive to any definitive conclusion due to the multiple differences in synthesis conditions, we could observe that, in general,

a) The highest PCEs correspond to DSCs applying the longest ZnO NRs. This is not surprising taking into account that the longer the NR the larger the amount of Dye adsorbed on the oxide and thus, the higher the PCE.

b) Good efficiencies correspond also to synthesis methods where a modification of the basic hydrothermal method is used. For example, the synthesis of NRs is made on metallic substrates, by electrochemical methods or by the application of additives during synthesis, among others. This is a good indication that the PCE is directly related to the synthesis conditions and methods applied for the ZnO NR growth.

Additionally, enormous research efforts are being invested to understand the causes behind this low PCE response and to find new ways to improve the ZnO properties. One of the most popular strategy is the synthesis of different nanostructures with improved

surface area like vertically-aligned branched nanorods, nanoforest, nanosheets, nanoflowers, nanorings, etc.[1, 13] Recently 3-Dimensional ZnO nanostructures called nanoforest, have demonstrated the enhancement on PCE when applied in DSC due to the higher surface area.[14, 15] Table 3.1 enlists the photovoltaic values obtained for DSCs applying all these different ZnO nanostructures. The first part of the table is ordered from low to high power conversion efficiency (PCE) since no electrode thickness is given. The second part of the table is ordered in ascending order depending on the ZnO electrode layer thickness. The highest performance of 7.5% PCE corresponds to a DSC applying a ~15 µm layer of hierarchical ZnO nanocrystals prepared by spray pyrolysis.[16] Other ZnO nanostructures synthesized by hydrothermal methods achieved also high solar cell performance for example nanosheets with 6.19% PCE applying an electrode of 35.6 µm thick,[17] nanoplates with 5.05% PCE and an electrode of 12 µm thick[18] or hollow spheres with 5.60% PCE and 12 µm electrode thickness.[19] Figure 3.1 represents some of these ZnO nanoforms applied in DSC in function of the obtained power conversion efficiencies (PCE).

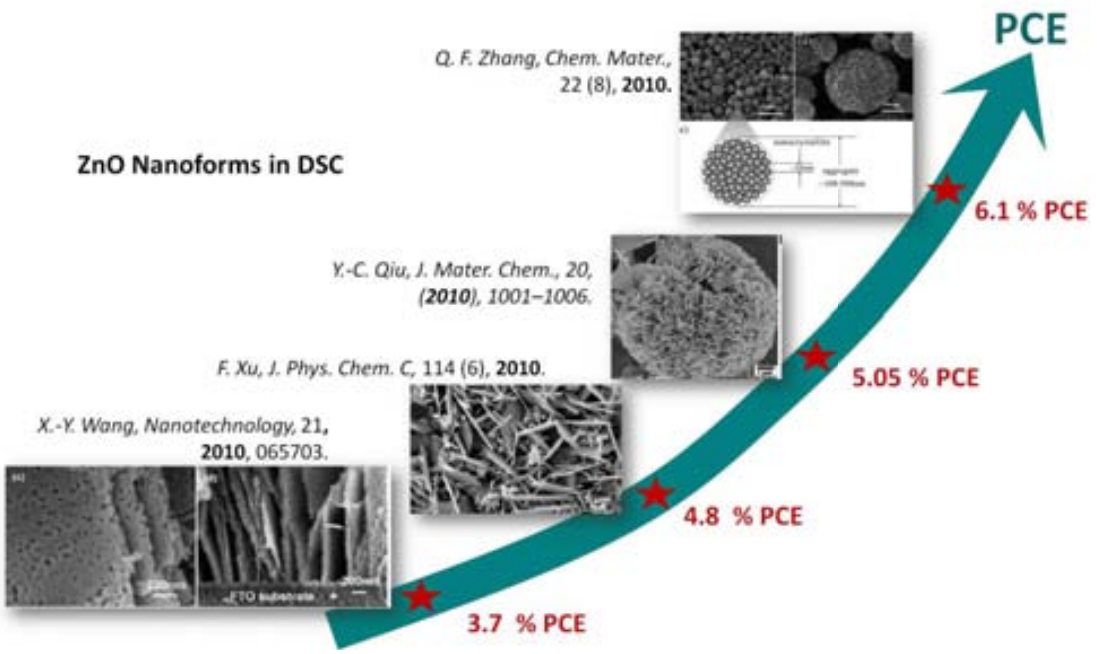

Figure 3.1 Different ZnO nanoforms reported in literature vs. the obtained power conversion efficiency (PCE) in DSCs.

Table 3.1 Literature review on different ZnO nanostructures and their application in DSCs. *Nanostruct.: Nanostructure, NW: Nanowires, H.: Hierarchical structure, NRs: Nanorods, MOCVD: Metal Organic Chemical Vapour Deposition, CVD: Chemical Vapour Deposition, HT: Hydrothermal, ALD: Atomic Layer Deposition, ECD: Electrochemical Deposition, Sonochem.: Sonochemical method, T. plasma: Thermal plasma. * Randomly oriented and horizontal ZnO NRs.*

Film Thickness (μm)	ZnO Nanostruct.	Synthesis method	Dye	Light Intensity (mW/cm²)	V_{oc} (V)	J_{sc} (mA/cm²)	FF (%)	PCE (%)	Ref.
-	dendritic NWs	MOCVD	N719	100	0.74	1.62	38	0.50	20
-	Nanocombs	CVD	N719	100	0.67	3.14	34	0.68	21
-	*Nanofibers	MOCVD	N719	100	0.69	2.87	44	0.88	22
-	*Nanocones	HT	N719	100	0.70	2.29	55	0.91	23
-	Flakes	HT	N719	100	0.67	2.33	59	0.99	24
-	Nanosheets	HT	N3	100	0.59	2.06	55	1.56	25
-	Nanotubes	ALD	N719	90.6	0.74	3.30	64	1.60	26
-	H. Nanostruct.	ECD	N719	100	0.60	5.10	54	1.63	27
-	Branched NRs	HT	N719	100	0.69	6.19	39	1.66	28
-	Nanoflowers	HT	N719	100	0.65	5.50	53	1.90	29
-	Nanotubes	HT	N719	100	0.65	5.50	61	2.20	30
-	Nanospikes	ECD	N719	100	0.68	6.07	60	2.51	31
-	Nanosheets	HT	N719	100	0.56	12.3	48	2.60	32
-	Nanobelts	ECD	N719	100	0.56	17.0	28	2.60	33
-	H. NRs-NPs	HT	N719	100	0.64	6.63	61	2.60	34
-	Nanosheets	ECD	Eosyn Y	100	-	-	-	2.70	35
-	Nanotetrapods	MOCVD	N719	100	0.61	9.71	55	3.27	36
-	Nanosheets	HT	N719	100	0.58	10.9	62	3.90	37
-	Nanosheets	ECD	D149	100	0.69	12.2	66	5.56	35
1.0	Nanotubes	HT	N719	42	0.54	3.40	53	2.30	38
1.3	H. NRs	ECD	Eosyn Y	100	0.52	5.39	57	1.60	39
2.0	Nanotubes	ALD	Porph.	98	0.50	1.30	66	0.50	40
2.0	Nanosheets	ECD	N3	80	0.37	4.20	53	1.00	41
2.0	Nanotubes	ECD	N3	80	0.39	4.70	53	1.20	41
3.0	Nanoflowers	HT	D149	100	0.52	3.35	48	0.84	42
3.3	Nanocactus	HT	D149	30-90	0.66	7.20	70	3.32	43
3.5	Nanoflowers	Microwave	N719	100	0.63	4.36	37	1.03	44
4.0	Nanosheets	HT	N719	100	0.56	13.8	44	3.30	45
5.0	*Nanofibers	Electrospun	N719	100	0.57	9.14	58	3.02	46
5.0	H. NRs	ECD	D149	100	0.56	12.4	58	4.08	47
5.0	H. NW-nanosheets	HT	N719	100	0.68	10.9	65	4.80	48
6.0-8.0	H. nanostruct.	HT	N3	100	0.69	1.51	52	0.54	49
6.8	Porous film	ECD	N719	100	0.58	8.00	69	3.20	50
7.0	NRs-Nanosheets	ECD	N719	100	0.74	10.9	38	3.12	51
7.1	Porous film	ECD	D149	100	0.57	10.7	73	4.40	50
7.0-8.0	Branched NRs	HT	N719	100	0.67	4.27	52	1.51	52
9.0	H. hollow spheres	Sonochem.	N719	100	0.73	9.56	62	4.33	53
10.0	*Nanosheets	HT	Evans	100	0.37	0.58	58	0.12	54
10.0	*Nanoflakes	HT	N719	100	0.63	7.00	44	3.64	55
12.0	Nanoplates	HT	N719	100	0.63	14.4	56	5.05	18
12.0	Hollow spheres	HT	N719	100	0.63	14.2	63	5.60	19
13.0	Nanoforest	HT	N719	100	0.68	8.78	53	2.63	14
14.0	Nanosheets	Surfactant	N719	100	0.64	7.89	63	3.20	56
15.0	*Branched NRs	HT	N719	100	0.59	5.52	55	1.82	57
15.0	H. Nanocrystallites	Spray pyrol.	N719	100	0.64	19.8	59	7.50	16
20.0	H. dislike shape	HT	N719	100	0.69	6.92	53	2.49	58
20.0	Nanosheets	HT	N719	100	0.62	9.37	63	3.70	59
20.0	*H. microflowers	HT	N719	100	0.68	11.3	53	4.12	60
20.0	Nanosheets	HT	D149	100	0.56	14.1	54	4.27	61
21.0	NRs+Microflowers	HT	N719	100	0.71	10.4	35	2.58	62
25.0	Tetrapods	T. plasma	N719	100	0.66	10.8	67	4.78	63
27.0	Porous nanosheets	HT	N719	100	0.57	14.7	61	5.16	64
35.6	H. nanosheets	HT	N719	100	0.69	12.7	70	6.19	17
42.2	Tetrapods	DC plasma	D149	100	0.61	12.4	65	4.90	65
320.0	Tetrapods	CVD	N3	100	0.58	3.76	47	1.02	66

Nevertheless, all these strategies have not unravelled the fundamental problems that attain the ZnO properties. The quality of ZnO NRs obtained by the low-temperature hydrothermal method (LT-HM) depend in great extent on many different synthesis parameters like temperature, reaction time, reactants concentration, among others.[12, 67] Taking into account all the above mentioned issues, the objective of this chapter is to understand the causes behind the low power conversion efficiency of DSCs applying vertically-aligned ZnO NR electrodes. In order to achieve our goal, two strategies have been considered:

a) Analysis of the effect of the synthesis methodology: A slight modification of the low temperature hydrothermal method, LT-HM, is made by the exchange of the synthesis reactor from glass-base to an autoclave reactor. The latter permits the increase of internal pressure of the reaction during ZnO NR growth.

b) The synthesis of different ZnO nanostructures in order to increase surface area. Increasing surface area increases the dye loading capacity and PCE of the final ZnO NR electrodes.

3.2 Synthesis of ZnO electrodes by a modification of the Low Temperature Hydrothermal Method (LT-HM)

We carried out the modification of the low-temperature hydrothermal method (LT-HM) described in detail in Chapter 2. The new synthesis method is similar to the LT-HM, in both cases the NR growth synthesis techniques use an equimolar 25 mM aqueous solution of $Zn(NO_3)_2$ and HMT. However, the glass PYREX bottle applied in the LT-HM was exchanged for an autoclave Parr Autodigestion bomb with PTFE-liner (A-HM). In this case, the hydrothermal solution was hermetically sealed inside the reactor at a pressure of $\sim 1.2 \cdot 10^7$ Pa. The reaction temperature was also modified from 96°C for the LT-HM, to 150°C for the A-HM.[68] The comparison of the obtained ZnO nanostructures prepared by the autoclave hydrothermal method (A-HM) and the low temperature hydrothermal method (LT-HM) is presented in this section as well as a proposed growth mechanism.

3.2.1 Comparison of two hydrothermal syntheses methods

Figure 3.2 shows the schematic representation of the reactors and images from both growth synthesis methods. A PYREX® Screw Cap bottle with capacity of 120 mL was used for the LT-HM and two different autoclave Parr Autodigestion Bombs with PTFE-liner of different capacities: 23 mL (model 4749, synthesis A-HM-1) and 45 mL (model 4744, synthesis A-HM-2) were used.

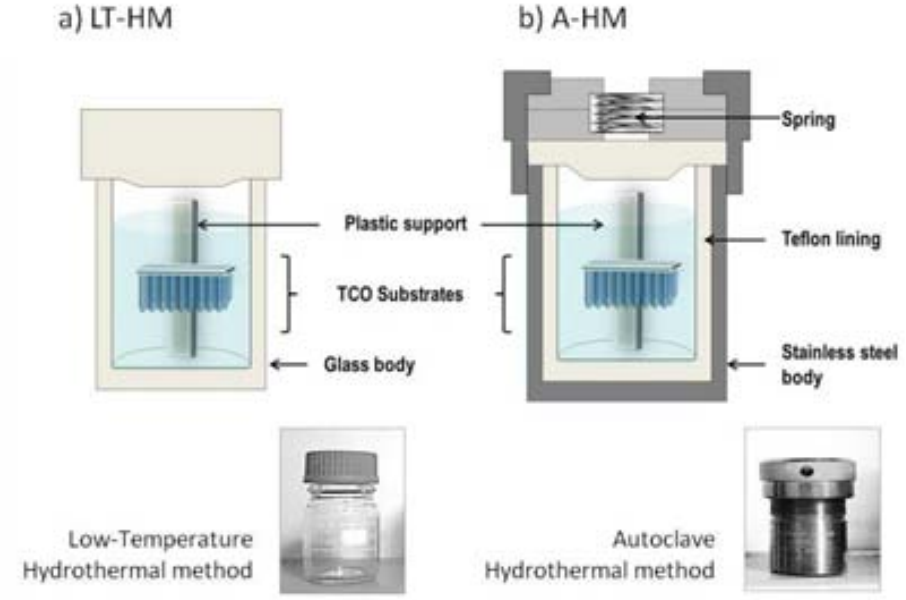

Figure 3.2 Schematic representation of both hydrothermal reactors and their images from a) the low-temperature hydrothermal method (LT-HM) and b) the autoclave hydrothermal method (A-HM).

The distance between the substrate and the bottom of the flask was also different in the A-HM due to different reactor sizes. The autoclave reactors need to be filled only 2/3 parts of the total volume due to the internal pressure. Autoclave 1 (total volume 23 mL) was filled with only 14 mL and the autoclave 2 (total volume 45 ml) with 28 mL of the hydrothermal solution. The PYREX® bottle reactor from LT-HM was filled with 110 mL of the hydrothermal solution. The optimum distance of the substrate from the bottom of the flask was 7 cm for the LT-HM (see details in chapter 2, section 2.2.2). New substrate supports were prepared for the A-HM; distances here were 1 cm for A-HM-1 and 2.5 cm for A-HM-2. The electrodes of ZnO NR prepared with the synthesis A-HM were grown continuously for 6 h, 12 h, 22 h and 28 h, changing the solution every 6 h-12 h. Figure 3.3

shows the cross section and top view SEM images comparison between LT-HM and A-HM grown for 6 h, 12 h and 22 h. NR length grown by the LT-HM increases with growth time and stabilizes after 22 h, as already reported.[12, 67] The method A-HM had a completely different response, NRs increased initially from 0.4-0.7 μm at 6 h growth time to 0.9-1 μm after 12 h and stabilized at about 1 μm at 22 h. The NR length and diameter are represented in Figure 3.5.

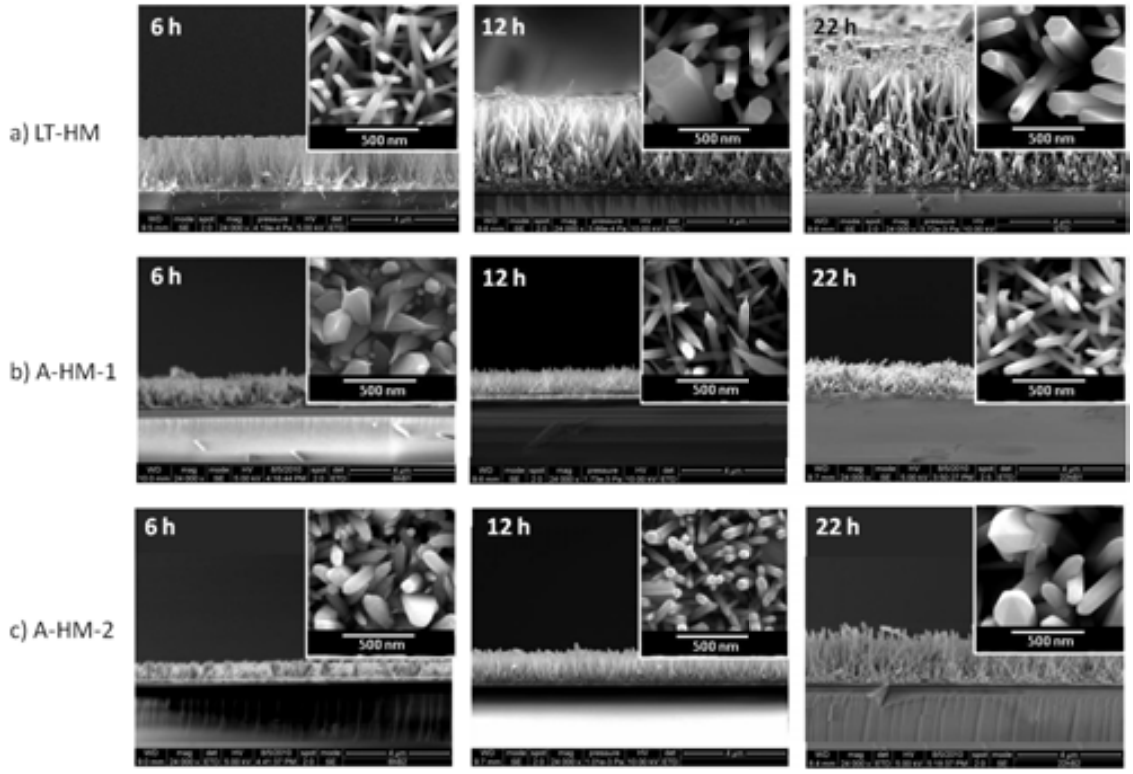

Figure 3.3 Lateral view and top view (inset) SEM images of the ZnO NRs grown for 6h, 12h and 22h with different methods: a) the Low temperature hydrothermal method -LT-HM, b) the Autoclave hydrothermal method 1- A-HM and c) the A-HM-2.

After 28 h growth time under the A-HM synthesis, a change in morphology was observed, the electrode length increased drastically from 1.1 μm to 3.5 μm for A-HM-1 and from 1.7 μm to 3.8 μm for A-HM-2. This drastic increase in length is due to the formation of an opened structure on top of the NRs, we called this new nanostructure, ZnO nanotrees (NTr). This new nanostructure, called NTr, is shown in the SEM image of Figure 3.4b and also schematically represented in Figure 3.4a. The bottom part of the electrode maintains the NR structure while the top of the electrode presents an open flower-like nanostructure. In combination, both bottom and upper parts of the electrode conforms a

nanotree-like structure. An advantage of this nanoform is that the NR confers good electron transport, while the top open structure boosts the harvesting of light. It is also remarkable the high homogeneity of the electrode (Figure 3.4c and d), which is obtainable in large areas. The top-view image in Figure 3.4e revealed clearly that changing the synthesis reactor from the glass bottle for the LT-HM to the autoclave reactor for the A-HM synthesis (Figure 3.2) the NR structure of the ZnO is no longer maintained, and the new NTr nanostructure appears.

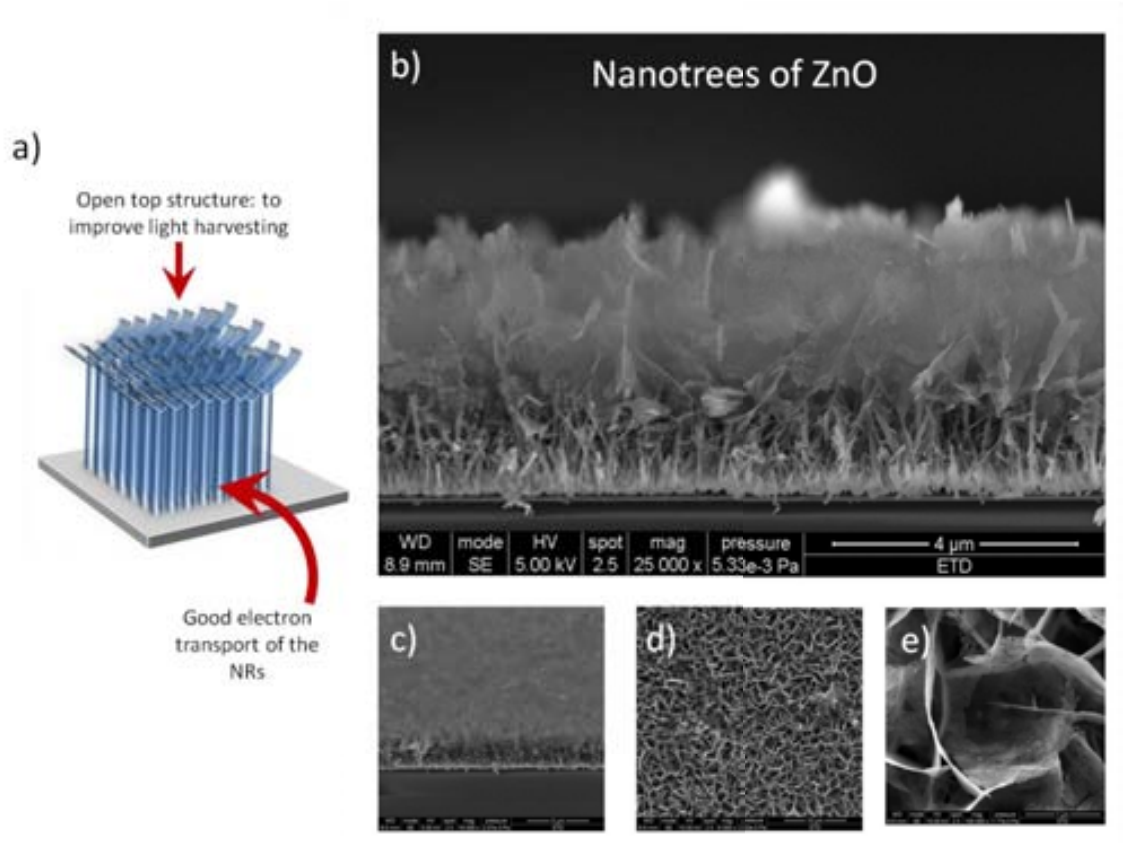

Figure 3.4 ZnO electrode growth by the A-HM-2: a) Schematic representation of the ZnO nanotrees (NTr) structure and SEM images of the NTr b) lateral view at 90°, c) lateral view tilted 85° and d)-e) top view images.

3.2.2 Evolution of the ZnO NR dimensions: length, diameter and aspect ratio

The length and diameter evolution of the ZnO NRs for the two hydrothermal methods are depicted in Figure 3.5. The measured dimensions are the average value obtained from the measurement of 10 NR of different sizes calculated from SEM images.[68-70] Comparison of the ZnO NR length obtained from both methods revealed that, for the same growth time, ZnO NRs obtained by the A-HM synthesis were 1/5 shorter than the NRs obtained by the LT-HM (Figure 3.5a). In the case of the diameters of the ZnO NRs obtained by the LT-HM, two different sizes were measured by SEM as a function of the growth time and a an hexagonal-shape diameter was observed as the main form, and was maintained constant after increasing the growth time. One diameter was found at between 200 - 500 nm and a smaller one between 50 - 80 nm. Different result was observed for the NRs obtained by the A-HM. In the case of the A-HM, these two different NR sizes were observed at 6h growth time. After which the NRs became thinner with more homogeneous NR diameters as the growth time increases, especially for the A-HM-1. At 22 h very thin and homogeneous NRs of about 60 nm were obtained for the A-HM-1, while the A-HM-2 and the LT-HM showed two NR diameter sizes. The latter is an indication of the effect of the distance between the bottom of the reactor and the substrate. The homogeneity of the ZnO NR diameters is indicated by the small error bars of the graph, an indication that the A-HM permits the synthesis of ZnO NRs with more reproducible and homogeneous ZnO NR dimensions.

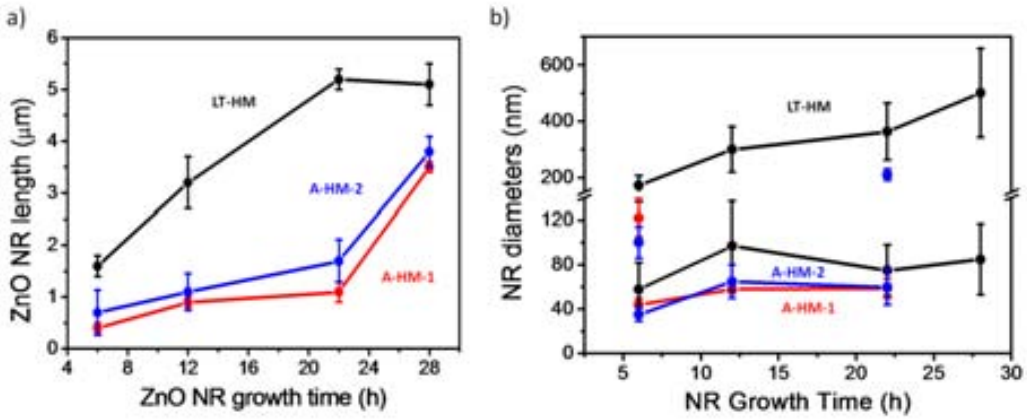

Figure 3.5 Evolution of the ZnO NR dimensions with growth time for the LT-HM (black line), the A-HM-1 (red line) and the A-HM-2 (blue line) hydrothermal methods: a) NR length, b) NR diameter.

Analysing the NRs evolution path, we observed that the NRs length completes its growth and stabilizes at about 5 μm for the LT-HM after 22 h of growth time, and between 0.9-1.1 μm, for the A-HM-1 and A-HM-2 respectively, after 12 h growth time. In the case of the synthesis A-HM, the new NTr structure appears after 22 h of growth time.

A schematic representation of the changes observed on the ZnO NRs with growth time for each syntheses methods, is shown in Figure 3.6. An interesting observation was the needle-tip morphology observed for the ZnO NRs obtained by the A-HM (see Figure 3.3b and Figure 3.6b and c). This needle-tip morphology is believed to be the responsible for the growth of thinner NRs with time, since the tip is probably acting as a seed for the growth of the following NR. At 28 h growth time and independently of the type of synthesis, the NRs ceased their growth, and a new nanostructure is formed for the A-HM, the NTr. Since almost all the synthesis conditions are maintained the same for both methods, we can conclude that the pressurized container (autoclave) used for the growth of the NR by the A-HM, is clearly the responsible for the formation of the needle-shape and the NTr morphology.

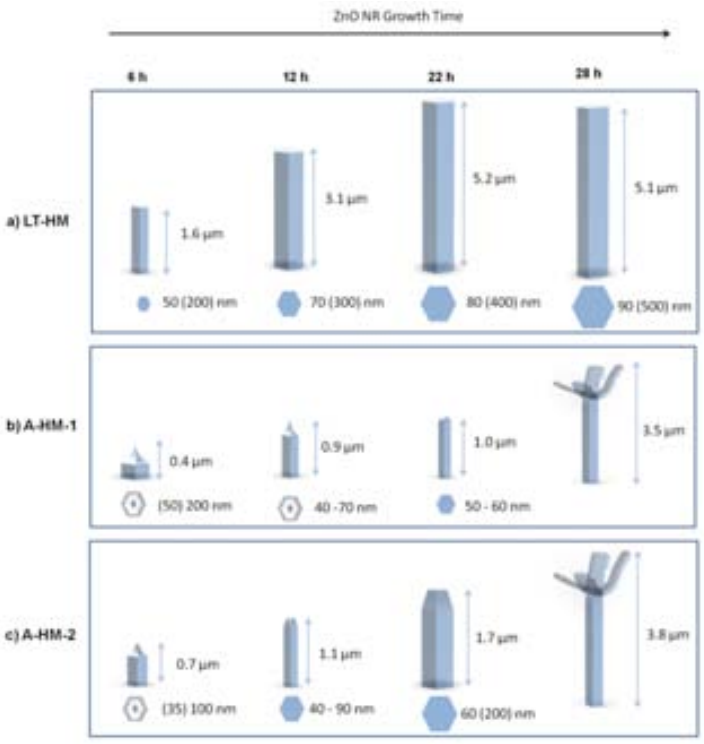

Figure 3.6 Schematic representation of the ZnO NR evolution for both hydrothermal methods: a) the LT-HM, b) the A-HM-1 and c) the A-HM-2. Lengths and diameters were calculated from SEM images. The diameters in parenthesis are the minority of NRs.

3. 3 Characterization of the modified ZnO nanostructures

The ZnO electrodes prepared by the A-HM for all the different growth times (6 h, 12 h, 22 h and 28 h) were characterized with different techniques presented in this section.

3.3.1. ZnO nanostructure morphology and aspect ratio by electronic microscopy analyses (SEM and TEM)

The different ZnO morphologies applying the A-HM synthesis grown at different reaction times and using the autoclave reactor 1 and 2 observed by SEM analyses are presented in Figure 3.3 and Figure 3.4. The scanning electron microscopy (SEM) images showed the needle shape and the different NR lengths compared with the LT-HM as commented in section 3.2.2. The new nanostructure, nanotrees (NTr), obtained at 28 h growth time by the A-HM-1 and the A-HM-2 is shown in Figure 3.4.

The ZnO morphology of the different nanostructures could be also observed by transmission electron microscopy (TEM) analyses. The ZnO electrodes were scratched and the ZnO nanostructures were suspended in ethanol, then one drop of this dispersion was placed on the TEM grid. Figure 3.7 shows TEM images of ZnO NTr obtained by the A-HM using the autoclave reactor 1 (a) and 2 (b). We could see from the latter images two types of nanostructure: a NR structure and an open ZnO nanostructure, which we also observed by SEM images (Figure 3.4). The comparison of the bottom part of the ZnO NTr, the NR structure, with the NRs obtained by the LT-HM at 28 h is shown in Figure 3.8. Thinner NRs were observed for the A-HM-1 synthesis with a diameter ~60 nm (Figure 3.8d) compared to ~400 nm for the LT-HM (Figure 3.8a). The NTr top structure is presented in Figure 3.9a.

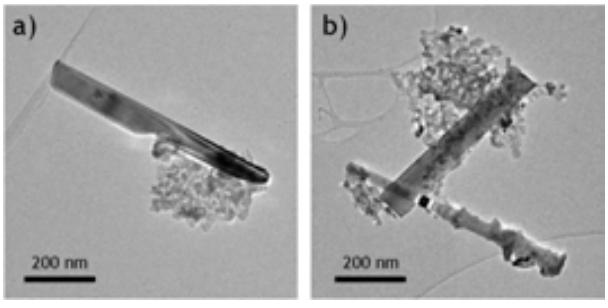

Figure 3.7 TEM images of scratched ZnO electrodes grown for 28 h prepared by a) the A-HM-1 and b) the A-HM-2.

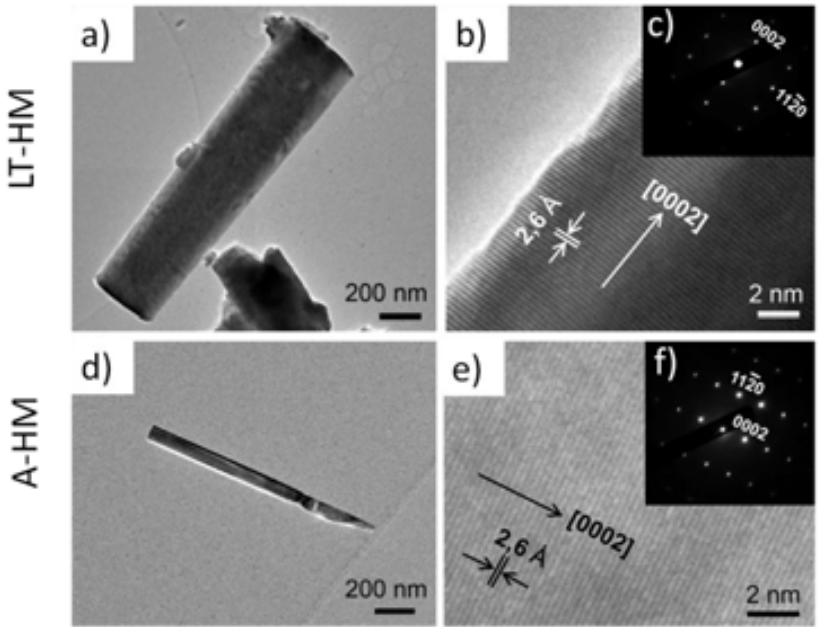

Figure 3.8 High resolution-TEM images of ZnO NRs prepared by the LT-HM (a-c) and the A-HM-1 (d-f) with low magnification (a, d), high magnification (b, e) and Selected-area electron diffraction (SAED) pattern (c, f).

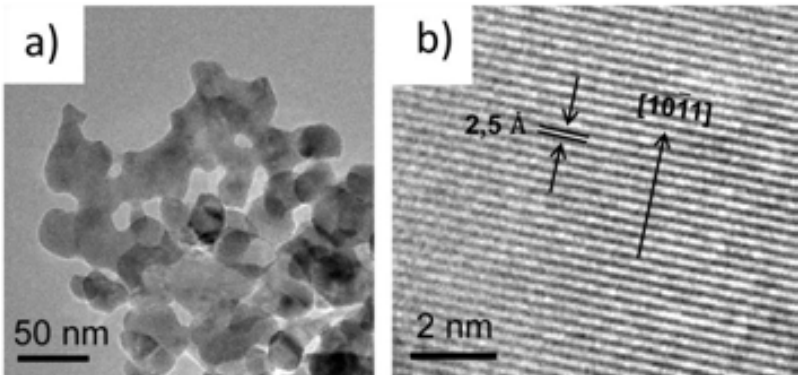

Figure 3.9 HR-TEM images of the ZnO top structure from an electrode prepared with the A-HM-1 at 28h growth time, a) low magnification and b) high magnification.

The aspect ratio defined as the NR length divided by the NR diameter was measured from the obtained SEM images of each ZnO growth condition.[3, 71] The larger the aspect ratio the larger will be the surface area of our ZnO NRs, which means more available area to adsorb dye to enhance the exciton formation in DSCs, thus, the aspect ratio is an important parameter to take into account.[1] Figure 3.10 shows the aspect ratio in function of the NR length for the LT-HM and the A-HM-1 and 2. No aspect ratios were measured on the ZnO NTr structure (prepared by the A-HM at 28 h) due to the presence of the top structure that

made not possible the measurement of the NR diameters from the SEM images. The aspect ratio was observed to increase when the NR length increased, however, decreased for the LT-HM grown at 28 h and the A-HM-2 grown at 22 h. This aspect ratio decrease was caused by the large NR diameters respect to a stabilized ZnO NR length. The synthesis A-HM-1 did not present the aspect ratio decrease given that the NR diameters were maintained small with homogeneous sizes (see section 3.2.2).

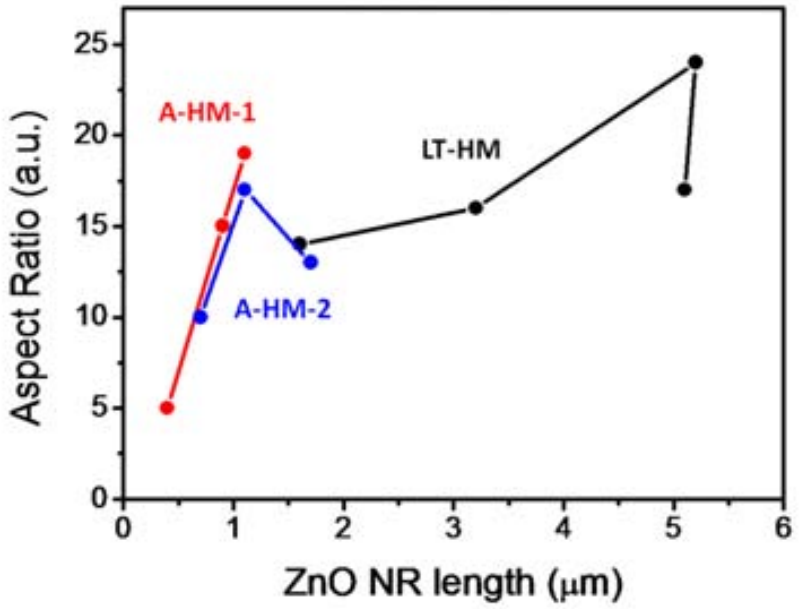

Figure 3.10 Aspect ratio in function of the NR length for each ZnO NR growth condition.

3.3.2. Crystalline structure by XRD and HR-TEM analyses

All the ZnO electrodes presented an hexagonal wurtzite crystalline structure characterized by X-rays (XRD), with peaks at 31.7°, 34.5°, 36.4°, 47.7°, 56.8°, 62.9°, 81.6° and 104.9° that correspond respectively with the planes: (1010), (0002), (10-11), (10-12), (1100), (10-13), (10-14) and (10-15) of the wurtzite structure, see Figure 3.11. The preferential orientation is observed by the higher intensity of the peak at 34.5° which indicates a vertical growth along c-axis, the direction [0001] perpendicular to the FTO substrate. Figure 3.11 shows the XRD graphs for electrodes prepared at 28 h growth time for the three synthesis methods. The ZnO electrodes grown by the A-HM show the same wurtzite peaks as the LT-HM, yet, the intensity of the peak (0002) was inferior due to the presence

of the new NTr structure with no vertical growth orientation. In addition, the peaks from FTO substrates can also be seen on the XRD diffractograms of the ZnO electrodes obtained by the A-HM, probably due to the thinner of the ZnO layer. Reported studies where the ZnO is obtained at higher pressures (above 10 GPa), presented a change in crystalline structure from the wurtzite form (the more stable in ambient conditions), into the rock salt structure (NaCl).[72] In our case, the crystalline ZnO structure was always the wurtzite form and not changes in the crystalline structure was observed in any case. The latter implies that the maximum pressure inside the autoclave of $1.2 \cdot 10^7$ Pa, is not high enough as to provoke the modification of the ZnO crystalline structure.

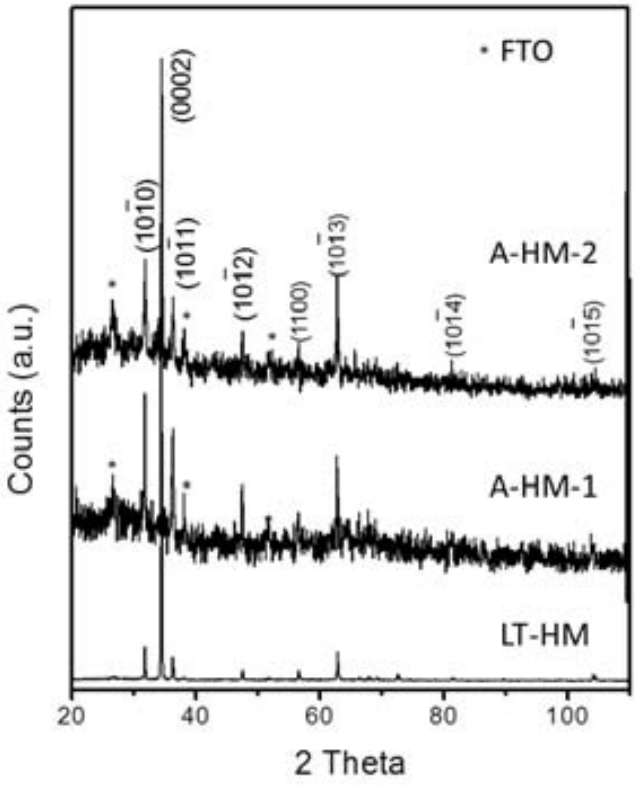

Figure 3.11 XRD pattern of ZnO electrodes grown for 28 h by the synthesis methods: the LT-HM, the A-HM-1 and the A-HM-2.

Further crystalline structure characterization of the different ZnO nanostructures was also carried out by high resolution TEM analyses. The comparison of the NR structure obtained by the LT-HM and the A-HM-1 at 28 h growth time is shown in Figure 3.8. The HR-TEM images confirm the highly crystalline structure of the ZnO nanostructures for both

synthesis methods. Figure 3.8b and e show a lattice spacing of 2.6 Å for the ZnO NRs, which corresponds to the distance between two (0002) planes of hexagonal ZnO, indicating that the NRs grow along the [0001] direction. The corresponding selected-area electron diffraction (SAED) patterns from the HR-TEM images are shown in Figure 3.8c and f and confirm the single-crystal nature of the ZnO nanostructures. On the other hand, the top structure from the NTr obtained by the A-HM at 28 h growth time, presents also the hexagonal wurtzite crystalline structure but the growth direction in this top structure is different than the [0001] direction, such as [10-11] or others depending on the area from the structure observed (Figure 3.9b).

3.3.3. Optical quality of the ZnO nanostructures: Photoluminescence (PL) and Time Resolved Photoluminescence (TRPL)

The optical properties of the electrodes obtained by the A-HM method were measured by photoluminescence (PL) and also by time resolved photoluminescence (TRPL).[68] These electrodes presented the same two emission bands as described in chapter 2, section 2.3.3, for the LT-HM method. One band at UV range attributed to the near-band-edge (NBE) at ~ 380 nm and a band at the visible range called orange band around ~ 650 nm. Figure 3.12 shows the PL spectra of the electrodes obtained by the A-HM-1 and the A-HM-2, and the intensity ratio between the orange band/NBE. The most interesting aspect observed in these graphs was the completely different behaviour of the orange band presented for the A-HM in comparison to the LT-HM (Figure 2.13). When the hydrothermal growth time increased, the intensity of the orange band for the A-HM electrodes decreased, which means the surface defects also decrease. The latter response was the opposite of the LT-HM electrodes. Figure 3.13 shows this different behaviour between the LT-HM and the A-HM-1, the surface defects increase from 6 h to 22 h growth time for the LT-HM, while for the A-HM-1 decrease. The intensity ratio between orange band and NBE in the A-HM increased from 6 h to 12 h growth time but decreased for 22h and 28h growth time, an indication of the relation between surface defects and NR length. The observed NR length for the A-HM increased from 6 h to 12 h growth time but stabilized at 22 h with similar NR length than the electrodes grown at 12 h, while at 28 h the new ZnO NTr structure appeared (Figure 3.5a). The formation of the ZnO NTr did not increase the surface defects on the ZnO electrodes. The surface defects comparison of both synthesis methods is

presented in Figure 3.14, the PL intensity of the peak at ~380 nm was normalized at 1 in order to compare the intensity of the orange band. Higher surface defects were observed on the electrode grown at 6 h by the A-HM-1 compared with the L-HM electrode at the same growth time, electrodes grown at 12 h for both methods have similar surface defects and lower surface defects were observed for the A-HM-1 electrodes grown at 22 h and 28 h compared to the L-HM electrodes with the same growth time (Figure 3.14). The same behaviour as the A-HM-1 was observed for the A-HM-2.

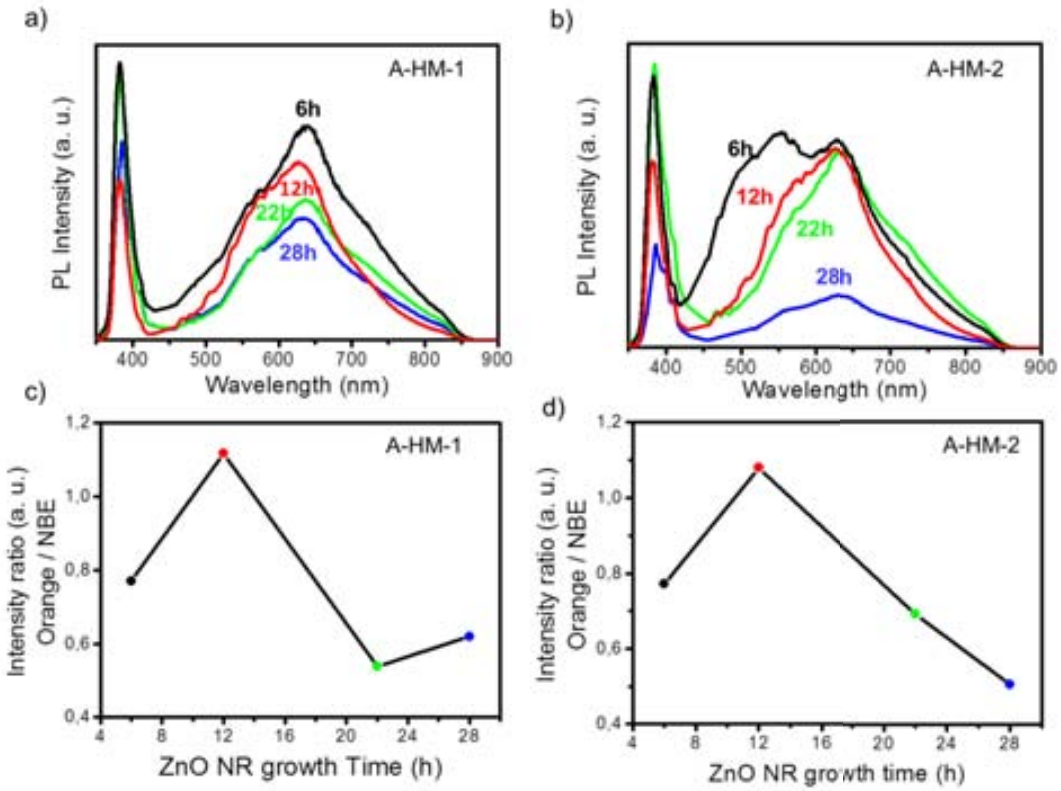

Figure 3.12 Room-temperature photoluminescence (PL) spectra for a) the A-HM-1 and b) the A-HM-2 electrodes and also the intensity ratios between orange band/NBE of the c) A-HM-1 and d) A-HM-2 electrodes.

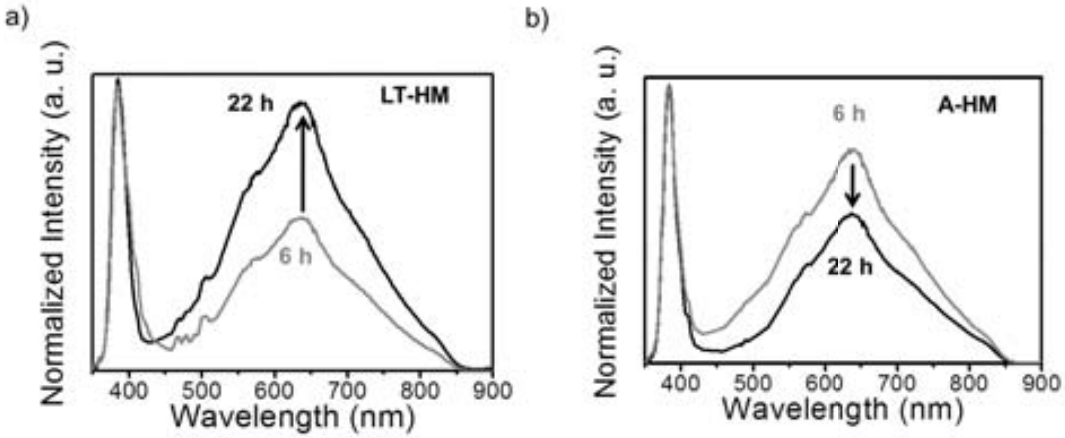

Figure 3.13 Room-temperature PL spectra of ZnO electrodes grown at 6 h and 22 h by a) the LT-HM and b) the A-HM-1.

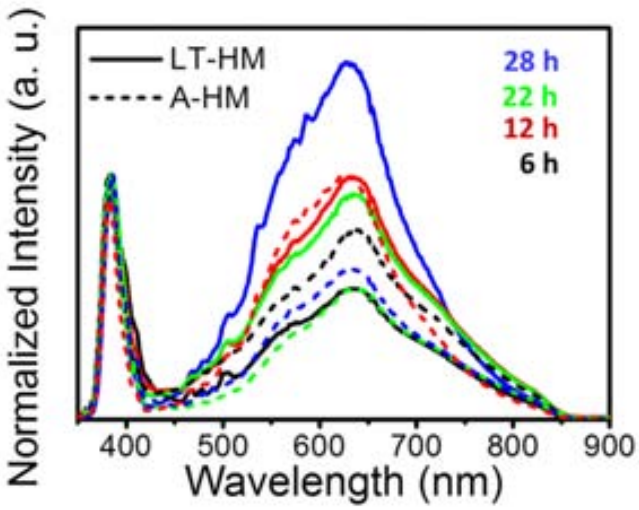

Figure 3.14 Room-temperature PL spectra of the LT-HM (solid line) and the A-HM-1 (dashed line) electrodes grown at 6 h (black), 12 h (red), 22 h (green) and 28 h (blue).

TRPL measurements allowed a more detailed and quantitative analysis of the free exciton lifetime on the different ZnO nanostructured electrodes from both synthesis methods. Figure 3.15a shows the TRPL spectra of the ZnO electrode obtained by the A-HM-2 at 22 h growth. When the dye was adsorbed on the ZnO NRs, the lifetime of the free exciton decreased as was also observed for the LT-HM electrode (see chapter 2, section 2.3.3). This lifetime decrease was attributed to the presence of more recombination channels.

The latter lifetime decrease when the dye was applied was also observed for all the other ZnO electrodes prepared by the A-HM. The TRPL measurements revealed that the electron lifetime for the ZnO NR obtained by the A-HM is considerable larger (between 50 and 140 ps depending on the NR length) than those obtained for the synthesis with the LT-HM (about 20-30 ps)[68] see Figure 3.15b. The latter is in agreement with the presence of less oxygen vacancies on the surface of the ZnO NRs grown by the A-HM for longer NR growth times (Figure 3.14). Higher surface defects indicate higher amount of electron traps and higher electron recombination. For this reason, the electron lifetime is shorter when higher surface defects exist. This difference on surface defects can be explained by the growth mechanisms on both methods. Temperature and pressure were the two different conditions between the LT-HM and the A-HM, however, as the post treatment annealing temperature of the electrodes was the same for both synthesis, only the pressure was the responsible for the surface defects. The pressurized atmosphere observed from the different reactors can saturate the solution with ions on the ZnO growth surface. Other groups observed the reduction of surface defects like oxygen vacancies by the introduction of doping elements with similar electronegativity as the oxygen ion, like chlorine[73] or fluorine.[74] They also observed a decrease of the visible band intensity at around 530 nm when the concentration of the ions in the precursor increases. We propose a similar phenomenon in our ZnO NRs prepared by the A-HM, though, in our synthesis the electronegative ions must be oxygen from the solution in the form of –OH or HCHO (formaldehyde) and can occupy the free sites of the O_{vac} reducing the surface defects. Thus, the pressurized reactor of the A-HM synthesis apply higher pressure when the NR length increases, rising the saturation of –OH or HCHO on the surface of the NR, and this explains why at 12 h growth time the surface defects increase but decrease at longer NR growth times.

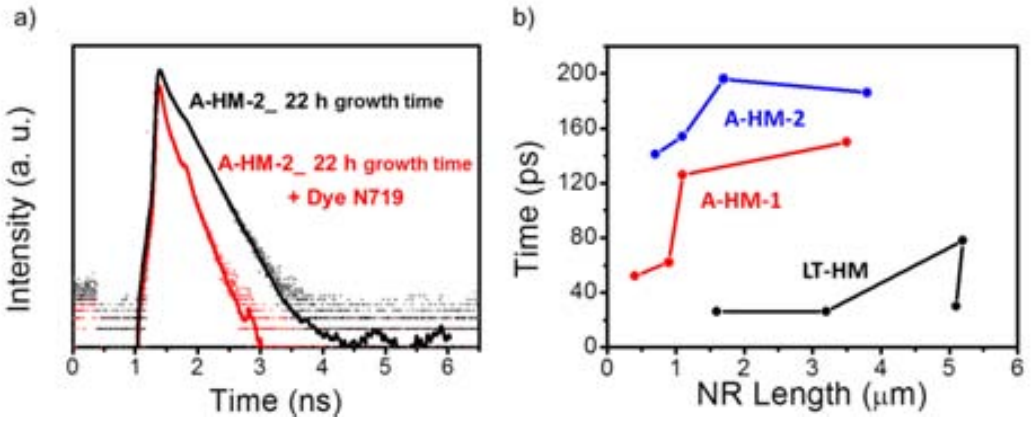

Figure 3.15 Time resolved Photoluminescence (TRPL) studies: a) for the ZnO NR electrode grown at 22 h obtained by the A-HM-2 without dye N719 and with N719 (3 h DLT) b) dependence of the electron lifetime with the NR length for the LT-HM and the A-HM-1 and the A-HM-2.

3.4 Application in Dye-sensitized Solar Cells

In this section we present the application of the ZnO electrodes prepared by the A-HM method in DSCs (the response of the ZNO NRs obtained by the LT-HM have been described in Chapter 2). First, the cells were optimized for each growth time of the A-HM synthesis and then, compared with the obtained results of the LT-HM electrodes. The study of the linkage between the dye and the ZnO is presented and also the effect of the different surface defects on this linkage.

3.4.1 Optimization of dye loading time

The optimization of the dye loading was carried out to the electrodes by their immersion in a solution of N719 dye using the same dye-loading time (DLT) as the optimum calculated for the LT-HM synthesis (chapter 2, section 2.4.3). The optimum DLT for the LT-HM electrodes at each growth time were: 2 h (6 h growth time), 3 h (12 h growth time), 6 h (22 h growth time) and 8 h (28 h growth time). The performances obtained for the A-HM were slightly lower than the ones of the LT-HM electrodes. However, when shorter dye-loading times were used for the A-HM electrodes, the power conversion efficiencies increased. The latter was not surprising since the A-HM electrodes have a thinner ZnO layer thickness and are usually shorter than the corresponding ZnO electrodes grown by the LT-HM. Figure 3.16 presents the best power conversion efficiency obtained for each ZnO electrode grown for 6 h, 12 h, 22 h and 28 h applying the A-HM-1 and the A-HM-2

methods at different dye-loading times. In general, the cells applying the ZnO NRs made by the A-HM-1 exhibited higher efficiencies compared to the A-HM-2, but graphs presented the same trend. The optimum DLT for both the A-HM (synthesis 1 and 2) electrodes measured were: 1 h (6 h growth time), 2 h (12 h growth time), 3 h (22 h growth time) and 3 h (28 h growth time).

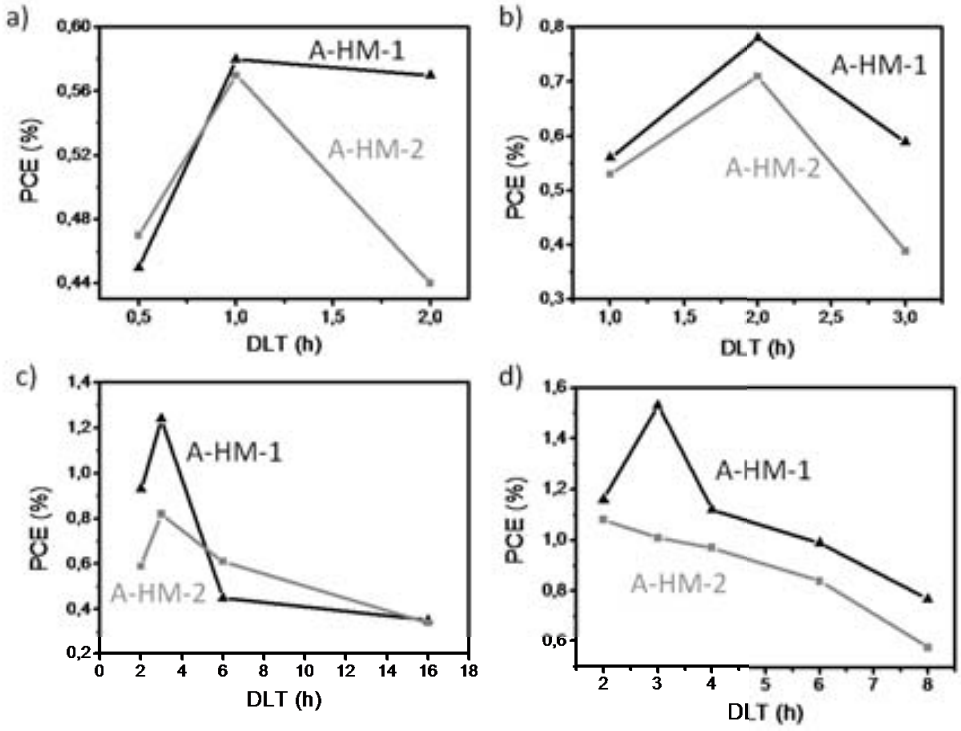

Figure 3.16 Dye loading time Vs. DSC power conversion efficiency for ZnO NRs obtained by the A-HM synthesis method and grown at different reaction times: a) 6 h, b) 12 h, c) 22 h and d) 28 h. The cells were measured at 100 mW·cm^{-2} (AM 1.5) light intensity and 72°C. Pt counter electrode from Solaronix (60 nm). Active area ~0.2 cm^2.

3.4.2 Performance comparison between the LT-HM and the A-HM

Several DSCs of each ZnO electrode with their optimum DLT were prepared and measured. The average photovoltaic response of the best 5 cells is shown in Figure 3.17a and Table 3.2. All the cells presented an increase on power conversion efficiency when the NR length increases, independently of the synthesis method (Table 3.2). Moreover, the cell performances improved after being measured the first day and kept some days in the dark at room temperature (see Table 3.2) due to the UV-light effect on the ZnO semiconductor, as commented in chapter 2, section 2.5.3. On the other hand, the A-HM-1 electrodes

showed a solar cell efficiency enhancement in comparison to the LT-HM electrodes grown for 22 h and 28 h. The A-HM-2 had also a slightly increase on the performance when the electrode was grown for 28 h. The latter is an unexpected result taken into account that the NR length of the A-HM electrodes is about 1/5 of the size of the NRs prepared by the LT-HM (Figure 3.17a). The current–voltage graphs of the best cells obtained in each condition are depicted in Figure 3.17b and the DSCs data for these cells are in Table 3.3. The DSC efficiencies obtained by both synthesis methods have a good correlation with the orange peak in the PL graph of Figure 3.14. The better results observed with shorter NR length when the A-HM is applied, were attributed to the lower surface defects observed in the ZnO electrodes grown by this method. These lower surface defects allowed higher solar cell efficiencies as result of an increase of the FF and V_{oc} values for the existence of lower recombination processes.

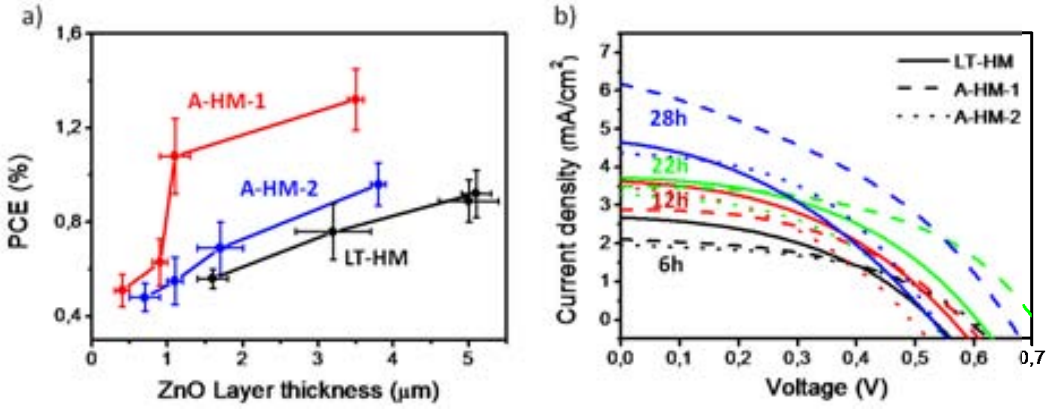

Figure 3.17 a) Average performance of DSCs (of 5) showing the effect of the ZnO NR length and the different synthesis methods the LT-HM, the A-HM-1 and the A-HM-2 and b) JV-curves of the best DSCs with the different hydrothermal methods and different growth time. Light intensity 100 mW·cm^{-2} (AM 1.5) and 72°C. Active area ~0.2 cm^2. Pt CE from Solaronix (~60 nm thickness).

Table 3.2 Average of DSCs performances of the LT-HM synthesis and the A-HM (of 5 cells) for each growth time. Light intensity 100 mW·cm^{-2} (AM 1.5) and 72°C. Active area ~0.2 cm^2. Pt CE from Solaronix (~60 nm thickness).

Measure	Growth Time	HT method	ZnO NR Length (μm)	Optimum DLT (h)	V_{oc} (V)	J_{sc} (mA·cm^{-2})	FF (%)	PCE (%)
At start	6 h	LT-HM	1.6 ± 0.2	2	0.49 ± 0.04	2.30 ± 0.34	44 ± 3	0.46 ± 0.05
		A-HM-1	0.4 ± 0.1	1	0.48 ± 0.02	1.74 ± 0.28	47 ± 2	0.39 ± 0.07
		A-HM-2	0.7 ± 0.2	1	0.47 ± 0.05	1.61 ± 0.28	46 ± 3	0.35 ± 0.07
	12 h	LT-HM	3.2 ± 0.5	3	0.49 ± 0.02	3.98 ± 0.32	41 ± 1	0.73 ± 0.05
		A-HM-1	0.9± 0.1	2	0.55 ± 0.06	2.20 ± 0.32	38 ± 6	0.46 ± 0.06
		A-HM-2	1.1 ± 0.1	2	0.52 ± 0.03	2.01 ± 0.33	45 ± 4	0.47 ± 0.06
	22 h	LT-HM	5.1 ± 0.2	6	0.52 ± 0.06	3.53 ± 0.22	43 ± 2	0.78 ± 0.08
		A-HM-1	1.1 ± 0.2	3	0.58 ± 0.06	3.65 ± 0.76	43 ± 4	0.92 ± 0.25
		A-HM-2	1.7 ± 0.3	3	0.53 ± 0.04	2.29 ± 0.24	46 ± 7	0.56 ± 0.16
	28 h	LT-HM	5.0 ± 0.4	8	0.54 ± 0.05	3.92 ± 0.46	38 ± 5	0.79 ± 0.06
		A-HM-1	3.5 ± 0.1	3	0.61 ± 0.03	4.65 ± 0.31	39 ± 3	1.11 ± 0.08
		A-HM-2	3.8 ± 0.1	3	0.56 ± 0.05	3.86 ± 0.35	40 ± 3	0.86 ± 0.09
At Max.	6 h	LT-HM	1.6 ± 0.2	2	0.55 ± 0.03	2.23 ± 0.31	44 ± 3	0.56 ± 0.04
		A-HM-1	0.4 ± 0.1	1	0.56 ± 0.03	1.91 ± 0.32	48 ± 2	0.51 ± 0.07
		A-HM-2	0.7 ± 0.2	1	0.56 ± 0.07	1.77 ± 0.21	49 ± 1	0.48 ± 0.06
	12 h	LT-HM	3.2 ± 0.5	3	0.56 ± 0.01	3.19 ± 0.56	41 ± 1	0.76 ± 0.12
		A-HM-1	0.9± 0.1	2	0.61 ± 0.06	2.33 ± 0.40	44 ± 5	0.63 ± 0.10
		A-HM-2	1.1 ± 0.1	2	0.57 ± 0.08	2.18 ± 0.81	47 ± 4	0.55 ± 0.10
	22 h	LT-HM	5.1 ± 0.2	6	0.54 ± 0.04	3.83 ± 0.30	44 ± 1	0.92 ± 0.10
		A-HM-1	1.1 ± 0.2	3	0.64 ± 0.06	3.55 ± 0.46	48 ± 5	1.08 ± 0.16
		A-HM-2	1.7 ± 0.3	3	0.57 ± 0.05	2.66 ± 0.54	46 ± 3	0.69 ± 0.11
	28 h	LT-HM	5.0 ± 0.4	8	0.58 ± 0.05	4.12 ± 0.50	39 ± 3	0.89 ± 0.09
		A-HM-1	3.5 ± 0.1	3	0.68 ± 0.02	4.67 ± 1.00	43 ± 5	1.32 ± 0.13
		A-HM-2	3.8 ± 0.1	3	0.60 ± 0.04	3.89 ± 0.38	42 ± 4	0.96 ± 0.09

Table 3.3 DSCs performances of the best cells obtained for each hydrothermal synthesis and growth time at the maximum performance (after some days of being prepared) and also the quantity of dye N719 adsorbed on the ZnO electrode and shunt and series resistances (R_{sh} and R_s). Light intensity 100 mW·cm^{-2} (AM 1.5) and 72°C. Active area ~0.2 cm^2. Pt CE from Solaronix (~60 nm thickness).

Growth Time	HT method	ZnO NR Length (μm)	DLT (h)	V_{oc} (V)	J_{sc} (mA·cm^{-2})	FF (%)	PCE (%)	Dye adsorbed (10^{-8} mol·cm^{-2})	R_{sh} (Ω·cm^2)	R_s (Ω·cm^2)
6h	LT-HM	1.6	2	0.528	2.67	41	0.61	2.5	2318	68
	A-HM-1	0.4	1	0.586	2.11	47	0.58	3.7	1417	83
	A-HM-2	0.7	1	0.594	1.96	49	0.57	2.9	3210	83
12h	LT-HM	3.2	3	0.561	3.62	41	0.87	3.4	1123	60
	A-HM-1	0.9	2	0.557	2.88	49	0.78	5.5	1468	62
	A-HM-2	1.1	2	0.493	3.45	42	0.71	3.4	1426	58
22h	LT-HM	5.1	6	0.603	3.72	45	1.01	6.1	796	48
	A-HM-1	1.0	3	0.705	3.50	50	1.24	7.4	1439	49
	A-HM-2	1.7	3	0.522	3.28	47	0.81	4.8	1490	50
28h	LT-HM	5.0	8	0.526	4.64	38	0.93	7.7	612	58
	A-HM-1	3.5	3	0.656	6.15	38	1.53	9.1	299	43
	A-HM-2	3.8	3	0.530	4.36	47	1.08	5.8	2565	41

The IPCE spectra of the DSC prepared by both hydrothermal methods at different growth time conditions are depicted in Figure 3.18. The IPCE peak at ~550 nm corresponds to the N719 dye, and it is similar for both syntheses methods, with values between 10-20 %. These IPCE values increased when the growth time increases as is expected for the presence of a thicker ZnO layer and more dye can be adsorbed. However, the IPCE peak corresponding to ZnO at ~380 nm was observed to be higher for the cells prepared by the A-HM (Figure 3.18) independently of the growth time. This IPCE peak at ~380 nm had no relation with the growth time; still, the higher values for the A-HM method explain its higher power-conversion efficiencies compared to the LT-HM due to a better charge transfer. The higher the IPCE peak at ~380 nm, the more efficient is the charge transfer from the ZnO to the FTO and lower the back transfer, recombination process, from the ZnO to the electrolyte.[75, 76]

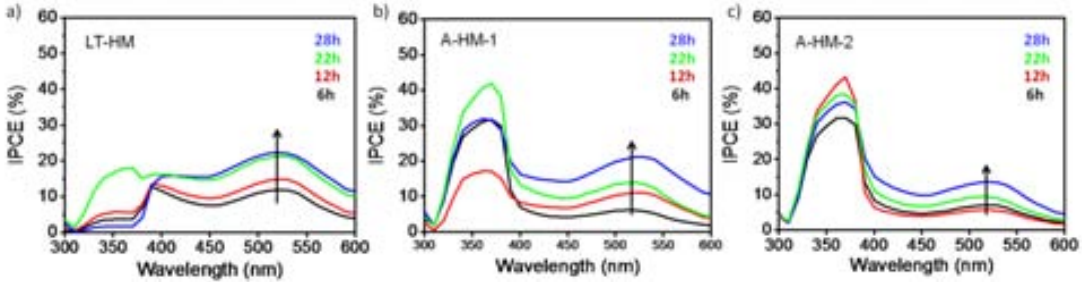

Figure 3.18 IPCE spectra obtained for the DSC applying a) the LT-HM, b) the A-HM-1 and c) the A-HM-2 at different growth times. Pt CE from Solaronix (~60 nm thickness). Growth time: 6h (black line), 12h (red line), 22h (green line) and 28h (blue line).

3.4.3 ZnO surface defects and dye binding

The quantity of dye adsorbed on the ZnO electrodes for the best solar cells was measured by a desorption technique described in chapter 6, section 6.6 (UV-visible analyses), results are shown in Table 3.3. An increase of dye adsorbed was observed when the NR length increases, which is an expected result due to a larger ZnO surface area available. Moreover, a larger amount of dye adsorbed on the ZnO electrode is observed when the A-HM-1 electrodes were used, in comparison with the LT-HM electrodes with the same NR growth times. We have attributed the latter response to the different surface defects observed on each electrode. The way the dye attaches to the semiconductor oxide surface determines the charge injection process taking place at the interface. This process

depends on the quality of the semiconductor oxide surface and also to the anchoring groups of the dye. The anchoring group between the dye and the surface of the oxide is usually made through physisorption (hydrogen bonding) or chemisorption (chemical bond formation) between the group –COOH of the dye and the –OH of the oxide surface. Figure 3.19 shows a schematic representation of all the possible types of bonding between the dye and the ZnO surface. The carboxylate group is known to anchor by unidentate, bidentate and bridging bidentate modes.[77-79] The type of binding between dye-ZnO depends on the structure of the dye, the pH and the semiconductor surface properties.[80] Recent works report that the presence of O_{vac} reduces the amount of dye adsorbed on the oxide due to the less –OH groups available.[81] Another possible linkage observed is with the presence of defects, like oxygen vacancies by the insertion of the O atom form the –COOH into the vacancy position (Figure 3.19e). The linkage through the defects of the oxide is highly stable and enhances electron injection, unfortunately at the cost of lower V_{oc}, FF and higher electron recombination.[82, 83] The latter corresponds with our DSC results, the A-HM electrodes grown at 6 h and 12 h have higher amount of defects than the LT-HM grown at the same growth time. Consequently, lower amount of dye is anchored through the O_{vac} resulting in lower power conversion efficiency. On the other hand, ZnO electrodes grown by the A-HM at 22 h and 28 h show lower surface defects, more dye is adsorbed by physisorption and/or chemisorption using the –OH from the ZnO surface and thus, a higher V_{oc} was obtained which produce higher power conversion efficiencies compared to the LT-HM electrodes (Figure 3.19g). In literature similar dye-loadings were obtained with ZnO nanostructures.[17, 34, 51]

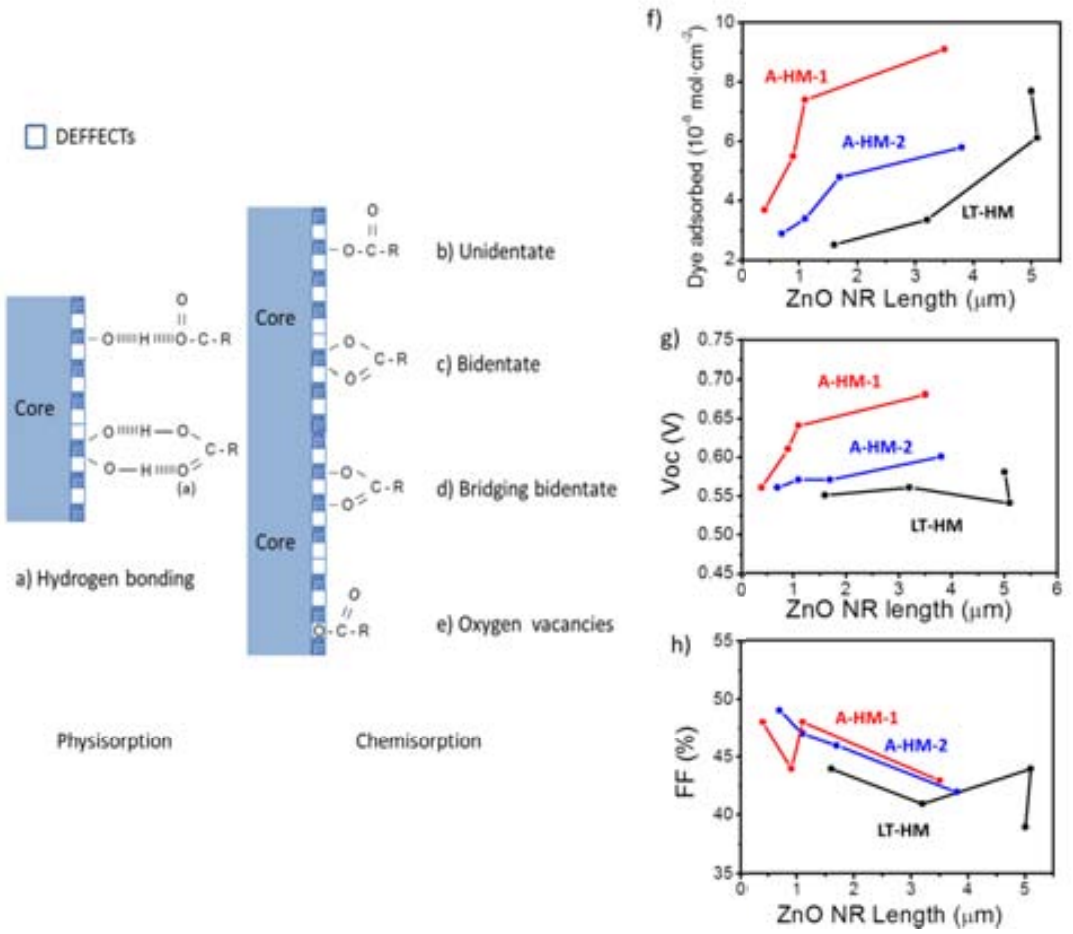

Figure 3.19 Schematic representation of the anchoring method between the dye and the ZnO surface, a) Physisorption by hydrogen bonding and chemisorption by hydrogen bond formation in different modes: b) unidentate, c) bidentate, d) bridging bidentate or e) oxygen vacancies. ZnO-based DSCs measurements in function of the ZnO NR length: f) dye adsorbed on the ZnO electrodes, g) V_{oc} and h) FF.

ATR-FTIR analyses of the ZnO electrodes/dye N719 were carried out in order to determine the type of bond obtained for each type of syntheses. Figure 3.20 shows the ATR-FTIR graphs for the pure dye N719 powder (a) and the ZnO electrodes grown for 12 h by the LT-HM (b) and the A-HM-1 (c), both ZnO electrodes (b and c) were dye-loaded with N719 dye solution for 2 h. From the IR spectra we can establish that the broad peak at 3400 cm^{-1} related to the –COOH group from the dye is not present in either of the electrodes (Figure 3.20a). Besides, the splitting carboxylate stretching bands: antisymmetric ν_{as} ($-COO^-$) at 1380 cm^{-1} and symmetric ν_s ($-COO^-$) at 1610 cm^{-1} can be used to determine the type of linkage between the dye and the oxide surface. The measurement of $\Delta = \nu_{as}$ ($-COO^-$) – ν_s ($-COO^-$) has been used in vibrational spectroscopic studies of metal

complexes of carboxylic acids to distinguish between possible modes of coordination. Unidentate complexes present a larger Δ value respect the ionic species, bidentate have a lower Δ, and bridging complexes should have a similar value of Δ compared with the ionic species.[77, 78] In our case, the ionic specie is the pure dye and presents a Δ value of 255 cm^{-1}, the ZnO electrodes obtained by the LT-HM and the A-HM-1, have Δ values of 242 cm^{-1} and 230 cm^{-1} respectively. The slightly lower values compared to the Δ of the dye suggest a bidentate coordination and some bridging coordination. The different Δ value for the LT-HM and the A-HM points out the presence of a different oxide surface as we already observed by PL studies and with DSC results. Moreover, the band at 1720 cm^{-1} related to C=O stretch mode of the protonated carboxylic acid was almost not observed in the FTIR spectra of the electrodes. Therefore, the presence of mainly carboxylate groups demonstrate that the complex is being adsorbed on the surface using the two carboxylic groups (that are trans to the NCS ligands).[84] Table 3.4 show all the IR peaks for the 3 samples and their assignment.

Table 3.4 ATR-FTIR data for the dye N719 powder, and ZnO NR electrodes grown by the LT-HM and the A-HM at 12 h. Both ZnO NRs electrodes were dye loaded for 2 h.

IR band (cm^{-1})			IR band assignment
Dye N719	**ZnO NR/Dye 12h – LT-HM**	**ZnO NR/Dye 12h – A-HM**	
3400			O-H stretching
2098	2105	2105	-NCS
	2053	1053	-NCS
1712			-C=O
1612	1616	1616	$-COO^-$ stretching
1357	1374	1370	$-COO^-$ asymmetric
1228	1171		C-O

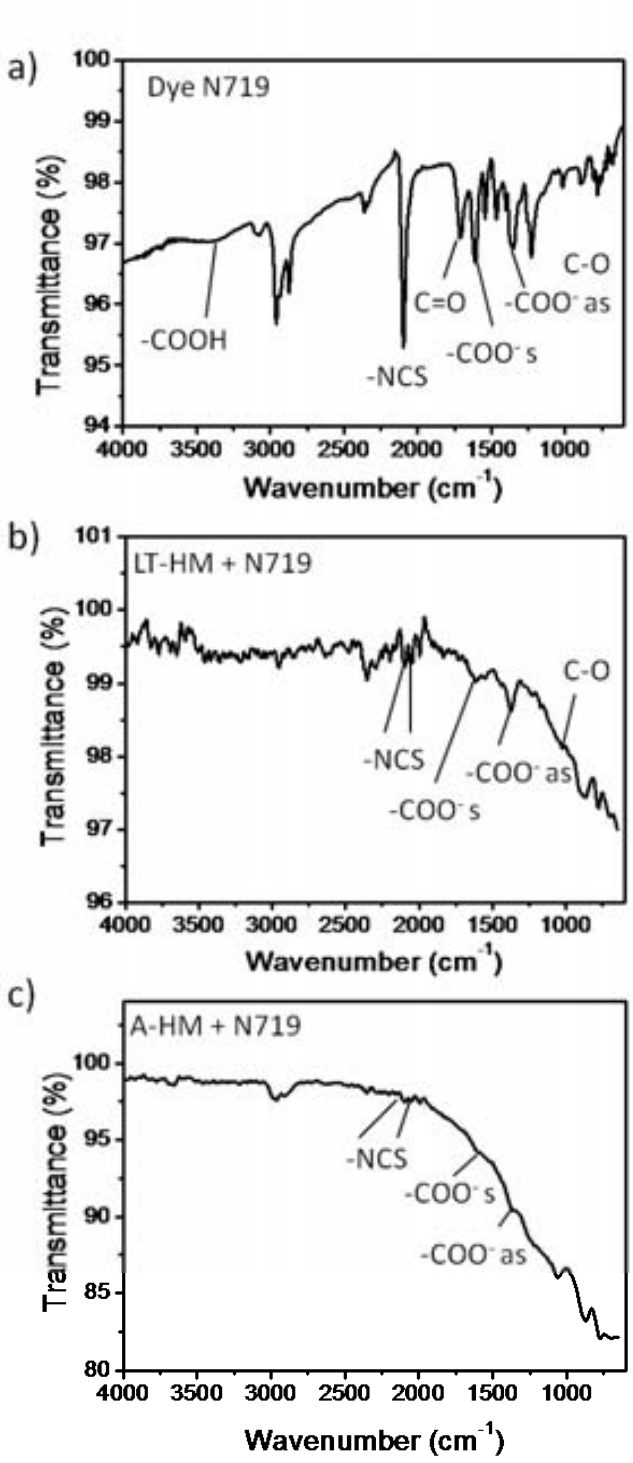

Figure 3.20 ATR-FTIR spectra for a) pure dye N719 powder, b) ZnO electrode of 12h growth time by the LT-HM and 2h of dye-loading time and c) ZnO electrode of 12 growth time by the A-HM-1 and 2h of dye-loading time.

3.5 Conclusions

A new hydrothermal synthesis method applying an autoclave reactor (A-HM) has been presented and compared with the standard low temperature hydrothermal method (LT-HM), carried out in a Pyrex glass reactor. Electrodes of ZnO NR were prepared maintaining the same synthesis conditions except for the slight pressure applied in the A-HM and high temperature as well as the distance from the substrate to the bottom of the flask due to different size reactors. Characterization of the A-HM electrodes by electron microscopy SEM and TEM, show NRs with lengths 1/5 shorter than those obtained by the LT-HM. The resulted NRs have also smaller and more homogeneous diameters than the NRs obtained with the LT-HM. Moreover, a new ZnO nanostructure, that we called it nanotrees (NTr) was obtained at 28h growth time by the A-HM. X-rays (XRD) analyses and selected-area electron diffraction (SAED) from TEM of these electrodes showed that the resulting ZnO NRs present a highly crystalline hexagonal wurtzite structure in all cases. Analyses by photoluminescence (PL) and time resolved photoluminescence (TRPL) of the A-HM electrodes grown at 22 h and 28 h showed less surface defects than the LT-HM electrodes and hence, have less electron traps and recombination centres. Higher power conversion efficiencies were obtained when the A-HM electrodes (growth time 22 h and 28 h) were applied in DSCs, confirming the improvement of the ZnO surface properties. A growth mechanism is proposed for the A-HM synthesis to explain the obtained ZnO morphology. Oxygen vacancies (O_{vac}) play an important role in the mechanism as anchoring points for the residual –OH and HCOH anions from the hydrothermal solution. The slightly higher pressure in the A-HM increases the concentration of –OH and HCOH on the surface of the NR and facilitates the anchoring of the anions. Therefore, A-HM electrodes (growth time 22 h and 28 h) have low quantity of O_{vac} and then, present higher FF, V_{oc} and low recombination processes compared to LT-HM electrodes. We demonstrated in this chapter that improved ZnO electrodes were prepared with a modified hydrothermal synthesis (A-HM), which has higher performance in DSCs compared with the LT-HM electrodes. However, ZnO NRs prepared by the LT-HM can be a good choice in other applications where recombination is important such as OLEDS or mechanical energy harvesting (piezoelectric) devices.

3.6 References

1. I. Gonzalez-Valls and M. Lira-Cantu, "Vertically-aligned nanostructures of ZnO for excitonic solar cells: a review". *Energy & Environmental Science* **2009,** 2 (1), 19-34.
2. L. Vayssieres, "Growth of arrayed nanorods and nanowires of ZnO from aqueous solutions". *Advanced Materials* **2003,** 15 (5), 464-466.
3. B. Cheng and E. T. Samulski, "Hydrothermal synthesis of one-dimensional ZnO nanostructures with different aspect ratios". *Chemical Communications* **2004,** (8), 986-987.
4. M. Guo, P. Diao, S. M. Cai and Bg, "Hydrothermal growth of well-aligned ZnO nanorod arrays: Dependence of morphology and alignment ordering upon preparing conditions". *Journal of Solid State Chemistry* **2005,** 178 (6), 1864-1873.
5. Q. Ahsanulhaq, A. Umar and Y. B. Hahn, "Growth of aligned ZnO nanorods and nanopencils on ZnO/Si in aqueous solution: growth mechanism and structural and optical properties". *Nanotechnology* **2007,** 18 (11), 115603.
6. C. H. Lu, L. M. Qi, J. H. Yang, L. Tang, D. Y. Zhang, J. M. Ma and Wa, "Hydrothermal growth of large-scale micropatterned arrays of ultralong ZnO nanowires and nanobelts on zinc substrate". *Chemical Communications* **2006,** (33), 3551-3553.
7. A. B. Djurisic, Y. H. Leung, K. H. Tam, Y. F. Hsu, L. Ding, W. K. Ge, Y. C. Zhong, K. S. Wong, W. K. Chan, H. L. Tam, K. W. Cheah, W. M. Kwok and D. L. Phillips, "Defect emissions in ZnO nanostructures". *Nanotechnology* **2007,** 18, 095702.
8. L. Schmidt-Mende and J. L. MacManus-Driscoll, "ZnO - nanostructures, defects, and devices". *Materials Today* **2007,** 10 (5), 40-48.
9. M. Guo, P. Diao, X. D. Wang and S. M. Cai, "The effect of hydrothermal growth temperature on preparation and photoelectrochemical performance of ZnO nanorod array films". *Journal of Solid State Chemistry* **2005,** 178 (10), 3210-3215.
10. J. J. Kim, K. S. Kim and G. Y. Jung, "Fabrication of flexible dye-sensitised solar cells with photoanodes composed of periodically aligned single crystalline vertical ZnO NRs by utilising a direct metal transfer method". *Journal of Materials Chemistry* **2011,** 21 (21), 7730-7735.
11. J. J. Qiu, X. M. Li, F. W. Zhuge, X. Y. Gan, X. D. Gao, W. Z. He, S. J. Park, H. K. Kim and Y. H. Hwang, "Solution-derived 40 mu m vertically aligned ZnO nanowire arrays as photoelectrodes in dye-sensitized solar cells". *Nanotechnology* **2010,** 21 (19), 195602.
12. I. Gonzalez-Valls, Y. H. Yu, B. Ballesteros, J. Oro and M. Lira-Cantu, "Synthesis conditions, light intensity and temperature effect on the performance of ZnO nanorods-based dye sensitized solar cells". *Journal of Power Sources* **2011,** 196 (15), 6609-6621.
13. Z. L. Wang, "Nanostructures of zinc oxide". *Materials Today* **2004,** 7 (6), 26-33.
14. S. H. Ko, D. Lee, H. W. Kang, K. H. Nam, J. Y. Yeo, S. J. Hong, C. P. Grigoropoulos and H. J. Sung, "Nanoforest of Hydrothermally Grown Hierarchical ZnO Nanowires for a High Efficiency Dye-Sensitized Solar Cell". *Nano Letters* **2011,** 11 (2), 666-671.
15. M. McCune, W. Zhang and Y. Deng, "High Efficiency Dye-Sensitized Solar Cells Based on Three-Dimensional Multilayered ZnO Nanowire Arrays with "Caterpillar-like" Structure". *Nano letters* **2012,** 12 (7), 3656-62.
16. N. Memarian, I. Concina, A. Braga, S. M. Rozati, A. Vomiero and G. Sberveglieri, "Hierarchically Assembled ZnO Nanocrystallites for High-Efficiency Dye-Sensitized Solar Cells". *Angewandte Chemie-International Edition* **2011,** 50 (51).
17. Y. Shi, C. Zhu, L. Wang, W. Li, C. Cheng, K. M. Ho, K. K. Fung and N. Wang, "Optimizing nanosheet-based ZnO hierarchical structure through ultrasonic-assisted precipitation for remarkable photovoltaic enhancement in quasi-solid dye-sensitized solar cells". *Journal of Materials Chemistry* **2012,** 22 (26).
18. Y. C. Qiu, W. Chen and S. H. Yang, "Facile hydrothermal preparation of hierarchically assembled, porous single-crystalline ZnO nanoplates and their application in dye-sensitized solar cells". *Journal of Materials Chemistry* **2010,** 20 (5), 1001-1006.
19. Z. Dong, X. Lai, J. E. Halpert, N. Yang, L. Yi, J. Zhai, D. Wang, Z. Tang and L. Jiang, "Accurate Control of Multishelled ZnO Hollow Microspheres for Dye-Sensitized Solar Cells with High Efficiency". *Advanced Materials* **2012,** 24 (8).

20. J. B. Baxter and E. S. Aydil, "Nanowire-based dye-sensitized solar cells". *Applied Physics Letters* **2005,** 86 (5).
21. A. Umar, "Growth of Comb-like ZnO Nanostructures for Dye-sensitized Solar Cells Applications". *Nanoscale Research Letters* **2009,** 4 (9).
22. S. Li, X. Zhang, X. Jiao and H. Lin, "One-step large-scale synthesis of porous ZnO nanofibers and their application in dye-sensitized solar cells". *Materials Letters* **2011,** 65 (19-20).
23. A. Umar, M. S. Akhtar, S. H. Kim, A. Al-Hajry, M. S. Chauhan and S. Chauhan, "Growth, Properties and Dye-Sensitized Solar Cells (DSSCs) Applications of ZnO Nanocones and Small Nanorods". *Science of Advanced Materials* **2011,** 3 (5), 695-701.
24. S. Al-Heniti, A. Umar, P. Singh, A. Sayari, A. Al-Hajry and A. A. Al-Ghamdi, "Nanocrystalline ZnO Flakes for Photovoltaic Device Applications". *Advanced Science Letters* **2010,** 3 (4), 543-547.
25. A. Elkhidir Suliman, Y. Tang and L. Xu, "Preparation of ZnO nanoparticles and nanosheets and their application to dye-sensitized solar cells". *Solar Energy Materials and Solar Cells* **2007,** 91 (18), 1658-1662.
26. A. B. F. Martinson, J. W. Elam, J. T. Hupp and M. J. Pellin, "ZnO nanotube based dye-sensitized solar cells ZnO nanotube based dye-sensitized solar cells". *Nano Letters* **2007,** 7 (8), 2183-2187.
27. Y.-T. Kim, J. Park, S. Kim, D. W. Park and J. Choi, "Fabrication of hierarchical ZnO nanostructures for dye-sensitized solar cells". *Electrochimica Acta* **2012,** 78.
28. X. Fang, L. Peng, X. Shang and Z. Zhang, "Controlled synthesis of ZnO branched nanorod arrays by hierarchical solution growth and application in dye-sensitized solar cells". *Thin Solid Films* **2011,** 519 (19).
29. C. Y. Jiang, X. W. Sun, G. Q. Lo, D. L. Kwong, J. X. Wang and Fc, "Improved dye-sensitized solar cells with a ZnO-nanoflower photoanode". *Applied Physics Letters* **2007,** 90 (26), 3.
30. S. Ameen, M. S. Akhtar, Y. S. Kim, O. B. Yang and H.-S. Shin, "Influence of seed layer treatment on low temperature grown ZnO nanotubes: Performances in dye sensitized solar cells". *Electrochimica Acta* **2011,** 56 (3).
31. S. Ameen, M. S. Akhtar and H. S. Shin, "Growth and characterization of nanospikes decorated ZnO sheets and their solar cell application". *Chemical Engineering Journal* **2012,** 195.
32. M. S. Akhtar, M. A. Khan, M. S. Jeon and O. B. Yang, "Controlled synthesis of various ZnO nanostructured materials by capping agents-assisted hydrothermal method for dye-sensitized solar cells". *Electrochimica Acta* **2008,** 53 (27), 7869-7874.
33. C. F. Lin, H. Lin, J. B. Li and X. Li, "Electrodeposition preparation of ZnO nanobelt array films and application to dye-sensitized solar cells". *Journal of Alloys and Compounds* **2008,** 462 (1-2), 175-180.
34. H. Dong, L. Wang, R. Gao, B. Ma and Y. Qiu, "Constructing nanorod-nanoparticles hierarchical structure at low temperature as photoanodes for dye-sensitized solar cells: combining relatively fast electron transport and high dye-loading together". *Journal of Materials Chemistry* **2011,** 21 (48).
35. T. Yoshida, J. B. Zhang, D. Komatsu, S. Sawatani, H. Minoura, T. Pauporte, D. Lincot, T. Oekermann, D. Schlettwein, H. Tada, D. Wohrle, K. Funabiki, M. Matsui, H. Miura and H. Yanagi, "Electrodeposition of Inorganic/Organic Hybrid Thin Films". *Advanced Functional Materials* **2009,** 19 (1), 17-43.
36. W. Chen, H. F. Zhang, I. M. Hsing and S. H. Yang, "A new photoanode architecture of dye sensitized solar cell based on ZnO nanotetrapods with no need for calcination". *Electrochem. Commun.* **2009,** 11 (5), 1057-1060.
37. E. Hosono, S. Fujihara, I. Honna and H. S. Zhou, "The fabrication of an upright-standing zinc oxide nanosheet for use in dye-sensitized solar cells". *Advanced Materials* **2005,** 17 (17), 2091-+.
38. M. Guo, P. Diao and S. M. Cai, "Photoelectrochemical properties of highly oriented ZnO nanotube array films on ITO substrates". *Chinese Chemical Letters* **2004,** 15 (9), 1113-1116.
39. S. Haller, T. Suguira, D. Lincot and T. Yoshida, "Design of a hierarchical structure of ZnO by electrochemistry for ZnO-based dye-sensitized solar cells". *Physica Status Solidi a-Applications and Materials Science* **2010,** 207 (10).

40. R. A. Jensen, H. Van Ryswyk, C. X. She, J. M. Szarko, L. X. Chen and J. T. Hupp, "Dye-Sensitized Solar Cells: Sensitizer-Dependent Injection into ZnO Nanotube Electrodes". *Langmuir* **2010,** 26 (3), 1401-1404.
41. Z. Liu, Y. Li, C. Liu, J. Ya, W. Zhao, L. E, D. Zhao and L. An, "Performance of ZnO dye-sensitized solar cells with various nanostructures as anodes". *Solid State Sciences* **2011,** 13 (6).
42. J. B. Chu, S. M. Huang, D. W. Zhang, Z. Q. Bian, X. D. Li, Z. Sun and X. J. Yin, "Nanostructured ZnO thin films by chemical bath deposition in basic aqueous ammonia solutions for photovoltaic applications". *Applied Physics a-Materials Science & Processing* **2009,** 95 (3), 849-855.
43. C.-T. Wu and J.-J. Wu, "Room-temperature synthesis of hierarchical nanostructures on ZnO nanowire anodes for dye-sensitized solar cells". *Journal of Materials Chemistry* **2011,** 21 (35).
44. N. Mir, M. Salavati-Niasari and F. Davar, "Preparation of ZnO nanoflowers and Zn glycerolate nanoplates using inorganic precursors via a convenient rout and application in dye sensitized solar cells". *Chemical Engineering Journal* **2012,** 181.
45. K. Kakiuchi, M. Saito and S. Fujihara, "Fabrication of ZnO films consisting of densely accumulated mesoporous nanosheets and their dye-sensitized solar cell performance". *Thin Solid Films* **2008,** 516 (8), 2026-2030.
46. W. Zhang, R. Zhu, X. Z. Liu, B. Liu and S. Ramakrishna, "Facile construction of nanofibrous ZnO photoelectrode for dye-sensitized solar cell applications". *Applied Physics Letters* **2009,** 95 (4).
47. V. M. Guerin, J. Rathousky and T. Pauporte, "Electrochemical design of ZnO hierarchical structures for dye-sensitized solar cells". *Solar Energy Materials and Solar Cells* **2012,** 102.
48. F. Xu, M. Dai, Y. N. Lu and L. T. Sun, "Hierarchical ZnO Nanowire-Nanosheet Architectures for High Power Conversion Efficiency in Dye-Sensitized Solar Cells". *Journal of Physical Chemistry C* **2010,** 114 (6), 2776-2782.
49. Y. S. Fu, J. Sun, Y. Xie, J. Liu, H. L. Wang and X. W. Du, "ZnO hierarchical nanostructures and application on high-efficiency dye-sensitized solar cells". *Materials Science and Engineering B-Advanced Functional Solid-State Materials* **2010,** 166 (3), 196-202.
50. C. Magne, T. Moehl, M. Urien, M. Graetzel and T. Pauporte, "Effects of ZnO film growth route and nanostructure on electron transport and recombination in dye-sensitized solar cells". *Journal of Materials Chemistry A* **2013,** 1 (6), 2079-2088.
51. J. Qiu, M. Guo and X. Wang, "Electrodeposition of Hierarchical ZnO Nanorod-Nanosheet Structures and Their Applications in Dye-Sensitized Solar Cells". *Acs Applied Materials & Interfaces* **2011,** 3 (7).
52. H.-M. Cheng, W.-H. Chiu, C.-H. Lee, S.-Y. Tsai and W.-F. Hsieh, "Formation of Branched ZnO Nanowires from Solvothermal Method and Dye-Sensitized Solar Cells Applications". *Journal of Physical Chemistry C* **2008,** 112 (42).
53. C.-X. He, B.-X. Lei, Y.-F. Wang, C.-Y. Su, Y.-P. Fang and D.-B. Kuang, "Sonochemical preparation of hierarchical ZnO hollow spheres for efficient dye-sensitized solar cells". *Chemistry* **2010,** 16 (29), 8757-61.
54. S. Suresh, A. Pandikumar, S. Murugesan, R. Ramaraj and S. P. Raj, "Photovoltaic performance of solid-state solar cells based on ZnO nanosheets sensitized with low-cost metal-free organic dye". *Solar Energy* **2011,** 85 (9).
55. J. Mou, W. Zhang, J. Fan, H. Deng and W. Chen, "Facile synthesis of ZnO nanobullets/nanoflakes and their applications to dye-sensitized solar cells". *Journal of Alloys and Compounds* **2011,** 509 (3).
56. H. Li, Y. Zhang and J. Wang, "ZnO Nanosheets Derived from Surfactant-Directed Process: Growth Mechanism, and Application in Dye-Sensitized Solar Cells". *Journal of the American Ceramic Society* **2012,** 95 (4).
57. P. Sudhagar, R. S. Kumar, J. H. Jung, W. Cho, R. Sathyamoorthy, J. Won and Y. S. Kang, "Facile synthesis of highly branched jacks-like ZnO nanorods and their applications in dye-sensitized solar cells". *Materials Research Bulletin* **2011,** 46 (9), 1473-1479.
58. J. X. Wang, C. M. L. Wu, W. S. Cheung, L. B. Luo, Z. B. He, G. D. Yuan, W. J. Zhang, C. S. Lee and S. T. Lee, "Synthesis of Hierarchical Porous ZnO Disklike Nanostructures for Improved Photovoltaic Properties of Dye-Sensitized Solar Cells". *Journal of Physical Chemistry C* **2010,** 114 (31), 13157-13161.

59. X. Y. Wang, Z. P. Tian, T. Yu, H. M. Tian, J. Y. Zhang, S. K. Yuan, X. B. Zhang, Z. S. Li and Z. G. Zou, "Effective electron collection in highly (110)-oriented ZnO porous nanosheet framework photoanode". *Nanotechnology* **2010,** 21 (6).
60. C. Cheng, Y. Shi, C. Zhu, W. Li, L. Wang, K. K. Fung and N. Wang, "ZnO hierarchical structures for efficient quasi-solid dye-sensitized solar cells". *Physical Chemistry Chemical Physics* **2011,** 13 (22).
61. E. Hosono, Y. Mitsui and H. S. Zhou, "Metal-free organic dye sensitized solar cell based on perpendicular zinc oxide nanosheet thick films with high conversion efficiency". *Dalton Transactions* **2008,** (40), 5439-5441.
62. A. D. Goncalves, M. R. Davolos and A. F. Nogueira, "Efficient Dye-Sensitized Solar Cells Based on the Combination of ZnO Nanorods and Microflowers". *Journal of Nanoscience and Nanotechnology* **2010,** 10 (10), 6432-6438.
63. C. H. Lee, W. H. Chiu, K. M. Lee, W. H. Yen, H. F. Lin, W. F. Hsieh and J. M. Wu, "The influence of tetrapod-like ZnO morphology and electrolytes on energy conversion efficiency of dye-sensitized solar cells". *Electrochimica Acta* **2010,** 55 (28), 8422-8429.
64. Z. Li, Y. Zhou, G. Xue, T. Yu, J. Liu and Z. Zou, "Fabrication of hierarchically assembled microspheres consisting of nanoporous ZnO nanosheets for high-efficiency dye-sensitized solar cells". *Journal of Materials Chemistry* **2012,** 22 (29).
65. W. H. Chiu, C. H. Lee, H. M. Cheng, H. F. Lin, S. C. Liao, J. M. Wu and W. F. Hsieh, "Efficient electron transport in tetrapod-like ZnO metal-free dye-sensitized solar cells". *Energy & Environmental Science* **2009,** 2 (6), 694-698.
66. Y. F. Hsu, Y. Y. Xi, C. T. Yip, A. B. Djurisic and W. K. Chan, "Dye-sensitized solar cells using ZnO tetrapods". *Journal of Applied Physics* **2008,** 103 (8).
67. I. Gonzalez-Valls and M. Lira-Cantu, "Dye sensitized solar cells based on vertically-aligned ZnO nanorods: effect of UV light on power conversion efficiency and lifetime". *Energy & Environmental Science* **2010,** 3 (6), 789-795.
68. I. Gonzalez-Valls, J. S. Reparaz, F. Güell, M. R. Wagner, G. Callsen, B. Ballesteros, A. Hoffmann and M. Lira-Cantu, "Low temperature growth of vertically-aligned ZnO nanorods for dye sensitized solar cells: unravelling their low power conversion efficiency". *Nano Letters* **2012**, submitted.
69. O. Lupan, T. Pauporte, I. M. Tiginyanu, V. V. Ursaki, H. Heinrich and L. Chow, "Optical properties of ZnO nanowire arrays electrodeposited on n- and p-type Si(1 1 1): Effects of thermal annealing". *Materials Science and Engineering B-Advanced Functional Solid-State Materials* **2011,** 176 (16), 1277-1284.
70. O. Lupan, T. Pauporte and B. Viana, "Low-Voltage UV-Electroluminescence from ZnO-Nanowire Array/p-GaN Light-Emitting Diodes". *Advanced Materials* **2010,** 22 (30), 3298-+.
71. C. J. Murphy and N. R. Jana, "Controlling the aspect ratio of inorganic nanorods and nanowires". *Advanced Materials* **2002,** 14 (1).
72. U. Ozgur, Y. I. Alivov, C. Liu, A. Teke, M. A. Reshchikov, S. Dogan, V. Avrutin, S. J. Cho and H. Morkoc, "A comprehensive review of ZnO materials and devices". *Journal of Applied Physics* **2005,** 98 (4).
73. J. B. Cui, Y. C. Soo, T. P. Chen and U. J. Gibson, "Low-temperature growth and characterization of Cl-doped ZnO nanowire arrays". *Journal of Physical Chemistry C* **2008,** 112 (12), 4475-4479.
74. H. Y. Xu, Y. C. Liu, J. G. Ma, Y. M. Luo, Y. M. Lu, D. Z. Shen, J. Y. Zhang, X. W. Fan and R. Mu, "Photoluminescence of F-passivated ZnO nanocrystalline films made from thermally oxidized ZnF2 films". *Journal of Physics-Condensed Matter* **2004,** 16 (28), 5143-5150.
75. M. J. DeVries, M. J. Pellin and J. T. Hupp, "Dye-Sensitized Solar Cells: Driving-Force Effects on Electron Recombination Dynamics with Cobalt-Based Shuttles". *Langmuir* **2010,** 26 (11), 9082–9087.
76. S. J. Pearton, "GaN and ZnO-Based Materials and Devices". **2012**; p 485 ISBN 3642235212, 9783642235214.
77. K. S. Finnie, J. R. Bartlett and J. L. Woolfrey, "Vibrational spectroscopic study of the coordination of (2,2 '-bipyridyl-4,4 '-dicarboxylic acid)ruthenium(II) complexes to the surface of nanocrystalline titania". *Langmuir* **1998,** 14 (10), 2744-2749.

78. M. K. Nazeeruddin, R. Humphry-Baker, P. Liska and M. Gratzel, "Investigation of sensitizer adsorption and the influence of protons on current and voltage of a dye-sensitized nanocrystalline TiO2 solar cell". *Journal of Physical Chemistry B* **2003,** 107 (34), 8981-8987.
79. E. Galoppini, "Linkers for anchoring sensitizers to semiconductor nanoparticles". *Coordination Chemistry Reviews* **2004,** 248 (13-14), 1283-1297.
80. A. Vittadini, A. Selloni, F. P. Rotzinger and M. Gratzel, "Formic acid adsorption on dry and hydrated TiO2 anatase (101) surfaces by DFT calculations". *Journal of Physical Chemistry B* **2000,** 104 (6), 1300-1306.
81. K.-J. Hwang, S.-J. Yoo, S.-S. Kim, J.-M. Kim, W.-G. Shim, S. Kim, II and J.-W. Lee, "Photovoltaic Performance of Nanoporous TiO(2) Replicas Synthesized from Mesoporous Materials for Dye-Sensitized Solar Cells". *Journal of Nanoscience and Nanotechnology* **2008,** 8 (10), 4976-4981.
82. S. Meng and E. Kaxiras, "Electron and Hole Dynamics in Dye-Sensitized Solar Cells: Influencing Factors and Systematic Trends". *Nano Letters* **2010,** 10 (4), 1238-1247.
83. N. Martsinovich and A. Troisi, "Theoretical studies of dye-sensitised solar cells: from electronic structure to elementary processes". *Energy & Environmental Science* **2011,** 4 (11), 4473-4495.
84. K. Cahyorini, K. Indriana and Narsito, "Dye-sensitized solar cells based on in situ sensitized of nitrogen doped TiO2". *CORD Conference Proceedings* **2011**, 1-5.

Chapter 4

Core-shell ZnO Nanorods

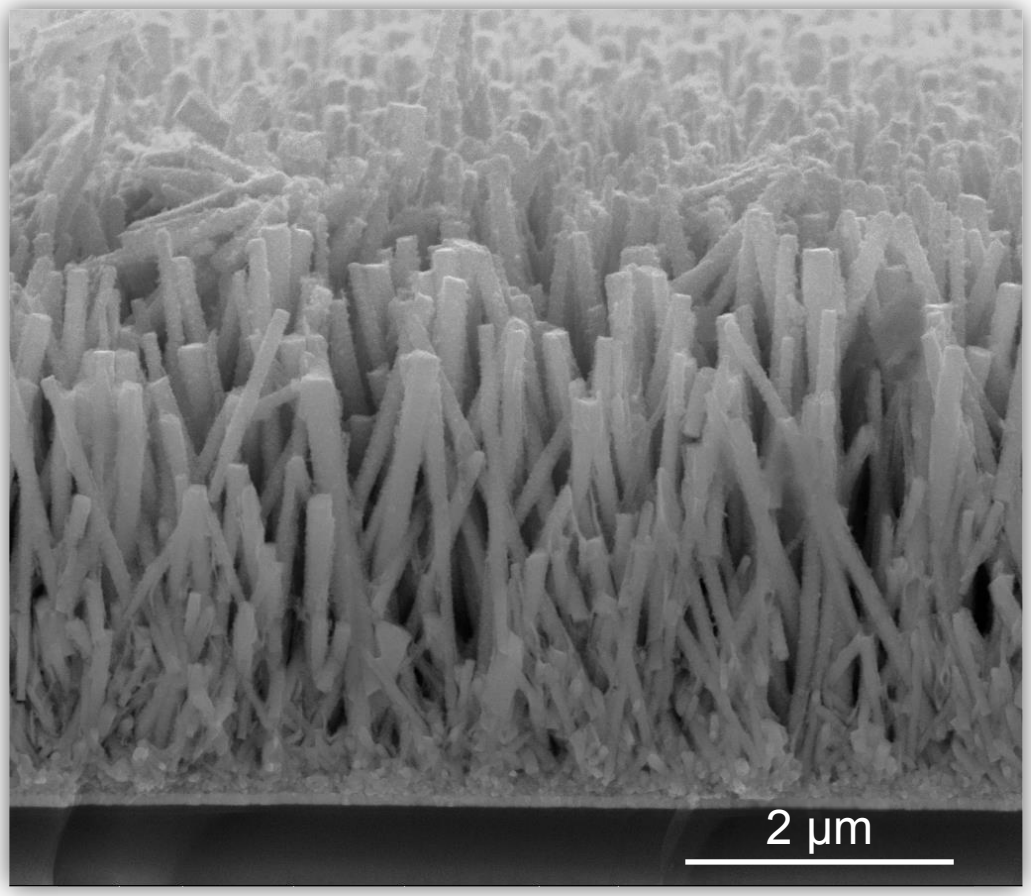

Chapter 4
Core-shell ZnO/In_xS_y Nanorods

4.1 Introduction

Among the recent innovative strategies to improve the ZnO nanorods (NR) properties for their application in DSC is the preparation of ZnO core-shell structures. The ZnO NRs functions as the skeleton or the core of the final nanostructure, and an inorganic semiconductor is deposited on its surface as an outer shell layer.[1-3] Shells of Al_2O_3, MgO, SiO_2, TiO_2, ZnS, CdSe or CdS as a thin layer, nanoparticles (NPs) or quantum dots (QDs) coated on ZnO electrodes for solar cells have been used.[4-11] A general overview of the different core-shell nanostructures find in the literature applied in DSC is summarized in Table 4.1. The table it is strictly focused on ZnO NRs and no other nanostructures, like tetrapods, nanoparticles, nanoflowers, etc., are included. We should mention at this point that the application of a thin outer layer of inorganic nanoparticles working as the replacement of the dye (the absorbed) in DSC has also been reported.[12, 13] These nanoparticles, usually of a few nanometers in size and therefore called quantum dots (QD), like CdS[14, 15] or CdSe,[16-21] can also be find as the outer shell for ZnO nanorods. Nevertheless, when these electrodes are part of a solar cell, usually called Quantum dots solar cells (QDSCs),[22] do not apply a dye for the fabrication of the final device. Consequently, these types of electrodes are beyond the main purpose of this work, and thus, are not included in Table 4.1. A schematic representation of vertically-aligned core-shell ZnO/In_xS_y NRs and the SEM and TEM images of the core-shell structures obtained in our laboratory are shown in Figure 4.1.

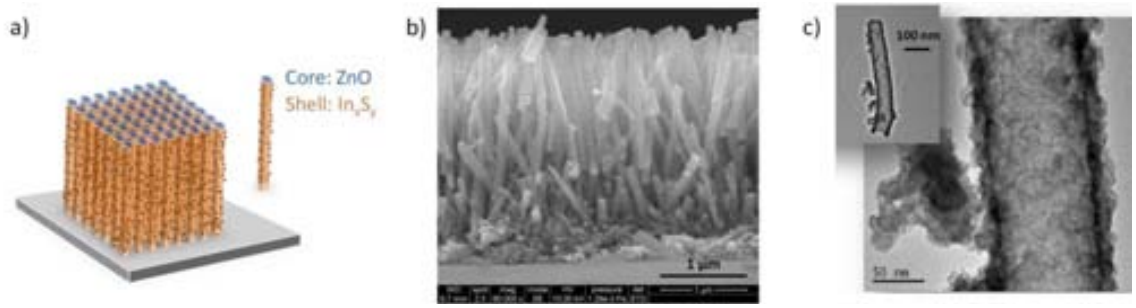

Figure 4.1 a) A schematic representation of vertically-aligned ZnO NRs covered with a shell layer of In_xS_y, b) SEM image of the core-shell ZnO/In_xS_y NRs and c) TEM images of the same core-shell ZnO/In_xS_y NRs obtained in our laboratory.

Table 4.1 Literature review on vertically-aligned ZnO NRs-core shell inorganic nanomaterials and their application as electrodes in DSC. *HT: Hydrothermal, PS: Plasma sputtering, CVD: Chemical Vapor Deposition, SILAR: Successive Ionic Layer Adsorption and Reaction, ALD: Atomic Layer Deposition, SAM: Self-Assembled Monolayer, NP: Nanoparticle, QD: Quantum dot, Merc: Mercurochrome.* *Solid-state Dye-sensitized Solar Cell (ss-DSC).

Film Thickness (μm)	Synthesis method	Shell layer	Dye	Light Intensity (mW/cm^2)	V_{oc} (V)	J_{sc} (mA/cm^2)	FF (%)	PCE (%)	Ref
-	HT	ZrO_2	D149	-	0.60	2.79	-	0.72	23
-	HT	Au NP	N719	100	0.62	4.20	-	1.20	24
1.5	HT + PS	TiO_2	C206	100	0.72	4.31	56	1.74	5
2.5	HT	ZnS NP	N3	100	0.68	1.87	60	0.76	25
2.5	HT	CdS QD	N3	100	0.68	7.00	40	1.90	26
2.5	HT	Mg-ZnO NP	N719	100	0.71	8.56	51	2.91	27
3.0	HT	TiO_2 NP	N719	100	0.60	3.54	37	0.79	28
3.0-4.0	HT	CdTe	N719	25	0.71	0.72	31	0.16	29
5.0	CVD	TiO_2	N719	100	0.59	2.57	60	0.92	30
5.0	HT	ZnO NP	N719	100	0.64	4.50	59	1.70	31
5.0	HT	ZnS	N719	100	0.56	8.38	42	1.92	32
5.3	HT + SILAR	ZnSe	N719	-	0.46	7.97	39	1.37	33
5.3	HT	ZnS	N719	-	0.53	11.98	44	2.72	34
5.5	HT	ZnO NP	Merc.	100	0.58	8.33	58	2.77	35
6.0	HT	ZnO NP	N719	100	0.60	7.00	52	2.19	36
7.0	HT	ZnO NP	N719	100	-	-	-	0.90	37
10.0	HT + ALD	TiO_2	C220	100	0.82	5.08	61	2.53	38
14.0	HT + dip coat	TiO_2	N719	100	0.59	10.55	61	3.80	39
15.0	HT + ALD	TiO_2	N719	-	0.80	4.78	59	2.21	4
50.0*	HT + SAM	TiO_2	Z907	100	0.80	12.40	59	5.86	40

The advantage of applying core-shell nanostructures of ZnO resides in the improvement of the surface structure.[34, 41] The dye attaches to the ZnO surface though a carboxylic acid group which degrades the ZnO nanostructure and decreases the solar cell efficiency (see chapter 2, section 2.4.3 and 2.5.4). The coverage of the ZnO surface could avoid the latter degradation and, additionally, could increase the electron injection from the dye to the ZnO semiconductor due to the reduction of recombination processes.[24, 26, 31, 41]

An inorganic semiconductor that attracted our attention as possible shell for ZnO NRs is In_xS_y. In a In:S ratio of 2:3, the In_2S_3 is well-known for its stability,[42, 43] non-toxicity,[43, 44] and good photoconductivity.[42, 45, 46] It has a band gap of 2.0-2.3 eV, suitable for the injection of photogenerated electrons from In_2S_3 to ZnO,[45] and the alignment of its conduction band with respect to the N719 Dye is suitable for charge injection from the dye. Figure 4.2 illustrates the energy band diagram of a DSC with a ZnO/In_2S_3 core-shell electrode and the electron charge transfer path. When a photon is absorbed by the dye N719, the excited electron can be transfer to the conduction band of the In_2S_3 shell layer and then to the ZnO NRs.[47]

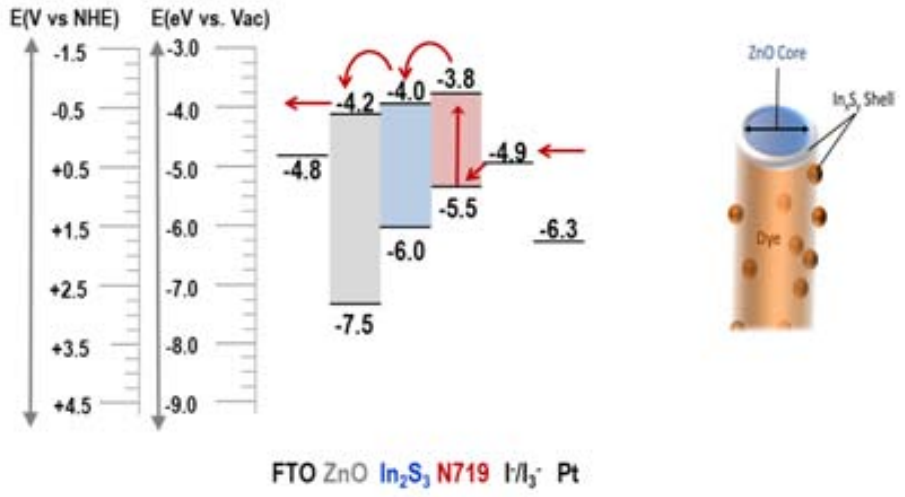

Figure 4.2 Energy diagram of a DSC based on core-shell ZnO/In_2S_3 thin film electrode, the dye N719 and an iodine redox electrolyte vs. Vacuum and vs. NHE (Normal Hydrogen Electrode).[47]

The synthesis of In_2S_3 can be carried out by several methods, such as spray ion layer gas reaction (ILGAR)[48-50], atomic layer deposition (ALD)[46, 51] or successive ion layer adsorption and reaction (SILAR).[23, 52] The deposition of In_2S_3 by the ILGAR technique consists of spraying an $InCl_3$ solution and a sulfurization in Ar:H_2S at 200 °C. The ALD method also uses the $InCl_3$ (or indium acetylacetonate) and H_2S as precursors, which are deposited on the substrate by evaporation. Among all the latter techniques, the SILAR technique is the most advantageous since it avoids the use of toxic H_2S gas and is also a low cost technique. The SILAR technique applies two aqueous solutions, one of $InCl_3$ and the other of Na_2S. Dittrich *et al.*[52] adapted the In_2S_3 SILAR technique using the same concentrations of precursors from the reported preparation of ZnS, CdS and $Zn_{1-x}Cd_xS$.[53] The mechanism for

the In_2S_3 SILAR deposition takes place by the following chemical reactions described in equation 4.1 to 4.3. First, the solution of Na_2S dissociates in water (equation 4.1), the presence of HCl controls the pH at 7-8, and is the responsible for the formation of HS^- anions (equation 4.2). These HS^- anions can be adsorbed on the In^{3+} surface, and not the S^{2-} anions, due to their less-strongly solvated character (equation 4.3).[53]

$$Na_2S + H_2O \leftrightarrow 2Na^+_{aq} + S^{2-}_{aq} \qquad (4.1)$$

$$S^{2-}_{aq} + H_2O \leftrightarrow HS^-_{aq} + OH^-_{aq} \qquad (4.2)$$

$$2InCl_3 + 3HS^- \leftrightarrow In_2S_3 + 3HCl \qquad (4.3)$$

We present in this chapter the synthesis and characterization of vertically-aligned core-shell ZnO/In_xS_y NR electrodes and their application in DSC. The shell layer was deposited on ZnO NRs electrodes obtained by the hydrothermal methods LT-HM (described in chapter 2)[54, 55] and the A-HM (applying the reactor 1, as described in chapter 3).[56] The synthesis of the In_xS_y shell layer was made employing the SILAR technique.[52] Different In_xS_y shell thicknesses were prepared on the ZnO NRs electrodes, the synthesis was optimized and characterized, and finally the as-prepared electrodes were applied in DSCs applying the N719 Dye and liquid electrolyte.[57] As will be explain in detail in this chapter, the initial application of the as-prepared electrodes in solar cells revealed good power conversion efficiency when the In:S ratio of the In_xS_y shell was not the stoichiometric 2:3 expected for a In_2S_3 layer. In order to study this effect, the In_xS_y shell on the ZnO NR was synthesized applying two different concentrations of the Na_2S solution, resulting in a shell layer with an stoichiometric In:S ratio of 2:3 and, with a low-sulfur content with In:S ratio of 10:3.

4.2 Synthesis and Characterization

In this section we describe the synthesis and characterization of the core-shell ZnO/In_xS_y nanorods. The nanostructure was obtained by the deposition of a layer of In_xS_y on top of the vertically-aligned ZnO NRs. The ZnO NRs were first prepared by the low-temperature hydrothermal method (LT-HM, chapter 2)[54, 55] and the autoclave hydrothermal method using the reactor 1 (A-HM, chapter 3).[56] The difference between the ZnO nanorods synthesized by these methods resides in the dissimilar optical quality of the ZnO NRs,

being the ZnO NR obtained by the LT-HM the ones with lower quality (higher amount of surface defects) in comparison with the A-HM. Another difference is that the NRs obtained by the A-HM are shorter in length, an important effect that will be detailed during this chapter. After the core-shell ZnO/In_xS_y nanostructures were prepared, these were characterized by SEM, TEM, XRD, EDS and FT-IR analysis.

4.2.1 In_xS_y shell preparation and characterization

The In_xS_y shell layer was deposited by the Successive Ion Layer Adsorption and Reaction (SILAR) technique reported by T. Dittrich *et al.*[52] who adapted the synthesis of ZnS, CdS and $Zn_{1-x}Cd_xS$[53] for In_2S_3. The method consists of two aqueous solutions of $InCl_3$ and Na_2S with a concentration of 0.1 M and 0.03 M respectively. The ZnO NRs electrode is first dipped in the $InCl_3$ solution. In a second step, the electrodes are immersed in the Na_2S solution and finally washed with distilled water. The process encompassing these three steps is called a SILAR cycle. In order to vary the shell thickness, several SILAR cycles must be applied to the ZnO NR electrodes. The ZnO electrodes used (described in Table 4.2) were grown for 6 h (electrode A) and 12 h (electrode B) both prepared by the LT-HM method. Figure 4.3 shows the top and the lateral view of the electrode A and electrode B after 3, 5 and 10 SILAR cycles. The final length of each core-shell ZnO/In_xS_y NR electrode was: 2.4 μm (3 cycles), 2.3 μm (5 cycles), 1.9 μm (10 cycles) for electrode A and 3.2 μm (3 cycles), 3.1 μm (5 cycles) and 3.0 μm (10 cycles) for electrode B as observed by the SEM images shown in Figure 4.3. A decrease in NR length is observed after the In_xS_y layer is deposited from 2.4 and 3.2 μm to 1.9 and 3.0 μm, for samples A and B respectively. This decrease in NR length was observed when the number of SILAR cycles was increased. The latter has been attributed to the acidity of the $InCl_3$ (pH=1-3) solution that can dissolve the ZnO semiconductor. From SEM top view image of the sample with 10 SILAR cycles (Figure 4.3c) we observed that the core of the ZnO NRs seems to be empty, resembling ZnO nanotubes (NTs).

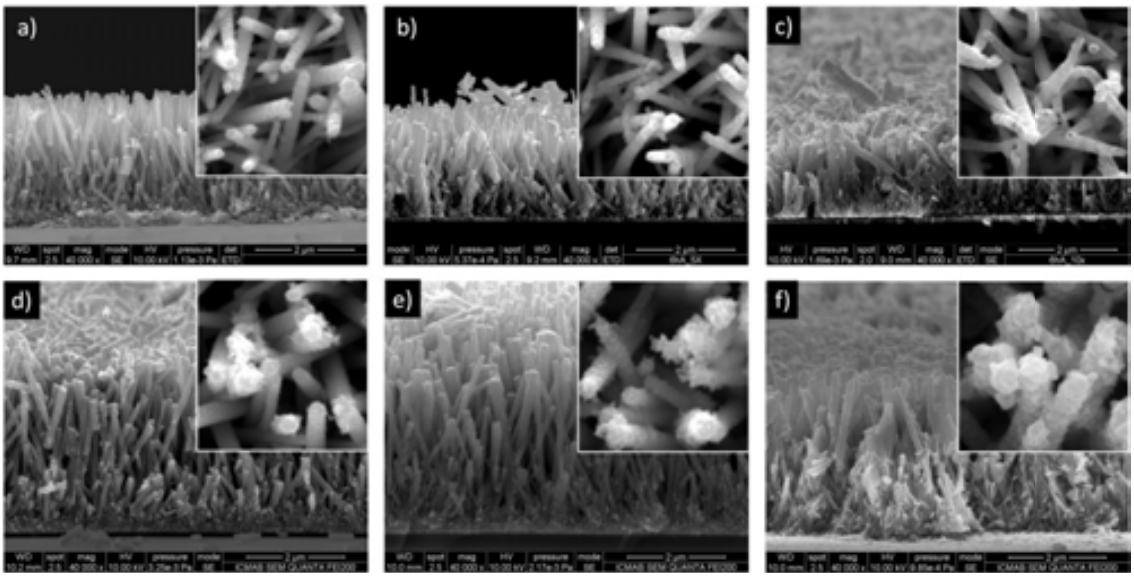

Figure 4.3 Lateral and top view SEM images of core-shell ZnO NRs prepared by the LT-HM and grown for 6h-electrode A (a-c) and 12h-electorde B (d-f) with different SILAR cycles: 3 (a, d), 5 (b, e) and 10 (c, f). The scale for the top images is 1 μm each side of the square.

In order to analyze the core-shell ZnO/In_xS_y nanostructure we used the SEM back-scattered electron (BSE) detector which applies high-energy electrons originated in the electron beam of the SEM microscope. The elastic scattering interactions of the atoms are then reflected and analyzed. The technique permits the characterization of different atoms since the heavy elements (with higher atomic number) backscatter electrons in a stronger way than light elements (lower atomic number). Thus, heavy metals appear brighter in the BSE image than light elements, such as organic materials, which appear with a dark color. In our samples, the In_xS_y shell should appear brighter than the ZnO. Our results, shown in Figure 4.4, demonstrate that increasing the SILAR cycles on these electrodes (20 and 40 cycles) resulted on almost all the ZnO NRs converted to nanotubes. The latter has been attributed to the presence of HCl from the acid $InCl_3$ solution which dissolves the ZnO NRs. As a consequence, not only the core of the ZnO NR is eliminated but also the NR length decreases when increasing the SILAR cycles. For example, for electrode A, the NR length for 20 SILAR cycles was about 1.4 μm, while increasing to 40 cycles resulted in 1.3 μm length (see Figure 4.4). We can also state that the vertical-aligned structure is partially destroyed and converted into a randomly distributed In_xS_y nanostructure after prolonged SILAR cycles, as we can see in Figure 4.4d.

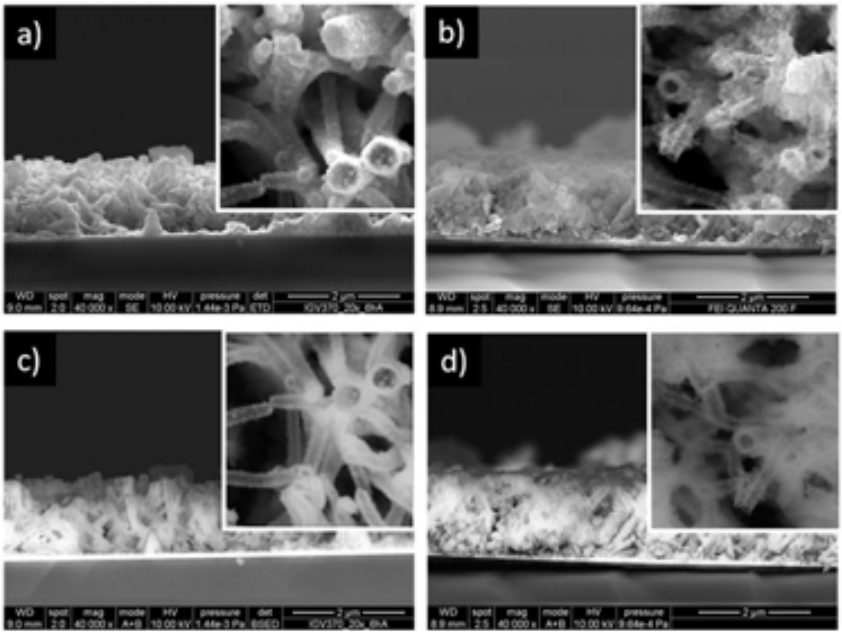

Figure 4.4 Lateral and top view SEM images (a, b) and backscattered electron images (c, d) of core-shell electrode A with 20 (a, c) and 40 (b, d) SILAR cycles. The scale for the top images is 1 μm each side of the square.

4.2.2 In_xS_y shell layer thickness

The In_xS_y layer thickness was measured by TEM analyses. Figure 4.5 shows the TEM images of the core-shell ZnO/In_xS_y NR prepared by the SILAR technique applying 3 (a, d), 5 (b, e) and 10 cycles (c, f). The thin film shell thickness increased from 3-9 nm for 3 cycles, to 4-12 nm for 5 cycles and 20-50 nm for 10 cycles. The crystalline structure of the core-shell electrodes was also investigated by TEM presenting in all cases a hexagonal wurtzite structure for the core ZnO NRs and an amorphous shell layer (Figure 4.6). Due to the amorphous nature of the shell layer, the x-ray analysis shows only the corresponding peaks of the wurtzite structure of the ZnO and the FTO substrate (Figure 4.7).

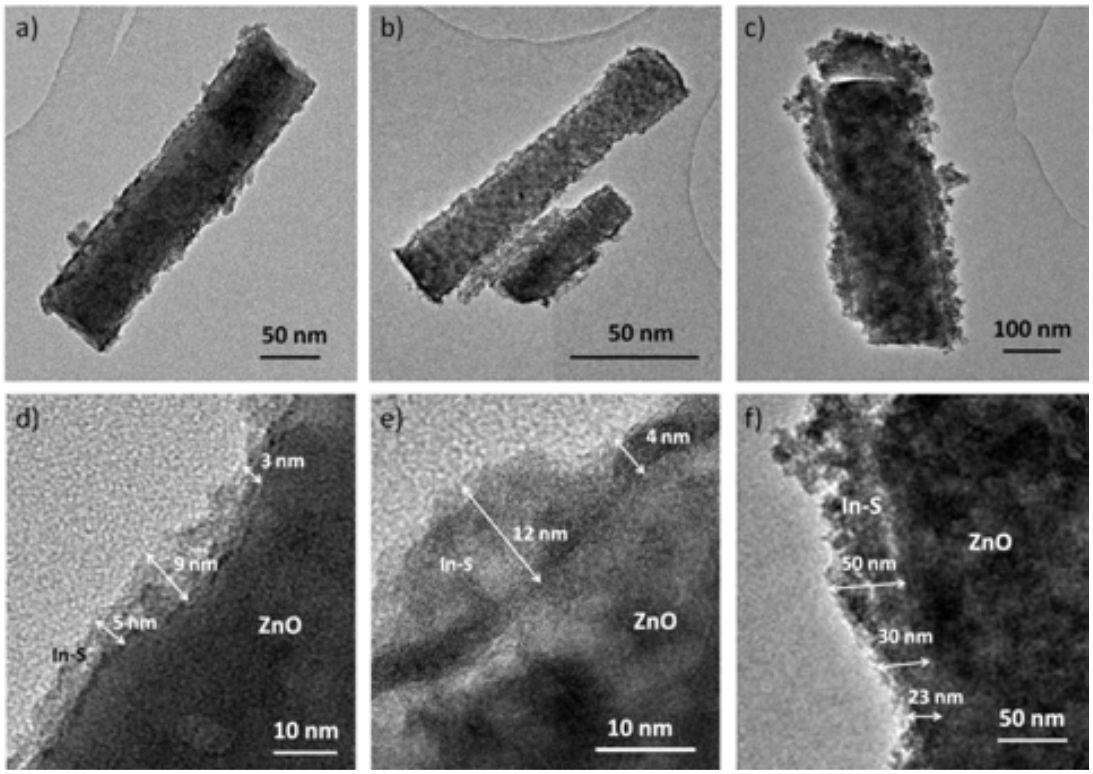

Figure 4.5 TEM images of ZnO NRs scratched from the electrode A with 3 (a, d) and 5 (b, e) SILAR cycles and the electrode B with 10 cycles (c, f).

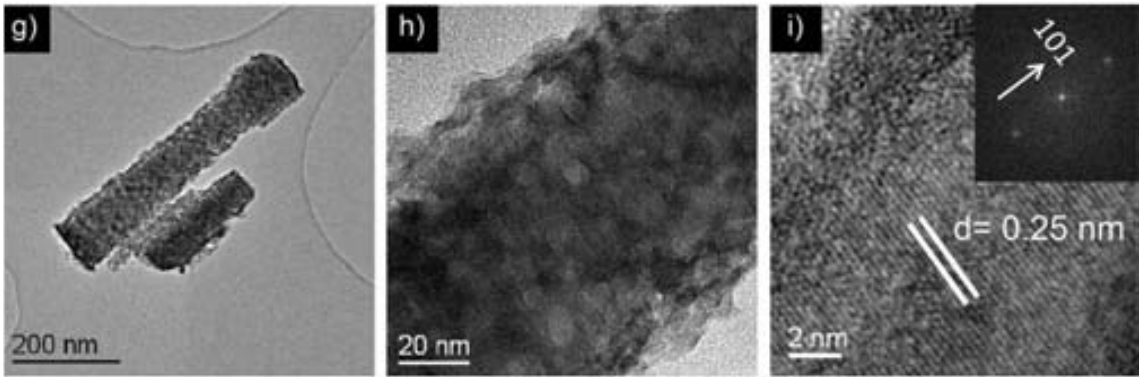

Figure 4.6 TEM and High resolution TEM images of ZnO NRs from electrode A with 5 SILAR cycles.

TEM analyses demonstrate an uniform formation of the In_xS_y shell layer covering all the ZnO NRs with different thicknesses depending on the number of SILAR cycles applied. This shell layer was observed to be amorphous.

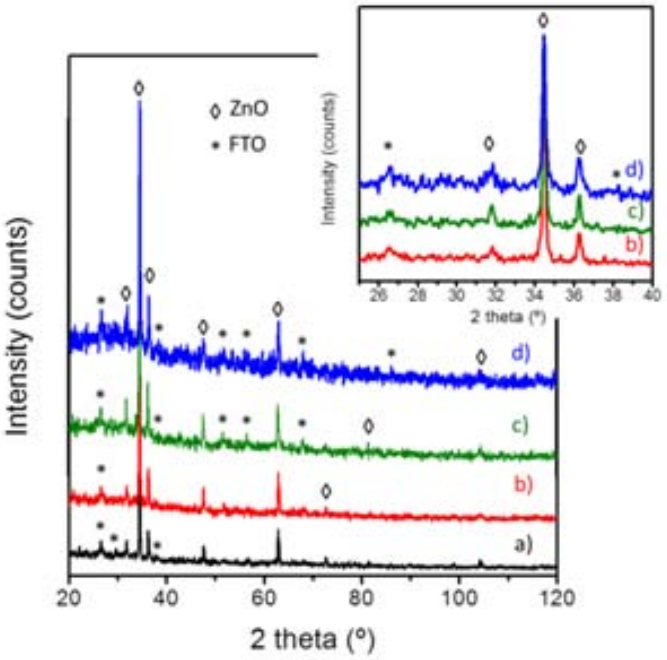

Figure 4.7 X-rays diffraction analyses (XRD) of electrodes: a) FTO/ZnO NRs and FTO/ZnO/In_xS_y NRs applying b) 3 SILAR cycles, c) 5 cycles and d) 10 cycles. The ZnO NRs were grown by the LT-HM at 6h. The inset figure is an amplification of a small part of the XRD spectra.

4.3 Application in Dye-sensitized solar cells

In this section we present the application of the core-shell ZnO/In_xS_y NR electrodes in DSC. The ZnO electrodes applied were synthesized by the LT-HM and the A-HM (as described in Chapter 2 and 3). The electrodes were labelled as it is shown in Table 4.2.

Table 4.2 Summary of the electrodes prepared with an In_xS_y shell layer.

ELECTRODE	ZnO NR		
	synthesis method	Growth time	Length (nm)
A	LT-HM	6h	1.6
B	LT-HM	12h	3.2
C	LT-HM	22h	5.1
D	A-HM	6h	0.4
E	A-HM	12h	0.9
F	A-HM	28h	1.1

The initial analyses of the as-prepared electrodes revealed improved power conversion efficiency when the In_xS_y shell was used in comparison with the bare ZnO electrodes. Nevertheless, we notice that the best power conversion efficiency was not achieved in samples where the In:S stoichiometric ratio of 2:3, expected for an In_2S_3 layer, was used. Only when a low S content was used during synthesis we were able to achieve improved efficiency. In order to study this effect, the In_xS_y shell on the ZnO NR was synthesized applying two concentrations of Na_2S: the first one to get the 2:3 stoichiometric ratio (In_2S_3) and a second one, of lower Na_2S concentration (based on the work from Dittrich *et al.*- ref 52), corresponding to a 10:3 ratio ($In_{10}S_3$). Thus, in this section we initiate describing the photovoltaic response observed when these two different Na_2S solutions are applied during shell deposition. Then, a description of the optimization of the DSCs applying always the low concentration of Na_2S is presented which results in best photovoltaic response. Finally, the end of this chapter debates on the reasons behind the improved solar cell performance when low concentration of S is used and the effect of the shell layer on the final photovoltaic devices.

4.3.1 Effect of the Na_2S concentration

Electrodes made of core-shell ZnO/In_xS_y nanostructures, obtained with two different Na_2S concentrations, 0.15 and 0.03 M, were analyzed in DSCs. This In_xS_y shell layer was freshly prepared before each DSC fabrication due to an observed power conversion decrease when the electrodes were kept some days under ambient atmosphere in air. The In_xS_y shell was deposited on the ZnO NR electrodes prepared by the LT-HM and the A-HM (see Table 4.2). For comparison purposes, the bare vertically-aligned ZnO electrodes obtained in the same conditions, without the In_xS_y shell, were also analyzed. The best results (of a series of 4 samples) for each type of electrode are shown in Table 4.3. In general, we have observed that devices with an In_xS_y layer deposited with the low Na_2S concentration solution (0.03 M), showed the best solar cell performance if compared with the DSCs without the In_xS_y shell. Whereas electrodes obtained with higher Na_2S solution concentration (0.15 M) presented the lowest power conversion efficiency, mainly due to the low current density observed.

Table 4.3 DSC parameters applying ZnO NRs with and without core-shell prepared with low (0.03 M) and high (0.15 M) Na_2S solution concentration. 100 mW·cm^{-2} illumination, AM 1.5G. Pt-CE prepared by EBPVD (50 nm).

ZnO electrode	Na_2S conc. (M)	SILAR cycles	V_{oc} (V)	J_{sc} (mA·cm^{-2})	FF (%)	PCE (%)
	-	-	0.48	2.06	40	0.40
A	0.03	3	0.58	2.11	64	0.79
	0.15	3	0.41	0.97	51	0.20
	-	-	0.56	2.29	42	0.54
B	0.03	5	0.59	4.11	61	1.50
	0.15	5	0.46	0.86	52	0.21

4.3.2 Optimization of the solar cell parameters

Based on the previously described results, the optimization of the solar cell parameters was carried out with core-shell ZnO/In_xS_y electrodes prepared with the low concentration of the Na_2S (0.03M), which correspond to a theoretical In:S ratio of 10:3. Thus, the synthesis of the In_xS_y layer was carried out applying the SILAR method for different cycles, with solution concentrations of 0.1 M for the $InCl_3$ solution and 0.03 M for the Na_2S solution.

The optimization of the photovoltaic properties was carried out by analyzing the effect that the shell layer thickness and the dye loading time (DLT) have on the solar cell performance. The shell layer thickness was modified by the deposition of different SILAR cycles (from 1 up to 20 cycles). The best solar cell results obtained applying electrode A are presented in Figure 4.8. For electrode A the highest power conversion efficiency was observed for samples obtained with 3 SILAR cycles of the In_xS_y shell (Figure 4.8a). The dye-loading time (DLT) was also optimized and found that, for electrode A, increasing the DLT from 2h to 4h increases the solar cell performance. Longer DLT resulted in the decrease of the power conversion efficiency of the device as observed in Figure 4.8b. The other electrodes B to F (Table 4.2) were optimized following the same procedure as electrode A. Nevertheless, the In_xS_y shell thicknesses applied to the electrodes B to F were prepared applying between 3 and 15 SILAR cycles as the solar cell performance was observed to decrease for thicker In_xS_y shells.

The best power conversion efficiency of 2.32% was obtained for the ZnO electrode B with an In_xS_y shell made with 5 SILAR cycles. Moreover, the best response for electrode B was observed after 6h of DLT, after this time the power conversion efficiency decreased. The

rest of the samples (electrodes C to F) showed, in general, low performance. Table 4.4 shows the best In_xS_y shell thickness, DLT and the photovoltaic performance observed for all the electrodes analyzed. In general, we have observed that the length of the ZnO NR electrodes is directly related to the number of the SILAR cycles required to obtain the best photovoltaic performance. The longer the ZnO NRs the larger the amount of SILAR cycles needed, as expected. Short ZnO NRs are prone to faster degradation due to the acidic condition of the shell deposition bath. Thus, it is not surprising that ZnO NRs obtained by the LT-HM (lengths between 1.6 and 5.1 μm), present higher power conversion efficiency if compared to those obtained by the A-HM (lengths between 0.4 and 3.5 μm). The latter problem was resolved by lowering the concentration of the solution applied during In_xS_y synthesis. The application of a more dilute SILAR solution (0.025M of $InCl_3$ and 0.0075M of Na_2S) for the shorter ZnO NR electrodes, those obtained by the A-HM, resulted in an effective improvement of the power conversion efficiency. Nevertheless, for the A-HM electrodes the optimum number of SILAR cycles was not directly related to the ZnO NR length, as observed for the LT-HM electrodes (see Table 4.4). The latter can probably be attributed to the higher complexity for the ZnO dissolution (easy to degrade) found in short NRs.

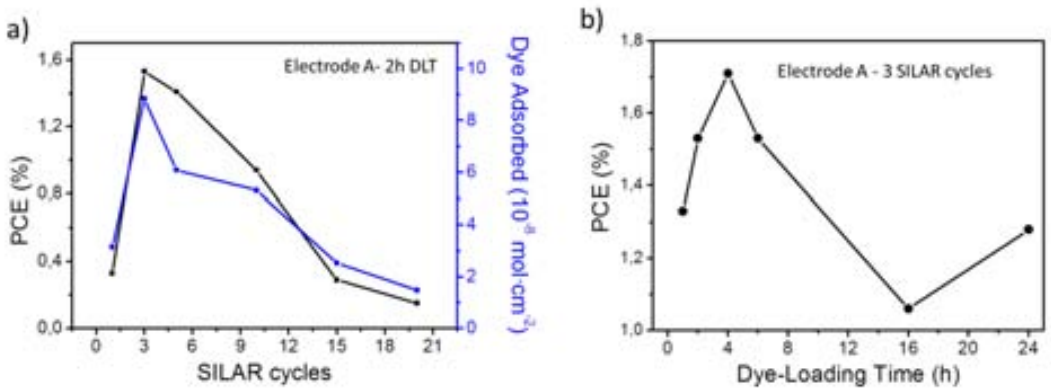

Figure 4.8 The power conversion efficiency (PCE) of the DSCs applying the ZnO/In_xS_y core-shell electrode A depending on the number of SILAR cycles (a) and different dye loading times, DLTs (b).

Table 4.4 The Solar Cell performance of the optimized core-shell ZnO/In_xS_y electrodes prepared by the LT-HM grown for 6h (A), 12h (B) and 22h (C) and prepared by the A-HM grown for 6h (D), 12h (E) and 28h (F). Applying 0.1 M $InCl_3$ and 0.03 M Na_2S SILAR concentrations for electrode A,B and C, while other SILAR concentrations: 0.025 M $InCl_3$ and 0.0075 M Na_2S were applied for electrodes D, E and F. Measured at 100 mW·cm^{-2} illumination, AM 1.5G. Pt-CE prepared by EBPVD (50 nm).

ZnO electrode	HT Method	NR growth time (h)	NR length (µm)	SILAR cycles	DLT (h)	V_{oc} (V)	J_{sc} (mA·cm^{-2})	FF (%)	PCE (%)
A	LT-HM	6	1.6	3	4	0.59	5.21	56	1.71
B	LT-HM	12	3.2	5	6	0.70	5.46	60	2.32
C	LT-HM	22	5.2	10	6	0.61	6.38	54	2.13
D	A-HM	6	0.4	5	2	0.66	2.63	53	0.91
E	A-HM	12	0.9	3	1	0.68	2.61	52	0.93
F	A-HM	28	3.5	3	3	0.61	5.18	54	1.70

The dye adsorbed on the ZnO electrodes of the DSCs was calculated by the dye-desorption method (described in chapter 6: experimental techniques, section 6.6.1). UV-vis absorption analysis of the solution was used to calculate the quantity of dye adsorbed per cell area. An important aspect to take into account is the time needed to obtain a completely dye desorption for the different electrodes. In the case of the bare ZnO NRs, less than one hour was required to desorb the dye from the electrode, while 2-3 h were needed for the core-shell NRs electrodes. The latter indicates that the interaction between the dye and the core-shell ZnO/In_xS_y NRs electrode is stronger, obtaining higher J_{sc} values with core-shell DSCs in comparison to the bare ZnO NRs. The quantity of dye adsorbed is in well agreement with the cell performance, solar cells with high power conversion efficiencies present the highest quantity of dye adsorbed (Figure 4.8a). The comparison between ZnO NRs electrodes grown under the same conditions (6h growth time, LT-HM) with and without the In_xS_y shell layer, showed higher dye quantity adsorbed for the core-shell electrode ($8.9 \cdot 10^{-8}$ mol·cm^{-2}) than for the bare ZnO electrode ($2.5 \cdot 10^{-8}$ M·cm^{-2}). We attribute this mainly to the porosity of the core-shell electrodes which results in higher surface area and higher amount of dye adsorbed on the core-shell NRs in comparison with the bare ZnO NRs. Figure 4.9 represents the average of the power conversion efficiencies obtained with the 3 best DSCs applying electrode A and B with different shell layer thicknesses.

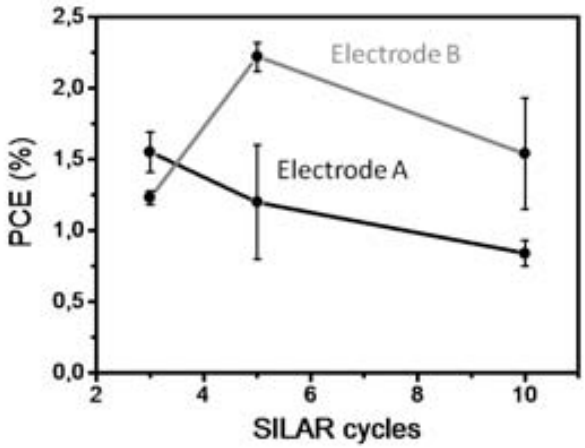

Figure 4.9 Average power conversion efficiencies (PCE) of the best 3 DSCs applying the electrode A and B with different SILAR cycles.

The IV-curves of the best cells from each electrode are shown in Figure 4.10a. Higher current densities were observed for electrodes prepared by the LT-HM (A, B and C). The highest V_{oc} and FF were measured with the electrode B obtaining a 2.32% efficiency (3.0 μm length) that is to our knowledge one of the highest obtained for core-shell electrodes of this type. Only longer core-shell NR length nanostructures DSCs achieved higher efficiencies using other shell layers (see Table 4.1).

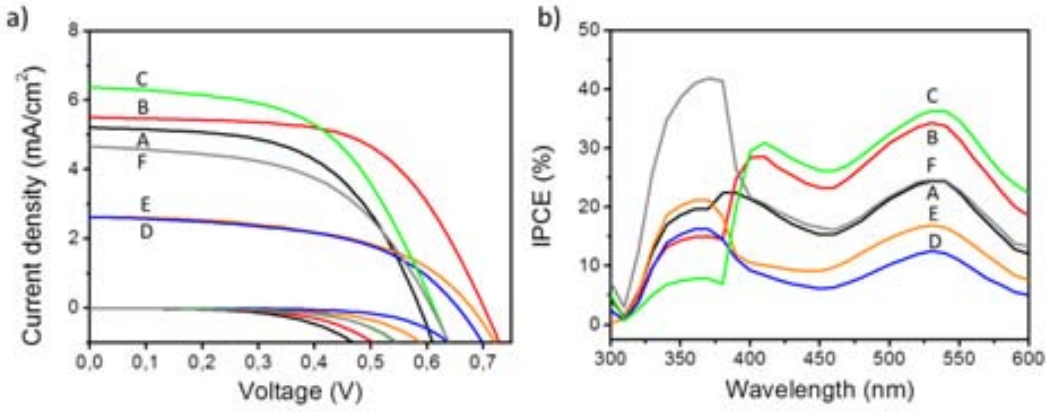

Figure 4.10 IV-curves and IPCE spectra of the best cells from table 4.5. Measured at 100 mW·cm^{-2} illumination, AM 1.5G. Pt-CE prepared by EBPVD (50 nm).

The IPCE spectra are represented in Figure 4.10b. The IPCE peak at ~530 nm corresponds to the dye N719, and present a trend that is identical with the current density shown in Figure 4.10a. The latter observation indicates that higher amount of dye in the cell gives higher current density which is the expected behavior. Electrode C (22h, LT-HM) presents the higher current density and IPCE value, with a peak at ~530 nm. This response is due to the larger length of the ZnO (around 5 μm) capable to adsorb higher amount of dye on its surface (as also described in chapter 3, see table 3.3). The IPCE peak at ~360 nm is related to the ZnO. The higher ~360 nm IPCE peak was measured for electrode F (28h, A-HM-1) and it was similar to the one measured with bare ZnO electrodes in chapter 3, Figure 3.18.

The comparison between bare and core-shell samples for electrode B (12h, LT-HM) is presented in Table 4.5, where the average DSC parameters from the best 5 cells are shown. All the photovoltaic parameters improved with the application of the core-shell ZnO/In_xS_y NR structure and hence, a 3 times higher efficiency was obtained.

Table 4.5 Average DSCs data using the electrode B (12h growth time by LT-HM) from the best 5 cells with bare ZnO NRs and core-shell electrodes (5 cycles, SILAR method 1). 100 $mW \cdot cm^{-2}$ illumination, AM 1.5G. Pt-CE prepared by EBPVD (50 nm).

Electrode B	NR length (μm)	V_{oc} (V)	J_{sc} ($mA \cdot cm^{-2}$)	FF (%)	PCE (%)	Max PCE (%)
Bare ZnO NRs	3.2 ± 0.5	0.54 ± 0.03	3.59 ± 0.61	41 ± 1	0.80 ± 0.09	0.87
Core-shell ZnO NRs	3.0 ± 0.1	0.64 ± 0.04	5.91 ± 0.49	57 ± 3	2.15 ± 0.12	2.32

4.3.3 Composition of the shell In_xS_y layer

EDS analyses of each core-shell ZnO/In_xS_y electrodes were carried out after different SILAR cycles in order to determine the relative quantity of the elements present in the shell layer. The analyses were carried out to the electrodes which showed the best photovoltaic properties: electrodes A and B (see Table 4.4). The EDS spectra of electrodes A and B revealed that increasing the number of SILAR cycles, the indium content increases together with a reduction on the Zn content (Figure 4.11). The latter is in well agreement with the formation of the inorganic In_xS_y shell layer and the dissolution of the ZnO NR due to the acidity of the reaction media, in agreement with the observations from the SEM/TEM analyses (section 4.2.1). Moreover, some chlorine atoms from the $InCl_3$ solution

were also observed. The presence of Cl in indium sulfide thin films has been also reported before applying the ILGAR technique.[58] Barreau *et al.,* pointed out that residual precursor elements are common when using chemical deposition techniques.[59] Figure 4.12 represents the atomic percentage of oxygen, zinc, indium, chlorine and sulfur on electrode A and B for 3, 5 and 10 SILAR cycles (the average of 4 different electrodes at each condition). These medium atomic percentage data is represented also in Table 4.6.

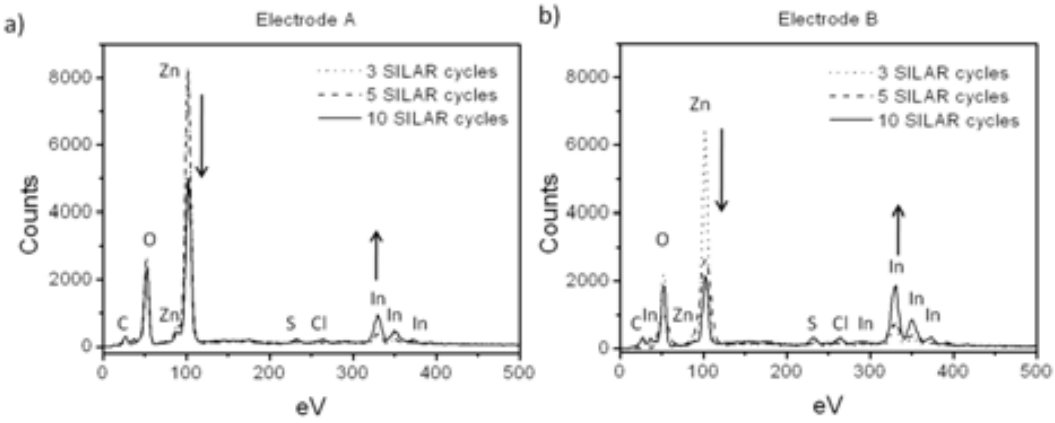

Figure 4.11 EDS graphs of electrodes A and B with 3, 5 and 10 SILAR cycles measured with the SEM instrument at 10 kV.

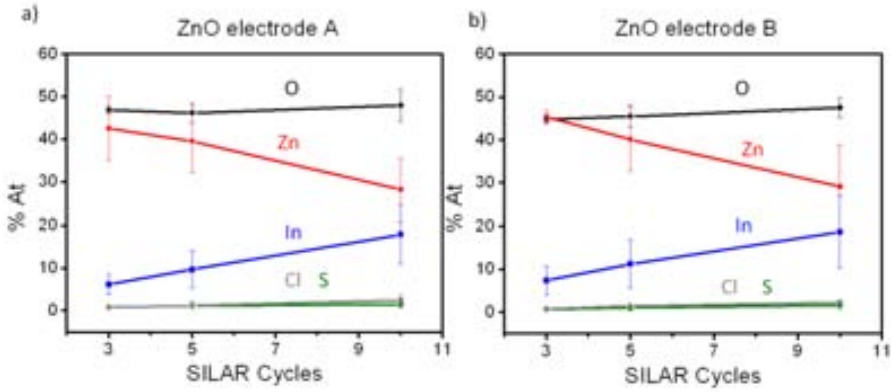

Figure 4.12 Atomic percentage graph of O, Zn, In, S and Cl measured by EDS analysis from the SEM instrument of ZnO/In_xS_y NR core-shell electrodes A and B at different SILAR cycles at 10 kV from 4 different electrodes for each condition.

Table 4.6 Medium EDS data from 4 ZnO NRs core-shell electrodes A and B of each condition (3, 5 and 10 cycles) using concentrations of 0.1 M and 0.03M for $InCl_3$ and Na_2S respectively.

ZnO electrode	SILAR cycles	Medium values O (% at)	Zn (% at)	In (% at)	S (% at)	Cl (% at)	Ratio Zn:In	In:S	S:Cl
A	3	49.9 ± 0.9	42.6 ± 7.5	6.2 ± 2.4	0.9 ± 0.1	0.8 ± 0.1	6.9	6.9	1.1
	5	46.2 ± 2.2	39.5 ± 7.2	9.7 ± 4.4	1.2 ± 0.9	1.2 ± 0.8	4.1	8.1	1.0
	10	48.0 ± 3.8	28.2 ± 7.3	17.9 ± 6.9	1.5 ± 0.8	2.6 ± 1.3	1.6	11.9	0.6
B	3	44.8 ± 0.9	45.4 ± 1.4	7.4 ± 3.4	0.7 ± 0.3	0.8 ± 0.3	6.1	10.6	0.9
	5	45.5 ± 2.5	40.1 ± 7.4	11.3 ± 5.6	1.0 ± 0.6	1.5 ± 0.4	3.5	11.3	0.7
	10	47.5 ± 2.3	29.1 ± 9.7	18.7 ± 8.3	1.6 ± 0.9	2.3 ± 0.5	1.6	11.7	0.7
Theoretical In:S ratio		44	43	10	3	0		10:3	

A significant factor observed from the EDS analyses, was that the best photovoltaic performance corresponded to electrodes where the In:S ratio is 10:1, lower S quantity than the theoretical ratio 10:3 (~3.3) during the In:S synthesis (Table 4.6).[52] The latter sulfur deficient In_xS_y shell formation was also observed by Barreau *et. al*. applying a chemical bath deposition method (CBD).[60] They compared two synthesis methods for In_2S_3 film preparation, chemical bath deposition (CBD) and physical vapor deposition (PVD), and found out higher film crystallinity for the PVD synthesis and lower oxygen and hydroxyl contamination than for the CBD. These reported results agree with our In_xS_y shell layer, we obtained an amorphous shell layer with deficient sulfur content than the theoretical expected data (Table 4.6). Moreover, the concentration of the oxygen was maintained almost constant or slightly increased when the number of SILAR cycles increased that is probably due to the oxygen or hydroxyl contamination mentioned in the Barreau *et. al*. paper.[60] Nevertheless, and as explained in section 4.3.1., this is not the stoichiometry In:S ratio of 2:3 expected for the formation of In_2S_3.

The synthesis formation of the In_2S_3 can be described as in equation 4.4.

$$2\ InCl_3 + 3\ Na_2S \longrightarrow In_2S_3 + 6\ NaCl \qquad (4.4)$$

For an In:S ratio of 2:3, a 0.1 M concentration of $InCl_3$ is used, together with a Na_2S concentration of 0.15 M.

EDS analyses of the SILAR reaction applying concentrations of 0.1 M $InCl_3$ and 0.15 M Na_2S solutions were performed on the electrode A. The electrodes presented now an In:S ratio between 0.6-0.9 that corresponds with the In_2S_3 semiconductor (theoretical value = 0.7) in Table 4.7. In addition, the ratio between S and Cl is much higher with the concentration 0.15 M of Na_2S, which highlight the difference between S and the residual element of the reaction, Cl. The oxygen in these samples was maintained at the same values indicating a less oxygen contamination of the In_xS_y shell layer.

Table 4.7 EDS results of tested core-shell electrodes A with 3, 5 and 10 cycles using concentrations of 0.1 M and 0.15M for $InCl_3$ and Na_2S solutions respectively.

ZnO electrode	SILAR cycles	O (% at)	Zn (% at)	In (% at)	S (% at)	Cl (% at)	Ratio		
							Zn:In	In:S	S:Cl
	3	31.5	38.7	4.0	4.7	0.4	9.7	0.8	11.8
A	5	31.6	41.1	4.6	7.74	0.4	8.9	0.6	19.4
	10	29.5	38.3	6.2	6.52	0.2	6.2	0.9	32.6
Theoretical In:S ratio		45	45	4	6	0		2:3	

In order to investigate the oxygen content on the In_xS_y shell layer, infrared ATR-FT-IR analyses were carried out on electrode B with ZnO NR and core-shell ZnO/In_xS_y NR applying the two concentrations of Na_2S (In_xS_y shell layer freshly prepared samples). The FT-IR spectra are shown in Figure 4.13, and the corresponding peak assignment for these 3 samples is presented in Table 4.8. A broad an asymmetric band at 3429 cm^{-1}, assigned to the stretching vibration hydroxyl O-H, is observed in the IR spectrum of the core-shell ZnO/In_xS_y NR obtained by the low Na_2S concentration of 0.03 M. The other samples, the ZnO NRs and the core-shell ZnO/In_xS_y NR (0.15 M of Na_2S) also present this peak but in lower intensity. The latter is probably due to the formation of $In(OH)_3$ shell layer when low Na_2S concentration was applied. These results explain the low sulfur content and the increase of oxygen content when the number of SILAR cycles increase (Table 4.6).

In general, the application of high Na_2S concentration during synthesis permits the formation of the In_xS_y shell layer with a In:S ratio of 2:3, Table 4.7. This stoichiometric ratio of In:S explains the low concentration of hydroxyl groups if compared to the rest of the samples. Two other peaks attributed to the O-H bending modes at ~1560 cm^{-1} and ~1428 cm^{-1} were observed for the three samples and the intensities observed correlate well with the intensity of the respective 3429 cm^{-1} band. This variety of O-H bending modes at the IR region between 1300 and 1650 cm^{-1} is in well correspondence to those observed for a bare ZnO film.[61] The peak at 2644 cm^{-1} corresponds to the thiol S-H vibration mode and was observed on both core-shell ZnO/In_xS_y NR samples. The IR bands at 1124 and 1051 cm^{-1} only present in the core-shell ZnO/In_xS_y NR (0.03 M of Na_2S) are assigned to the In-OH deformation modes as was reported before when $In(OH)_3$ was prepared.[62, 63] The IR region from ~900 to ~660 cm^{-1} is assigned to the Zn-O bond,[64] whose peaks were the same for the 3 samples.

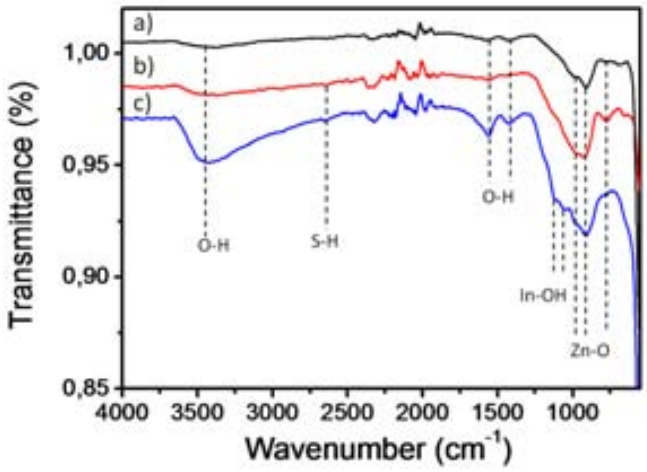

Figure 4.13 ATR-FTIR of a) ZnO NRs, b) core-shell ZnO/In_xS_y NR applying high Na_2S concentration- 5 cycles and c) core-shell ZnO/In_xS_y NR applying low Na_2S concentration- 5 cycles.

Table 4.8 ATR-FTIR data for the ZnO NRs, and both core-shell ZnO/In_xS_y NR (5 SILAR cycles) applying a 0.15 M and 0.03 M concentration of Na_2S and the band assignment.

IR band (cm^{-1})			IR band assignment
ZnO NRs	**ZnO/In_xS_y (0.15M) NR Core-shell**	**ZnO/In_xS_y (0.03M) NR Core-shell**	
3429	3429	3429	O-H stretching
	2663	2664	S-H stretching
1567	1555	1560	O-H bending
1414	1441	1428	O-H bending
		1124	In-OH
		1051	In-OH
986	985	979	Zn-O
909	926	913	Zn-O
777	774	774	Zn-O
691	662		Zn-O

Comparison of the FTIR analyses of the freshly prepared and the 3-day aged in air core-shell ZnO/In_xS_y NR electrodes (obtained with the Na_2S concentration) is presented in Figure 4.14. Both samples show similar peaks: similar band and intensity of the O-H band at ~3410 cm^{-1}. For the wavelength peaks at ~980 and ~910 cm^{-1} a decrease in peak intensity was observed, and new peaks appeared at 1242, 865 and 834 cm^{-1} , attributed to the ZnO degradation. These results indicate that the degradation of the core-shell ZnO/In_xS_y NR after 3 days exposure to air is related to an increase in the hydroxide concentration and sample hydration. Unfortunately, these new –OH sites are not linked to any Dye molecule and thus, it could be the reason of the decrease in power conversion efficiency when applied in a DSC, as indicated in section 4.3.1.

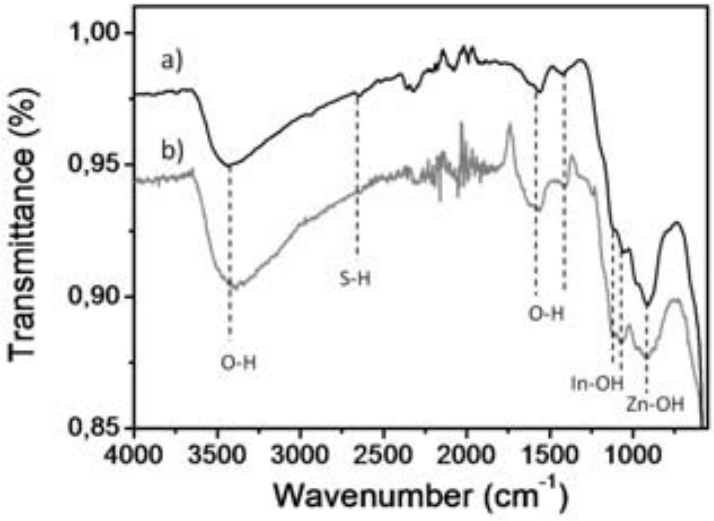

Figure 4.14 ATR-FTIR of core-shell ZnO/In_2S_3 NR (0.03 M of Na_2S and 10 SILAR cycles) a) freshly prepared and b) after 3 days kept in air for electrode B.

All the IR results observed for the samples indicate that a more complex nanomaterial is present as part of the electrode, than a simple ZnO and In_xS_y combination. The clear ZnO degradation, together with the formation of indium hydroxide, $In(OH)_3$, indium hydroxide–sulfide, $In(OH)_xS_y$, or a mixture of both is possible. We rule out the presence of In_2O_3 since the conversion of $In(OH)_3$ to In_2O_3 can only take place after thermal annealing at high temperatures,[62, 65] or after the sample is irradiated by an electron beam (e.g. form a TEM microscope).[66] The quantification of the exact amount of each compound is, however, rather difficult due to the thickness of the shell layer which is only of a few nm.[60]

4.3.4 Proposed working mechanism behind the core-shell ZnO/In_xS_y NR

Thus as a summary, our results indicate that

a) For the same ZnO NR length and SILAR cycles, the best photovoltaic response, 2.3% efficiency, is observed for low S content on the In:S ratio (10:1) in the shell of the ZnO NRs, followed by the application of the bare ZnO NRs with no core-shell, 0.87 % efficiency. The application of a stoichiometric In_2S_3 shell (2:3 In:S ratio) on the ZnO NRs results in the lowest photovoltaic performance, 0.21 % efficiency.

b) For the low S content (10:1, In:S ratio) the higher presence of -OH and S-H stretching bands in the FTIR spectra, indicates the possible presence of $In(OH)_3$ or indium hydroxide–sulphide, $In(OH)_xS_y$, or the combination of both.

c) The decrease on power conversion efficiency observed on the DSC after 3 day exposure of the electrodes to air is related to an increase in the hydroxides concentration and sample hydration.

The relation between electrode composition and power conversion efficiency of the DSC is represented in the energy band diagram of the DSCs with the different electrodes, as depicted in Figure 4.15 . We represent the three possible scenarios: a) The 2:3 ratio of In:S or the stoichiometry composition, In_2S_3 (obtained with high concentration of Na_2S during synthesis) which results in an electrode composition close to ZnO/In_2S_3, b) The bare ZnO electrode without shell layer, and c) The 10:1 ratio of In:S (obtained with low concentration of Na_2S during synthesis) with a final electrode composition closed to $ZnO/In(OH)_xS_y$ or $ZnO/In(OH)_3$. Table 4.9 shows the photovoltaic parameters observed for DSC applying comparable ZnO electrodes (all grown for 12 h by the same synthesis method). In the case of the shell layer, the synthesis was also made by the same number of SILAR cycles.

Table 4.9 Average DSCs data using the electrode B (12h growth time by LT-HM) from the best 5 cells with bare ZnO NRs and core-shell electrodes (5 cycles, SILAR method 1). 100 $mW \cdot cm^{-2}$ illumination, AM 1.5G. Pt-CE prepared by EBPVD (50 nm).

In:S ratio	Electrode composition	NR length (μm)	V_{oc} (V)	J_{sc} ($mA \cdot cm^{-2}$)	FF (%)	PCE (%)	Max PCE (%)
2:3	ZnO/In_2S_3	-	0.46	0.86	52	0.21	0.21
-	ZnO	3.2 ± 0.5	0.54 ± 0.03	3.59 ± 0.61	41 ± 1	0.80 ± 0.09	0.87
10:3	$ZnO/In(OH)_xS_y$	3.0 ± 0.1	0.64 ± 0.04	5.91 ± 0.49	57 ± 3	2.15 ± 0.12	2.32

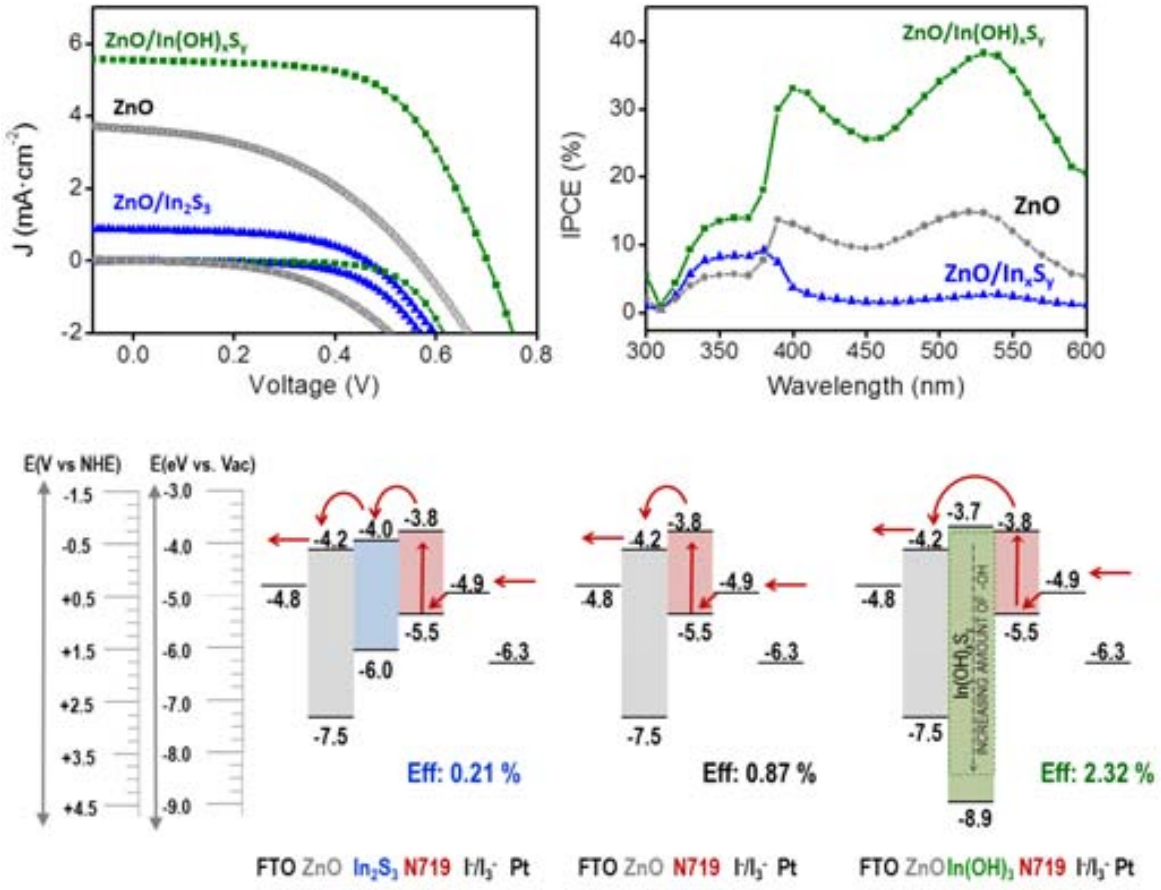

Figure 4.15 Energy diagram for a DSC applying ZnO as electron transport layer and a shell layer of In_2S_3 (left) and In(OH)xSy or $In(OH)_3$ (right). The dye N19 acts as the light harvesting material, an I^-/I_3^- electrolyte as the hole transport layer. Values (eV) vs. Vacuum and vs. NHE (Normal Hydrogen Electrode).

From the energy diagrams in Figure 4.15, we can observe that electron injection from the Dye N719 to any of the inorganic semiconductors (ZnO or In_xS_y, $In(OH)_xS_y$ or $In(OH)_3$), should be possible, since the HOMO level of the dye lies above the valence band (VB) of the inorganic materials (ref:10). The latter is correct since photovoltaic response is observed in all cases. Nevertheless, different recombination processes could be taking place in each electrode and could be the reason of the different power conversion efficiencies obtained.

In the case of the 2:3 ratio of In:S (In_2S_3) synthesized with high concentration of Na_2S, the power conversion efficiency is the lowest, and we ascribe this response to the SILAR synthesis method applied which has been proved to form an outer layer of the inorganic semiconductor (instead of high surface area quantum dots for example), and thus fast

internal recombination and low quantum efficiencies have been observed.[18] Another possibility that can contribute to the low power conversion efficiency is the low amount of –OH sites for the anchoring of the Dye, resulting in poor dye loading and low (but not null) photovoltaic response.

In the case of low concentration of S during synthesis, the formation of the indium hydroxide, $In(OH)_3$, indium hydroxide–sulfide, $In(OH)_xS_y$, or a mixture of both is possible. The band gap of the intermediate indium hydroxide–sulfide, $In(OH)_xS_y$, is located in between the band gap of In_2S_3 at 2.0 eV and the band gap of $In(OH)_3$ at 5.2 eV.[67, 68] The band gap broaden as the amount of sulfur (-S) content decreases and the concentration of hydroxide (–OH) increases.[67-69] A similar response has been observed for $In_2S_{3-3x}O_{3x}$ as reported by Robles[70], et al.: when the oxygen content of In_2S_3 increases, its band gap increases from 2 eV to 2.9 eV. Nevertheless, our FTIR analyses revealed high concentration of –OH, which indicates more probability for the presence of $In(OH)_xS_y$ or/and $In(OH)_3$ than a compound similar to $In_2S_{3-3x}O_{3x}$. In this case a high insulating layer of an inorganic semiconductor is part of the shell of the ZnO NR. The formation of an outer layer of an insulating oxide in between the ZnO and the Dye is a strategy already used to improve power conversion efficiency in DSCs. Coating of the oxide electrode with oxides such as Al_2O_3, Nb_2O_5, SnO_2, ZrO_2 or SiO_2 among others,[71-74] is known to improve dye adsorption and increase the sensitized photocurrent. The V_{oc} and the FF are observed to be strongly improved[71-74] just as observed for our DSC (see Figure 4.15, and Table 4.6). The shell layer must be of a few nm thick and present a wide band gap. All these characteristics are present in the shell layer synthesized in our work, where a thickness between 3-50 nm (depending on the SILAR cycles), is obtained for the shell layer, and a wide band gap above 5 eV is known for $In(OH)_xS_y$ and for $In(OH)_3$ (see Figure 4.15). Thus, the good power conversion efficiency could probably be ascribed to the inhibition of the electron back transfer from the oxide to the redox electrolyte by the insulating oxide.[62, 75] Finally, the presence of higher amount of hydroxide groups, which facilitate dye attachment through its carboxylic acid group, could also enhance power conversion efficiency by increasing the linking sites available for the attachment of the Dye.

4.4 Conclusions

Vertically-aligned core-shell ZnO/In_xS_y NR electrodes were prepared by the SILAR method and applied in DSCs. The electrodes were fully characterized by SEM, TEM, DRX, EDS and FT-IR. Six different core-shell electrodes were prepared: A (6h, LT-HM), B (12h, LT-HM), C (22h, LT-HM), D (6h, A-HM), E (12h, A-HM) and F (28h, A-HM). The In_xS_y shell layer was obtained applying two different concentrations of Na_2S (0.03 M and 0.15 M), maintaining the $InCl_3$ at a constant concentration of 0.1 M. The best DSCs results were obtained applying low concentration of Na_2S with an In:S ratio of ~10:1, which was sulphur deficient (theoretical ratio of 10:3). EDX and FTIR analyses of the electrodes confirmed the sulphur-deficient shell layer, as well as a high –OH content of the shell layer, probably due to the formation of $In(OH)_xS_y$ or/and $In(OH)_3$. The presence of high amount of –OH can probably enhance power conversion efficiency by increasing the sites for dye attachment, increasing the dye-loading capacity of the core-shell ZnO/In_xS_y NR electrodes. The presence of $In(OH)_xS_y$ or/and $In(OH)_3$ shell layer can act as an electron blocking layer improving the DSC performance. An enhanced efficiency of 2.32% was achieved with the core-shell ZnO/In_xS_y NR electrode B (3.0 μm NRs length, 5 SILAR cycles and 6h of immersion dye-loading time).

4.5 References

1. A. Kay and M. Gratzel, "Dye-sensitized core-shell nanocrystals: Improved efficiency of mesoporous tin oxide electrodes coated with a thin layer of an insulating oxide". *Chemistry of Materials* **2002,** 14 (7), 2930-2935.
2. T.-C. Tien, F.-M. Pan, L.-P. Wang, F.-Y. Tsai and C. Lin, "Coverage Analysis for the Core/Shell Electrode of Dye-Sensitized Solar Cells". *Journal of Physical Chemistry C* **2010,** 114 (21), 10048-10053.
3. N. G. Park, M. G. Kang, K. M. Kim, K. S. Ryu, S. H. Chang, D. K. Kim, J. van de Lagemaat, K. D. Benkstein and A. J. Frank, "Morphological and photoelectrochemical characterization of core-shell nanoparticle films for dye-sensitized solar cells: Zn-O type shell on SnO2 and TiO2 cores". *Langmuir* **2004,** 20 (10), 4246-4253.
4. M. Law, L. E. Greene, A. Radenovic, T. Kuykendall, J. Liphardt and P. D. Yang, "ZnO-Al2O3 and ZnO-TiO2 core-shell nanowire dye-sensitized solar cells". *Journal of Physical Chemistry B* **2006,** 110 (45), 22652-22663.
5. M. Wang, C. Huang, Y. Cao, Q. Yu, W. Guo, Q. Liu, J. Liang and M. Hong, "A plasma sputtering decoration route to producing thickness-tunable ZnO/TiO(2) core/shell nanorod arrays". *Nanotechnology* **2009,** 20 (28).
6. N. O. V. Plank, H. J. Snaith, C. Ducati, J. S. Bendall, L. Schmidt-Mende and M. E. Welland, "A simple low temperature synthesis route for ZnO-MgO core-shell nanowires". *Nanotechnology* **2008,** 19 (46).

7. M. Seol, H. Kim, Y. Tak and K. Yong, "Novel nanowire array based highly efficient quantum dot sensitized solar cell". *Chemical Communications* **2010,** 46 (30), 5521-5523.
8. S. Buhbut, S. Itzhakov, E. Tauber, M. Shalom, I. Hod, T. Geiger, Y. Garini, D. Oron and A. Zaban, "Built-in Quantum Dot Antennas in Dye-Sensitized Solar Cells". *Acs Nano* **2010,** 4 (3), 1293-1298.
9. M. Liberatore, L. Burtone, T. M. Brown, A. Reale, A. Di Carlo, F. Decker, S. Caramori and C. A. Bignozzi, "On the effect of Al2O3 blocking layer on the performance of dye solar cells with cobalt based electrolytes". *Applied Physics Letters* **2009,** 94 (17).
10. I. Mora-Sero, D. Gross, T. Mittereder, A. A. Lutich, A. S. Susha, T. Dittrich, A. Belaidi, R. Caballero, F. Langa, J. Bisquert and A. L. Rogach, "Nanoscale Interaction Between CdSe or CdTe Nanocrystals and Molecular Dyes Fostering or Hindering Directional Charge Separation". *Small* **2010,** 6 (2), 221-225.
11. Z. Yang, C.-Y. Chen, P. Roy and H.-T. Chang, "Quantum dot-sensitized solar cells incorporating nanomaterials". *Chemical Communications* **2011,** 47 (34), 9561-9571.
12. V. Aroutiounian, S. Petrosyan, A. Khachatryan and K. Touryan, "Quantum dot solar cells". *Journal of Applied Physics* **2001,** 89 (4).
13. A. J. Nozik, "Quantum dot solar cells". *Physica E-Low-Dimensional Systems & Nanostructures* **2002,** 14 (1-2), 115-120.
14. C.-Z. Yao, B.-H. Wei, L.-X. Meng, H. Li, Q.-J. Gong, H. Sun, H.-X. Ma and X.-H. Hu, "Controllable electrochemical synthesis and photovoltaic performance of ZnO/CdS core-shell nanorod arrays on fluorine-doped tin oxide". *Journal of Power Sources* **2012,** 207, 222-228.
15. K. Becker, J. M. Lupton, J. Mueller, A. L. Rogach, D. V. Talapin, H. Weller and J. Feldmann, "Electrical control of Forster energy transfer". *Nature Materials* **2006,** 5 (10), 777-781.
16. J. Xu, X. Yang, Q.-D. Yang, T.-L. Wong, S.-T. Lee, W.-J. Zhang and C.-S. Lee, "Arrays of CdSe sensitized ZnO/ZnSe nanocables for efficient solar cells with high open-circuit voltage". *Journal of Materials Chemistry* **2012,** 22 (26), 13374-13379.
17. A. M. Funston, J. J. Jasieniak and P. Mulvaney, "Complete Quenching of CdSe Nanocrystal Photoluminescence by Single Dye Molecules". *Advanced Materials* **2008,** 20 (22), 4274-4280.
18. S. Gimenez, A. L. Rogach, A. A. Lutich, D. Gross, A. Poeschl, A. S. Susha, I. Mora-Sero, T. Lana-Villarreal and J. Bisquert, "Energy transfer versus charge separation in hybrid systems of semiconductor quantum dots and Ru-dyes as potential co-sensitizers of TiO2-based solar cells". *Journal of Applied Physics* **2011,** 110 (1).
19. M. Sykora, M. A. Petruska, J. Alstrum-Acevedo, I. Bezel, T. J. Meyer and V. I. Klimov, "Photoinduced charge transfer between CdSe nanocrystal quantum dots and Ru-polypyridine complexes". *Journal of the American Chemical Society* **2006,** 128 (31), 9984-9985.
20. S. N. Sharma, Z. S. Pillai and P. V. Kamat, "Photoinduced charge transfer between CdSe quantum dots and p-phenylenediamine". *Journal of Physical Chemistry B* **2003,** 107 (37), 10088-10093.
21. J. Huang, D. Stockwell, Z. Huang, D. L. Mohler and T. Lian, "Photoinduced ultrafast electron transfer from CdSe quantum dots to re-bipyridyl complexes". *Journal of the American Chemical Society* **2008,** 130 (17), 5632-+.
22. I. Hod, V. Gonzalez-Pedro, Z. Tachan, F. Fabregat-Santiago, I. Mora-Sero, J. Bisquert and A. Zaban, "Dye versus Quantum Dots in Sensitized Solar Cells: Participation of Quantum Dot Absorber in the Recombination Process". *Journal of Physical Chemistry Letters* **2011,** 2 (24), 3032-3035.
23. N. O. V. Plank, I. Howard, A. Rao, M. W. B. Wilson, C. Ducati, R. S. Mane, J. S. Bendall, R. R. M. Louca, N. C. Greenham, H. Miura, R. H. Friend, H. J. Snaith and M. E. Welland, "Efficient ZnO Nanowire Solid-State Dye-Sensitized Solar Cells Using Organic Dyes and Core-shell Nanostructures". *Journal of Physical Chemistry C* **2009,** 113 (43), 18515-18522.
24. Z. H. Chen, Y. B. Tang, C. P. Liu, Y. H. Leung, G. D. Yuan, L. M. Chen, Y. Q. Wang, I. Bello, J. A. Zapien, W. J. Zhang, C. S. Lee and S. T. Lee, "Vertically Aligned ZnO Nanorod Arrays Sentisized with Gold Nanoparticles for Schottky Barrier Photovoltaic Cells". *Journal of Physical Chemistry C* **2009,** 113 (30), 13433-13437.

25. X. L. Yu, J. G. Song, Y. S. Fu, Y. Xie, X. Song, J. Sun and X. W. Du, "ZnS/ZnO Heteronanostructure as Photoanode to Enhance the Conversion Efficiency of Dye-Sensitized Solar Cells". *Journal of Physical Chemistry C* **2010,** 114 (5), 2380-2384.
26. X. Song, X. L. Yu, Y. Xie, J. Sun, T. Ling and X. W. Du, "Improving charge separation of solar cells by the co-sensitization of CdS quantum dots and dye". *Semiconductor Science and Technology* **2010,** 25 (9), 095014.
27. C. J. Raj, S. N. Karthick, K. V. Hemalatha, M.-K. Son, H.-J. Kim and K. Prabakar, "Magnesium doped ZnO nanoparticles embedded ZnO nanorod hybrid electrodes for dye sensitized solar cells". *Journal of Sol-Gel Science and Technology* **2012,** 62 (3), 453-459.
28. X. Y. Gan, X. M. Li, X. D. Gao, F. W. Zhuge and W. D. Yu, "ZnO nanowire/TiO2 nanoparticle photoanodes prepared by the ultrasonic irradiation assisted dip-coating method". *Thin Solid Films* **2010,** 518 (17), 4809-4812.
29. S. Sarkar, A. Makhal, K. Lakshman, T. Bora, J. Dutta and S. K. Pal, "Dual-Sensitization via Electron and Energy Harvesting in CdTe Quantum Dots Decorated ZnO Nanorod-Based Dye-Sensitized Solar Cells". *Journal of Physical Chemistry C* **2012,** 116 (27), 14248-14256.
30. A. Irannejad, K. Janghorban, O. K. Tan, H. Huang, C. K. Lim, P. Y. Tan, X. Fang, C. S. Chua, S. Maleksaeedi, S. M. H. Hejazi, M. M. Shahjamali and M. Ghaffari, "Effect of the TiO(2) shell thickness on the dye-sensitized solar cells with ZnO-TiO(2) core-shell nanorod electrodes". *Electrochimica Acta* **2011,** 58, 19-24.
31. D. K. P. Wong, C. H. Ku, Y. R. Chen, G. R. Chen and J. J. Wu, "Enhancing Electron Collection Efficiency and Effective Diffusion Length in Dye-Sensitized Solar Cells". *Chemphyschem* **2009,** 10 (15), 2698-2702.
32. L. Liu, Y. Chen, T. Guo, Y. Zhu, Y. Su, C. Jia, M. Wei and Y. Cheng, "Chemical Conversion Synthesis of ZnS Shell on ZnO Nanowire Arrays: Morphology Evolution and Its Effect on Dye-Sensitized Solar Cell". *Acs Applied Materials & Interfaces* **2012,** 4 (1), 17-23.
33. J. Chung, J. Myoung, J. Oh and S. Lim, "Successive ionic layer adsorption and reaction of ZnSe shells for ZnO nanowire-based dye-sensitized solar cells". *Journal of Physics and Chemistry of Solids* **2012,** 73 (4), 535-539.
34. J. Chung, J. Myoung, J. Oh and S. Lim, "Synthesis of a ZnS Shell on the ZnO Nanowire and Its Effect on the Nanowire-Based Dye-Sensitized Solar Cells". *Journal of Physical Chemistry C* **2010,** 114 (49), 21360-21365.
35. C. H. Ku and J. J. Wu, "Chemical bath deposition of ZnO nanowire-nanoparticle composite electrodes for use in dye-sensitized solar cells". *Nanotechnology* **2007,** 18 (50), 505706.
36. L.-Y. Lin, M.-H. Yeh, C.-P. Lee, C.-Y. Chou, R. Vittal and K.-C. Ho, "Enhanced performance of a flexible dye-sensitized solar cell with a composite semiconductor film of ZnO nanorods and ZnO nanoparticles". *Electrochimica Acta* **2012,** 62, 341-347.
37. C. Y. Jiang, X. W. Sun, K. W. Tan, G. Q. Lo, A. K. K. Kyaw and D. L. Kwong, "High-bendability flexible dye-sensitized solar cell with a nanoparticle-modified ZnO-nanowire electrode". *Applied Physics Letters* **2008,** 92 (14), 143101.
38. J. S. Bendall, L. Etgar, S. C. Tan, N. Cai, P. Wang, S. M. Zakeeruddin, M. Graetzel and M. E. Welland, "An efficient DSSC based on ZnO nanowire photo-anodes and a new D-pi-A organic dye". *Energy & Environmental Science* **2011,** 4 (8), 2903-2908.
39. Y. Feng, X. Ji, J. Duan, J. Zhu, J. Jiang, H. Ding, G. Meng, R. Ding, J. Liu, A. Hu and X. Huang, "Synthesis of ZnO@TiO2 core-shell long nanowire arrays and their application on dye-sensitized solar cells". *Journal of Solid State Chemistry* **2012,** 190, 303-308.
40. C. Xu, J. Wu, U. V. Desai and D. Gao, "High-Efficiency Solid-State Dye-Sensitized Solar Cells Based on TiO2-Coated ZnO Nanowire Arrays". *Nano Letters* **2012,** 12 (5), 2420-2424.
41. M. Wang, C. Huang, Y. Cao, Q. Yu, W. Guo, Q. Huang, Y. Liu, Z. Huang, J. Huang, H. Wang and Z. Deng, "The effects of shell characteristics on the current-voltage behaviors of dye-sensitized solar cells based on ZnO/TiO(2) core/shell arrays". *Applied Physics Letters* **2009,** 94 (26).
42. X. Gan, X. Li, X. Gao, J. Qiu and F. Zhuge, "TiO(2) nanorod arrays functionalized with In(2)S(3) shell layer by a low-cost route for solar energy conversion". *Nanotechnology* **2011,** 22 (30).
43. N. Revathi, P. Prathap and K. T. R. Reddy, "Thickness dependent physical properties of close space evaporated In2S3 films". *Solid State Sciences* **2009,** 11 (7), 1288-1296.

44. P. M. R. Kumar, T. T. John, C. S. Kartha, K. P. Vijayakumar, T. Abe and Y. Kashiwaba, "Effects of thickness and post deposition annealing on the properties of evaporated In2S3 thin films". *Journal of Materials Science* **2006,** 41 (17), 5519-5525.
45. T. Dittrich, D. Kieven, M. Rusu, A. Belaidi, J. Tornow, K. Schwarzburg and M. Lux-Steiner, "Current-voltage characteristics and transport mechanism of solar cells based on ZnO nanorods/In2S3/CuSCN". *Applied Physics Letters* **2008,** 93 (5).
46. S. K. Sarkar, J. Y. Kim, D. N. Goldstein, N. R. Neale, K. Zhu, C. M. Elliot, A. J. Frank and S. M. George, "In(2)S(3) Atomic Layer Deposition and Its Application as a Sensitizer on TiO(2) Nanotube Arrays for Solar Energy Conversion". *Journal of Physical Chemistry C* **2010,** 114 (17), 8032-8039.
47. W. Lee, S.-K. Min, G. Cai, R. S. Mane, T. Ganesh, G. Koo, J. Chang, S.-J. Baek, S.-H. Lee and S.-H. Han, "Polymer-sensitized photoelectrochemical solar cells based on water-soluble polyacetylene and beta-In(2)S(3) nanorods". *Electrochimica Acta* **2008,** 54 (2), 714-719.
48. D. Kieven, T. Dittrich, A. Belaidi, J. Tornow, K. Schwarzburg, N. Allsop and M. Lux-Steiner, "Effect of internal surface area on the performance of ZnO/In2S3/CuSCN solar cells with extremely thin absorber". *Applied Physics Letters* **2008,** 92 (15).
49. T. Dittrich, D. Kieven, A. Belaidi, M. Rusu, J. Tornow, K. Schwarzburg and M. C. Lux-Steiner, "Formation of the charge selective contact in solar cells with extremely thin absorber based on ZnO-nanorod/In2S3/CuSCN". *Journal of Applied Physics* **2009,** 105 (3).
50. J. Tornow, K. Schwarzburg, A. Belaidi, T. Dittrich, M. Kunst and T. Hannappel, "Charge separation and recombination in radial ZnO/In2S3/CuSCN heterojunction structures". *Journal of Applied Physics* **2010,** 108 (4).
51. N. Naghavi, R. Henriquez, V. Laptev and D. Lincot, "Growth studies and characterisation of IN2S3 thin films deposited by atomic layer deposition (ALD)". *Applied Surface Science* **2004,** 222 (1-4), 65-73.
52. C. Herzog, A. Belaidi, A. Ogacho and T. Dittrich, "Inorganic solid state solar cell with ultra-thin nanocomposite absorber based on nanoporous TiO(2) and In(2)S(3)". *Energy & Environmental Science* **2009,** 2 (9), 962-964.
53. Y. F. Nicolau and J. C. Menard, "SOLUTION GROWTH OF ZNS, CDS AND ZN1-XCDXS THIN-FILMS BY THE SUCCESSIVE IONIC-LAYER ADSORPTION AND REACTION PROCESS - GROWTH-MECHANISM". *Journal of Crystal Growth* **1988,** 92 (1-2), 128-142.
54. I. Gonzalez-Valls and M. Lira-Cantu, "Dye sensitized solar cells based on vertically-aligned ZnO nanorods: effect of UV light on power conversion efficiency and lifetime". *Energy & Environmental Science* **2010,** 3 (6), 789-795.
55. I. Gonzalez-Valls, Y. H. Yu, B. Ballesteros, J. Oro and M. Lira-Cantu, "Synthesis conditions, light intensity and temperature effect on the performance of ZnO nanorods-based dye sensitized solar cells". *Journal of Power Sources* **2011,** 196 (15), 6609-6621.
56. I. Gonzalez-Valls, J. S. Reparaz, F. Güell, M. R. Wagner, G. Callsen, B. Ballesteros, A. Hoffmann and M. Lira-Cantu, "Low temperature growth of vertically-aligned ZnO nanorods for dye sensitized solar cells: unravelling their low power conversion efficiency". *Nano Letters* **2012**, submitted.
57. I. Gonzalez-Valls, B. Ballesteros and M. Lira-Cantu, "Innovative vertically-aligned ZnO Nanorods – Indium sulfide core-shell with enhanced performance in Dye-sensitized Solar Cells". **2012,** In preparation.
58. N. A. Allsop, A. Schoenmann, A. Belaidi, H. J. Muffler, B. Mertesacker, W. Bohne, E. Strub, J. Roehrich, M. C. Lux-Steiner and C. H. Fischer, "Indium sulfide thin films deposited by the spray ion layer gas reaction technique". *Thin Solid Films* **2006,** 513 (1-2), 52-56.
59. N. Barreau, "Indium sulfide and relatives in the world of photovoltaics". *Solar Energy* **2009,** 83 (3), 363-371.
60. N. Barreau, J. C. Bernede, H. El Maliki, S. Marsillac, X. Castel and J. Pinel, "Recent studies on In2S3 containing oxygen thin films". *Solid State Communications* **2002,** 122 (7-8), 445-450.
61. B. M. Keyes, L. M. Gedvilas, X. Li and T. J. Coutts, "Infrared spectroscopy of polycrystalline ZnO and ZnO : N thin films". *Journal of Crystal Growth* **2005,** 281 (2-4), 297-302.

62. C. Shifu, Y. Xiaoling, Z. Huaye and L. Wei, "Preparation, characterization and activity evaluation of heterostructure In(2)O(3)/In(OH)(3) photocatalyst". *Journal of hazardous materials* **2010,** 180 (1-3), 735-40.
63. S. K. Poznyak and A. I. Kulak, "Characterization and photoelectrochemical properties of nanocrystalline In2O3 film electrodes". *Electrochimica Acta* **2000,** 45 (10), 1595-1605.
64. A. Umar, M. S. Akhtar, S. H. Kim, A. Al-Hajry, M. S. Chauhan and S. Chauhan, "Growth, Properties and Dye-Sensitized Solar Cells (DSSCs) Applications of ZnO Nanocones and Small Nanorods". *Science of Advanced Materials* **2011,** 3 (5), 695-701.
65. H. Zhu, X. Wang, Z. Wang, C. Yang, F. Yang and X. Yang, "Self-assembled 3D microflowery In(OH)(3) architecture and its conversion to In2O3". *Journal of Physical Chemistry C* **2008,** 112 (39), 15285-15292.
66. G. Miehe, S. Lauterbach, H.-J. Kleebe and A. Gurlo, "Indium hydroxide to oxide decomposition observed in one nanocrystal during in situ transmission electron microscopy studies". *Journal of Solid State Chemistry* **2013,** 198, 364-370.
67. R. Bayon, R. Musembi, A. Belaidi, M. Bar, T. Guminskaya, M. C. Lux-Steiner and T. Dittrich, "Highly structured TiO2/In(OH)(x)S-y/PbS/PEDOT : PSS for photovoltaic applications". *Solar Energy Materials and Solar Cells* **2005,** 89 (1), 13-25.
68. S. Chen, X. Yu, H. Zhang and W. Liu, "Preparation, characterization and activity evaluation of heterostructure In2O3/In(OH)(3) photocatalyst". *Journal of Hazardous Materials* **2010,** 180 (1-3), 735-740.
69. S. Avivi, Y. Mastai and A. Gedanken, "Sonohydrolysis of In3+ ions: Formation of needlelike particles of indium hydroxide". *Chemistry of Materials* **2000,** 12 (5), 1229-1233.
70. R. Robles, N. Barreau, A. Vega, S. Marsillac, J. C. Bernede and A. Mokrani, "Optical properties of large band gap beta-In2S3-3xO3x compounds obtained by physical vapour deposition". *Optical Materials* **2005,** 27 (4), 647-653.
71. E. Palomares, J. N. Clifford, S. A. Haque, T. Lutz and J. R. Durrant, "Slow charge recombination in dye-sensitised solar cells (DSSC) using Al2O3 coated nanoporous TiO2 films". *Chemical Communications* **2002,** (14), 1464-1465.
72. E. Palomares, J. N. Clifford, S. A. Haque, T. Lutz and J. R. Durrant, "Control of charge recombination dynamics in dye sensitized solar cells by the use of conformally deposited metal oxide blocking layers". *Journal of the American Chemical Society* **2003,** 125 (2), 475-482.
73. G. R. A. Kumara, A. Konno and K. Tennakone, "Photoelectrochemical cells made from SnO2/ZnO films sensitized with eosin dyes". *Chemistry Letters* **2001,** (2), 180-181.
74. H. J. Snaith and C. Ducati, "SnO2-Based Dye-Sensitized Hybrid Solar Cells Exhibiting Near Unity Absorbed Photon-to-Electron Conversion Efficiency". *Nano Letters* **2010,** 10 (4), 1259-1265.
75. K. Hara, K. Sayama and H. Arakawa, "Semiconductor-sensitized solar cells based on nanocrystalline In2S3/In2O3 thin film electrodes". *Solar Energy Materials and Solar Cells* **2000,** 62 (4), 441-447.

Chapter 5
Polymer Solar Cells
With ZnO nanostructures

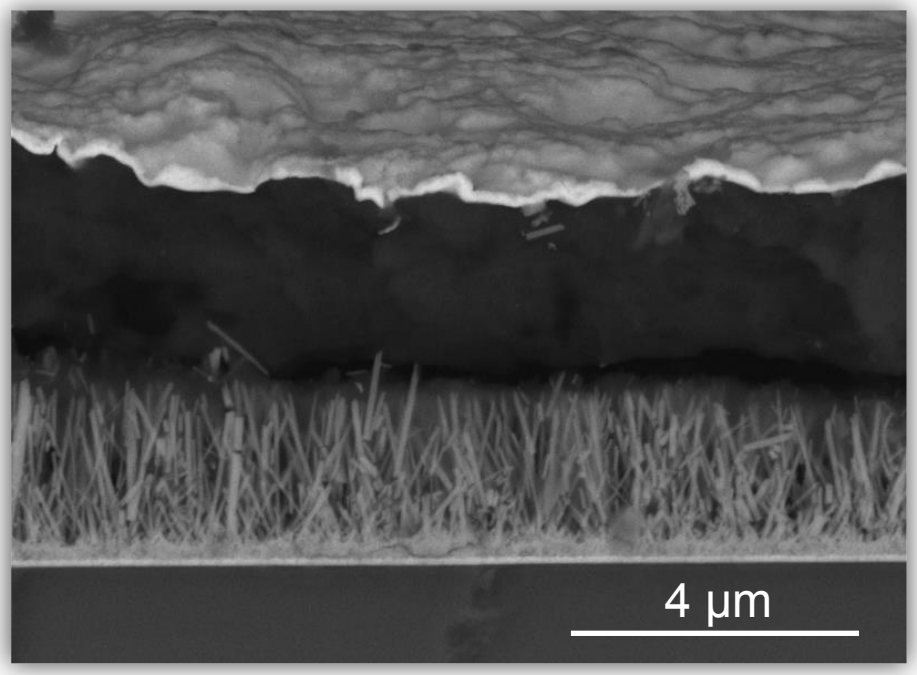

Chapter 5

Polymer solar cells with ZnO nanostructures

5.1 Introduction

Organic solar cells (OSC) or also known as polymer solar cells (PSC) are promising devices characterized by their flexibility and low-cost production, with power conversion efficiencies reaching now the 11%.[1] The application of organic materials with high optical absorption coefficients permits their fabrication as thin films and compatible with flexible plastic substrates. Furthermore, PSCs can be fabricated in large area and scalable production techniques such as the roll-to-roll process.[2-4] The active layer of the PSCs consist of a mixture of a donor material, normally a polymer such as P3HT and an acceptor material, a soluble form of fullerene (C_{60} derivative, such as PCBM).[5] Both organic materials are interconnected together in a bulk heterojunction (BHJ) layer to enhance the exciton dissociation formed at the interface. Since organic materials have short exciton lifetime and low mobility, the use of the BHJ allows a layer thickness increase from 20 nm for a bi-layer structure to 100-200 nm.[5-9] However, thicker organic layers would increase the light absorption and the device efficiency. Nevertheless, thicker active layers results in higher series resistance and electron recombination.[10] An innovative strategy to increase the active layer thickness is the application of new nanostructured oxides characterized by their good electron extracting properties. An optimized semiconductor oxide interface can enhance the charge generation and the electron transport while reducing the recombination processes within the BHJ layer.[11, 12] One attractive semiconductor oxide is ZnO and especially the vertically-aligned ZnO nanorods (NR). These nanostructures exhibit direct electron pathways, high electron mobility[13] and can be prepared by low cost fabrication techniques[14] and they are air stable nanostructures.[15] Another advantage is their longer photoinduced polaron lifetimes compared to PCBM.[8, 16, 17] Moreover, vertically-aligned ZnO NRs are well known to increase the interfacial area and to avoid the incomplete exciton dissociation observed in the BHJ layer due to isolation of the active materials.[18] ZnO NR electrodes with high surface-area-to-volume ratio are valuable nanostructures to enhance the charge generation and charge extraction in PSCs.

In this chapter, we apply vertically aligned ZnO NRs as the electron transport layer (ETL) in PSCs with P3HT:PCBM as the active layer in an inverted configuration of the type:

FTO/ZnONRs/P3HT:PCBM/PEDOT:PSS/Ag. Figure 5.1 shows a schematic representation (a) and the band energy diagram for the PSCs prepared in this chapter (b). When the polymer P3HT absorbs photons from the light, the exciton electron-hole occurs at the P3HT:PCBM ZnO interface. The charge separation takes places when the electrons flow to the PCBM followed by ZnO and then to the TCO electrode, while the holes formed in the P3HT instantly move to the PEDOT:PSS layer and Ag electrode.[19] In this configuration, the PEDOT:PSS act as the hole transport layer (HTL). The ZnO NR electrodes applied in this chapter were prepared by two similar synthesis techniques, the low temperature hydrothermal method (LT-HM described in chapter 2)[20, 21] and the autoclave hydrothermal method (A-HM described in chapter 3).[22] The main difference between them is the pressure imposed throughout the synthesis of the ZnO NRs when the autoclave method is applied. The application of these two synthesis permits the preparation of ZnO NRs with different electrode morphologies, surface areas and optical quality (surface defects).[18-20] ZnO NRs with lengths between 400 nm and 5 μm were chosen to carry out the photovoltaic studies presented in this chapter. These two types of ZnO NRs were also modified with an outside layer of In_xS_y, resulting in core-shell ZnO/In_xS_y NRs. These nanostructures were also analyzed in PSCs.

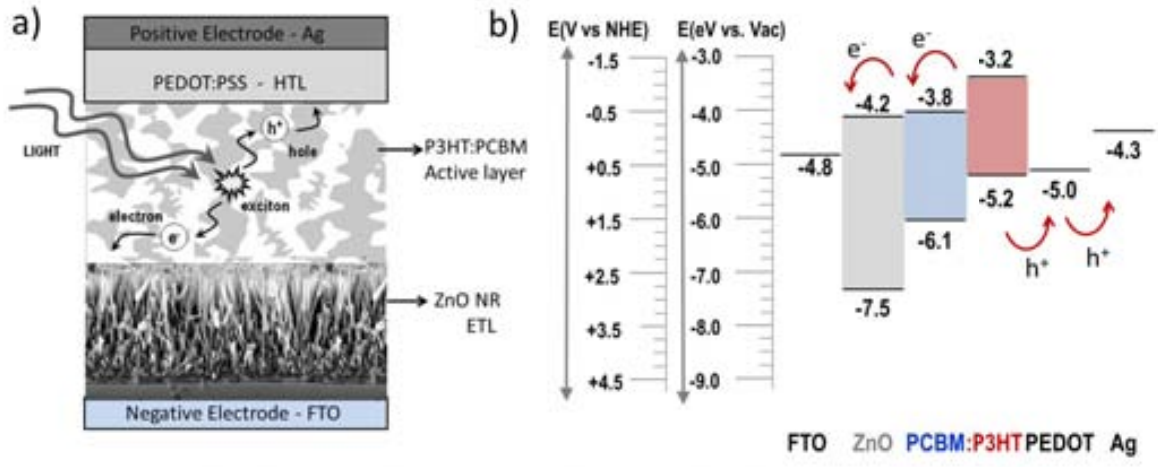

Figure 5.1 a) Schematic representation of a PSC with ZnO NRs and b) the band energy diagram vs. vacuum and vs. NHE (Normal Hydrogen Electrode) of the same PSC.[23, 24]

The application of vertically-aligned ZnO NRs as the electron transport material (ETM) has been reported in PSCs with P3HT:PCBM active layer. Table 5.1 summarizes the most recent photovoltaic results obtained from the literature. Many of the papers in literature used MoO_3 as hole transport layer (HTL), some others V_2O_5 and in other cases, the HTL layer was not

employed. An Ag thin film was the most applied back metal electrode; however, some works replaced the silver by gold or aluminum. An important aspect is the ZnO NRs length, most of the reported works apply NR lengths around 100-500 nm. Only two papers presented NRs of 2 μm in length.[25, 26] The data from Table 5.1 is ordered in function of the ZnO NR length, in an ascending order. The highest efficiency obtained was 4.1% applying a 400 nm length ZnO NRs electrode covered with ZnO NPs. When no NPs were added on top of the NRs, an efficiency of 1.42% was obtained. Power conversion efficiencies (PCE) of 3.56%[27] and 3.90%[28] were achieved for 100 nm and 450 nm ZnO NRs lengths respectively. Both cells had a HTL of V_2O_5 and this could be the reason for the high FF observed in those cells (60% and 65% respectively). Other groups that used a HTL of MoO_3 reported FF around 37-52% and the FF were ~34-50% when no HTL was applied in the cells (Table 5.1). Only one group reported PSCs with ZnO NRs and PEDOT:PSS as the HTL, achieving a FF of 47% and a power conversion efficiency of 1.23%.[25]

Table 5.1 Reported data of PSCs using ZnO NRs as electron acceptor and P3HT:PCBM as organic active layer. The cells were measured at 100 mW·cm^{-2}. CB= Chlorobenzene, *o*-DCB= o-Dichlorobenzene, $CHCl_3$=Chloroform, HTL=Hole Transport Layer, CE=Counter-electrode, 2-NT= 2-Naphthalenethiol.

ZnO NR Length (nm)	P3HT:PCBM concentration and solvent used (mg/mL)	P3HT:PCBM Deposition speed (rpm)	Comments	V_{oc} (V)	J_{sc} (mA/cm^2)	FF (%)	PCE (%)	Ref.
100	30:30 in CB	-	HTL= MoO_3	0.51	5.70	38	1.11	29
100	20:20 in *o*-DCB	-	No HTL	0.50	10.21	49	2.52	27
100	20:20 in *o*-DCB	-	HTL= V_2O_5	0.55	10.75	60	3.56	27
120	40:32 in *o*-DCB	400	No HTL	0.46	8.20	34	1.28	24
120	40:32 in *o*-DCB	400	No HTL/ C_{60}	0.53	11.60	34	2.09	24
120	25:15 in *o*-DCB	400	No HTL/ 2-NT	0.61	12.10	50	3.71	30
200	12:9.6 in CB	-	No HTL	0.40	7.29	35	1.02	31
200	12:9.6 in CB	-	HTL= MoO_3	0.44	8.55	45	1.71	31
200	40:40 in $CHCl_3$:CB	-	No HTL	0.48	10.00	43	2.03	32
220	15:12 in CB	-	HTL= MoO_3 /CE=Al	0.55	9.02	44	2.15	33
250	Ratio (1:1) in CB	2000	HTL= MoO_x /CE=Au	0.27	9.92	37	0.98	34
300	30:18 in CB	-	No HTL	0.57	9.60	50	2.70	8
400	25:25 in CB	By Dr Blade	HTL= MoO_3	0.43	8.34	40	1.42	35
400	25:25 in CB	By Dr Blade	HTL= MoO_3/NR+NP	0.57	13.75	52	4.10	35
450	30:24 in CB	-	HTL= V_2O_5	0.58	10.40	65	3.90	28
500	20:20 in $CHCl_3$	800	No HTL/CE=Ag	0.42	12.77	19	1.73	26
2000	20:20 in $CHCl_3$	800	No HTL/CE=Ag	0.30	6.35	12	0.51	26
2000	Ratio (1:0.6) $CHCl_3$	-	HTL= PEDOT:PSS/ CE=Au	0.45	6.76	47	1.23	25

5.2 Application of ZnO nanostructures in PSCs

Polymer solar cells (PSC) with ZnO NR electrodes were prepared with an inverted configuration of FTO/ZnO NRs/P3HT:PCBM/PEDOT:PSS/Ag. The electrodes of ZnO NRs were synthesized by the LT-HM and the A-HM (using autoclave reactor 1) with and without an In_xS_y shell layer as already described (chapters 2, 3 and 4).[20-22] Then the ZnO NRs substrates were annealed for 5 min at 140°C and the active layer solution was spin-coated on top at different spin velocities. Afterwards, the PEDOT:PSS layer was spin-coated and annealed at 140°C for 5 min. The deposition of the hole conductor PEDOT:PSS layer for all the cells was fixed at 1000 rpm. Finally, a ~100 nm silver counter electrode, used as the back contact, was deposited by thermal evaporation (Figure 5.2).

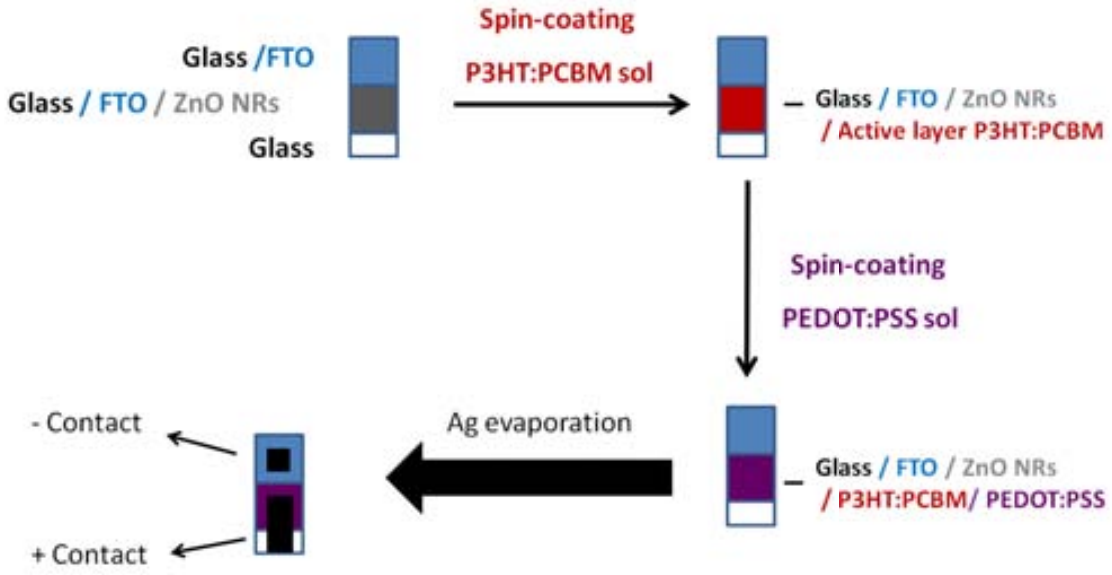

Figure 5.2 Scheme representation of all the PSC preparation steps. First, a spin-coating process of P3HT:PCBM solution was made on the ZnO NR electrode, then the deposition of PEDOT:PSS and finally, the Ag counter electrode evaporation.

Eight PSCs, used as reference devices, were fabricated applying a layer of ZnO NPs of ~100 nm thickness (prepared by sol-gel and the Pacholski *et al.* method).[20] For these reference devices, the P3HT:PCBM concentration used was 24 mg:24 mg, in chlorobenzene (CB) and deposited by spin coating at 1500 rpm. Figure 5.3 shows the front and back images of a PSC before and after optimization of the active area, this is, the elimination of extra organic material outside and at the edges of the solar cell. All the solar cells showed an improvement in the V_{oc} and FF, and a reduction of the J_{sc}. The latter is a well described phenomenon[36, 37]

attributed to the effect of the residual active material which is known to increase the shunt resistance of the device affecting V_{oc} and FF. The decrease of the J_{sc} is due to the reduction of the amount of material that adsorbs photons from light. Thus, the best reference solar cell showed an increase of the V_{oc} and FF from 0.21 V to 0.44 V for the V_{oc}, and from 28% to 36% for the FF, after removing the extra organic material. At the same time, the J_{sc} of the device was reduced from 11.95 $mA \cdot cm^{-2}$ to 5.99 $mA \cdot cm^{-2}$. These changes on the photovoltaic parameters affect directly the power conversion efficiency of the PSC, which increased from 0.68% to 0.92%. The active areas of all the solar cells reported in this chapter were optimized to 0.25-0.3 cm^2.

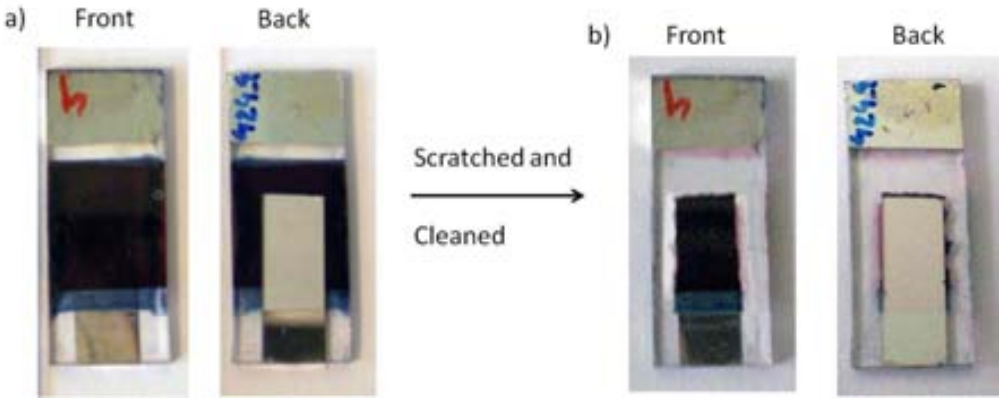

Figure 5.3 PSC images of a cell from the front and back side a) as prepared and b) after being scratched the extra active area and cleaned.

The efficiency of inverted PSC cells applying ZnO as the electron transport layer is known to improve after several hours stored in the dark or after being submitted to UV light irradiation. This effect has been attributed to the activation of ZnO when the UV light strikes the cell. UV light desorbs O_2 from the ZnO surface and produces electron traps by photogenerated holes. The later process recovers the rectification properties of ZnO improving the efficiency of the device.[38, 39] The solar cells analyzed in this chapter were measured at time zero (right after preparation) and also after 24 h and 48 h stored in the dark. We observed an increase of the solar cell performance after kept in the dark at room temperature for 24 h. Some cells presented a slightly higher performance after 48 h, but for comparison purposes, only the data obtained after 24 h is presented in this chapter.

5.2.1 Optimization of the P3HT:PCBM solution conditions

The deposition of the active layer P3HT:PCBM solution applied on the ZnO NRs, was first optimized for best solar cell performance. We studied the effect of materials concentration, type of solvent and spin-coating deposition velocity. In the first set of experiments, three concentrations of the mixture P3HT:PCBM were analyzed: 24:24 mg/mL, 40:24 mg/mL and 40:40 mg/mL. All other parameters were maintained the same: the solvent used was chlorobenzene (CB), the spin coating velocity was fixed at 400 rpm and the ZnO NR electrodes used were all grown for 6h (~1.6 μm length) by the LT-HM method.

We noticed that the photovoltaic performance of the PSCs improved when the solution was placed on top of the FTO/ZnO electrode before the spin coating was started. The latter has been attributed to the better infiltration of the polymer solution inside the NRs. Best results were obtained for the 40:40 mg/mL solution concentration of P3HT:PCBM (Table 5.2). Increasing the concentration from 24:24 to 40:40 mg/mL increases the current density of the cell linearly, due to the presence of higher quantity of active material to harvest light. Although other groups used ratios of (1:0.8)[24] or (1:0.6)[8, 25, 40] with lower quantity of PCBM, our cells presented better performances when a ratio of (1:1) is used, in agreement with previous reported results.[34, 35] The concentration of P3HT:PCBM was fixed at 40:40 mg/mL in chlorobenzene and deposited at 1500 rpm, 800 rpm, 400 rpm and at 2 x 400 rpm spin coating velocities. The application of different velocities permitted the fabrication of the active layer with different thickness. The best photovoltaic response was obtained for the thickest active layer with 2 x 400 rpm deposition speed (Table 5.2).

Table 5.2 Effect of the different P3HT:PCBM solution conditions on the PSCs parameters with ZnO ~1.6 µm NR length electrodes. At the start (time 0 h) and after 24 h kept in the dark at room temperature. AM1.5 light irradiation of 1000 $W \cdot m^{-2}$. CB= Chlorobenzene.

Cells Measured	P3HT:PCBM Concentration (mg/mL)	solvent	Deposition speed (rpm)	V_{oc} (V)	J_{sc} (mA/cm^2)	FF (%)	PCE (%)
At start (0 h)	24:24	CB	400	0.21	2.08	26	0.39
	40:24			0.33	8.20	31	0.85
	40:40			0.45	8.59	32	0.91
	40:40	CB	1500	0.22	4.19	30	0.28
			800	0.35	5.03	24	0.43
			400 + 400	0.37	9.29	32	1.12
	40:40	m-xylol	400 + 400	0.25	3.17	30	0.24
		chloroform	400 + 400	0.33	7.16	29	0.68
After 24 h	24:24	CB	400	0.30	5.44	26	0.43
	40:24			0.47	8.67	29	1.18
	40:40			0.42	9.61	33	1.48
	40:40	CB	1500	0.40	4.65	30	0.44
			800	0.38	7.09	28	0.75
			400 + 400	0.49	9.65	32	1.51
	40:40	m-xylol	400 + 400	0.25	2.84	27	0.19
		chloroform	400 + 400	0.36	7.45	28	0.74

It is well-known that the intrinsic morphology of the active layer affects directly the power conversion efficiency of the solar cell. The morphology is greatly affected by the different solvent or mixture of solvents used to disperse the P3HT:PCBM mixture. The modification of the solvent can introduce order or disorder on the side-chains of the polymer and change their optical properties.[41] Thus, solvents with different polarity, like chloroform and m-xylol, were also analyzed and compared with the results obtained applying chlorobenzene. Moreover, the use of these solvents could also help the infiltration of the solution into the ZnO NRs electrode. Nevertheless, the photovoltaic response of the solar cells applying chlorobenzene was always higher than those applying chloroform or m-xylol as shown in Table 5.2.

5.2.2 ZnO NRs electrodes obtained by two synthesis methods: application in PSCs

After the optimization of the active layer concentration, PSCs were fabricated applying the vertically aligned ZnO electrodes obtained by the two synthesis methods prepared in this thesis: the LT-HM (in a PYREX glass bottle) and the A-HM (in an autoclave reactor, model 4749 from Parr). We have reported the careful analyses of the NRs by photoluminescence (PL) and Time resolved photoluminescence (TRPL) in chapter 2 and 3.[22] Our results have shown faster PL decay observed for the ZnO NR obtained by the LT-HM (time constant, τ_{EFF} = 20-40 ps) in comparison with the ZnO NRs obtained by the A-HM (time constant, τ_{EFF} = 40-140 ps). The latter has been attributed to a larger contribution of the nonradiative recombination (surface defects). These results underline superior optical quality of the NR obtained by the A-HM.[20] The latter affected the photovoltaic response of Dye sensitized Solar Cells (DSCs) when applied as electrodes: the ZnO NRs obtained with less surface defects (by the A-HM) resulted in superior power conversion efficiencies. For this reason, in this chapter we analyzed the effect that these two types of ZnO NRs have on the photovoltaic properties of PSCs.

For each synthesis method, four different ZnO NR morphologies were analyzed. The different morphologies were obtained by modifying the growth time during synthesis (6 h, 12 h, 22 h and 28 h) resulting in ZnO NR lengths between 400 nm and 5.0 μm and different diameters shown in Table 5.3. The concentration of the active layer solution was fixed at 40:40 mg/mL in chlorobenzene. The deposition speed of the active organic blend was tuned to different spinning velocities (800 rpm, 400 rpm and 2 x 400 rpm) and applied on each ZnO electrode. Here, we present a complete study with different ZnO NR lengths, ranging from 400 nm up to 5 μm. Some other studies have reported PSCs applying ZnO NRs of a fixed length, usually between 100 –500 nm,[24, 27-29, 31-35] and only two works applied 2 μm ZnO NRs[25, 26] (Table 5.1).

Table 5.3 shows the best photovoltaic response obtained for each ZnO electrode. Values are shown at start and after 24h of being prepared and stored in the dark at room temperature. Best solar cell response was observed for ZnO NR lengths shorter than 1 μm, and applying deposition speed of 800 rpm for the BHJ blend. The thickness of the active layer, P3HT:PCBM, must be increased when the ZnO NR length increases. Thus, for ZnO NR lengths between 1-1.5 μm NR the spinning speed of 400 rpm improved the results. Above 1.5 μm NR lengths, the

optimum active layer deposition was made applying two consecutive coatings of the active layer at 400 rpm.

Table 5.3 Application of different ZnO NR electrodes in PSCs with a solution concentration 40:40 mg/mL of P3HT:PCBM in chlorobenzene. At the start (time 0 h) and after 24 h kept in the dark at room temperature. AM1.5 light irradiation of 1000 $W \cdot m^{-2}$.

Growth synthesis	Cells Measured	ZnO NR growth time (h)	Average NR length (μm)	Average NR diameter (nm)	Deposition speed (rpm)	V_{oc} (V)	J_{sc} (mA/cm^2)	FF (%)	PCE (%)
LT-HM	At start (0 h)	6	1.6 ± 0.2	115 ± 8	400 + 400	0.37	9.29	32	1.12
		12	3.2 ± 0.5	198 ± 23	400 + 400	0.32	7.53	27	0.65
		22	5.2 ± 0.2	279 ± 55	400 + 400	0.33	9.78	29	0.94
		28	5.1 ± 0.4	293 ± 89	400 + 400	0.35	7.32	28	0.72
	After 24 h	6	1.6 ± 0.2	115 ± 8	400 + 400	0.49	9.65	32	1.51
		12	3.1 ± 0.5	198 ± 23	400 + 400	0.48	8.83	28	1.17
		22	5.2 ± 0.2	219 ± 55	400 + 400	0.40	10.36	31	1.28
		28	5.1 ± 0.4	293 ± 89	400 + 400	0.45	9.69	28	1.23
A-HM	At start (0 h)	6	0.4 ± 0.1	83 ± 17	800	0.36	10.66	31	1.21
		12	0.9 ± 0.1	58 ± 9	800	0.32	8.51	27	0.74
		22	1.1 ± 0.2	59 ± 18	400	0.28	8.09	29	0.66
		28	3.5 ± 0.1	-	400 + 400	0.23	5.71	30	0.39
	After 24 h	6	0.4 ± 0.1	83 ± 17	800	0.49	11.63	35	1.96
		12	0.9 ± 0.1	58 ± 9	800	0.49	10.24	30	1.53
		22	1.1 ± 0.2	59 ± 18	400	0.50	10.27	31	1.59
		28	3.5 ± 0.1	-	400 + 400	0.46	8.25	28	1.07

Figure 5.4a shows the direct relation observed between the power conversion efficiencies (PCE) and the NR length. Shorter NR show higher photovoltaic performance. Below 0.5 μm NR length an efficiency of 2.0 % was obtained, while ZnO NR lengths between 0.5-2.0 μm achieved efficiencies around 1.5 %, and above 3 μm the efficiencies were lower than 1.3 % (Figure 5.4a). The calculated aspect ratio (defined as the NR length divided by the NR diameter)[42] of each ZnO NR electrode was also represented as a function of the power conversion efficiency (Figure 5.4b). There is a general acceptance that increasing the aspect ratio of the NR results in high power conversion efficiency.[43, 44] In our work, the ZnO NR electrodes with the lowest aspect ratio presented the highest performance, corresponding to the NRs obtained by the A-HM synthesis method. The comparison of the power conversion efficiency of devices applying ZnO NR with similar aspect ratios (see Figure 5.4b) shows that the ZnO NRs synthesized by the LT-HM present lower power conversion efficiency that the NRs obtained by the A-HM. These results are in agreement with the presence of different

surface defects for the ZnO NRs obtained by different synthesis methods as already described in chapter 3. The optical quality of the NRs (surface defects) is directly related to the interaction between the ZnO and the P3HT:PCBM active layer at the interface. Thus, it can also alter the BHJ blend solution infiltration into the ZnO NRs resulting in low power conversion efficiency as observed in this work when increasing NR length. Other groups also reported a poor penetration of the blend P3HT:PCBM solution, only covering the top surface of the ZnO NRs.[35] These results are an indication that the factors affecting the ZnO NR properties and solar cell performance are the result of the combination of many and variable issues, and not only limited by the aspect ratio (dimensions) or density of the ZnO NRs.

The lowest photovoltaic performance was observed for the ZnO electrode grown for 28h by the A-HM synthesis. The latter has been attributed to the change in morphology observed for this ZnO sample. The ZnO electrode shows a NR morphology for the bottom part, while an open form, similar to nanosheets, is observed on top (see Figure 3.4). This sheet-like structure is believed to prevent the infiltration of the P3HT:PCBM active layer solution in to the ZnO electrode, resulting in low power conversion efficiency. The FF of these cells are very low, 28-35 % and an important aspect is that the FF decreases when the NR length increases (Table 5.3). The decrease of FF values is a direct consequence of the increase of recombination processes due to electrical shorts. Figure 5.4c represents the shunt resistances (R_{sh}) defined as $R_{sh}=dV/dI_{(V=0)}$ and series resistances (R_s) defined as $R_s=dV/dI_{(I=0)}$.[45, 46] R_{sh} and R_s were measured from the IV- curves of the best solar cells under illumination. A decrease on the R_{sh} from 120 to 60 $\Omega\cdot cm^2$ was observed when the NR length increased, while the R_s was maintained constant (around 20-40 $\Omega\cdot cm^2$). The decrease in solar cell performance have been attributed to the Rsh (recombination loses) and has been observed by other groups with resistivity values of 50-390 $\Omega\cdot cm^2$ (R_{sh}) and 22-47 $\Omega\cdot cm^2$ (R_s),[33] or 250-620 $\Omega\cdot cm^2$ (R_{sh}) and 2-6 $\Omega\cdot cm^2$ (R_s)[27] for similar PSCs.

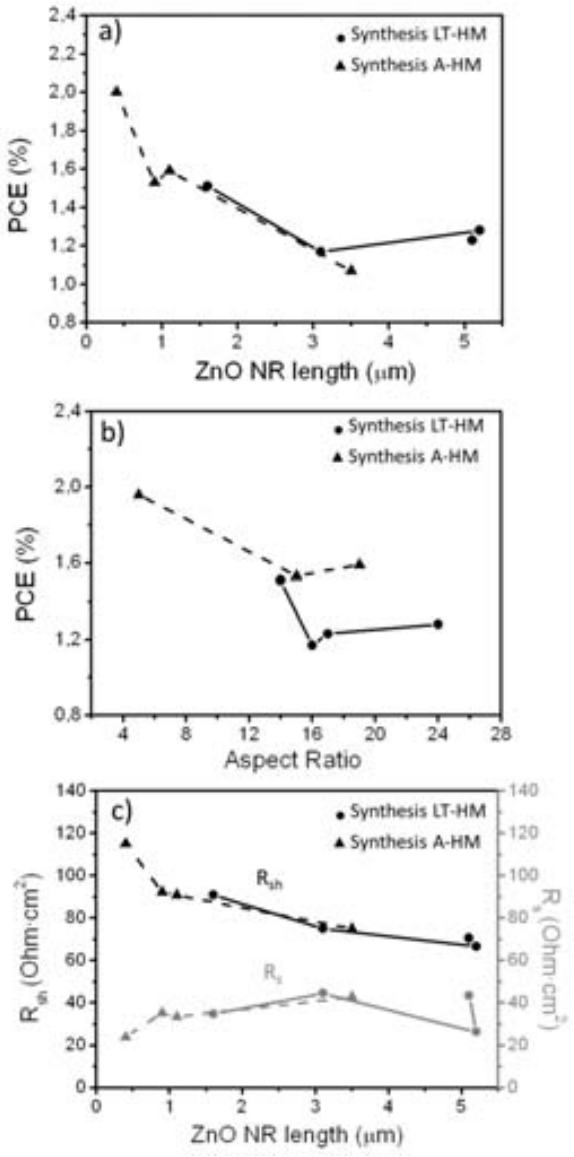

Figure 5.4 a) Representation of PSC power conversion efficiencies (PCE) in function of ZnO NR length, b) aspect ratio of each ZnO NR electrode in function of power conversion efficiencies (PCE) and c) Shunt resistances (R_{sh}) and series resistances (R_s) as a function of the ZnO NR length for both synthesis methods.

Figure 5.5a depicts the current-voltage curves of two cells prepared applying the LT-HM and the A-HM methods with similar NR length around 1.1-1.6 μm and similar aspect ratios (6h L-HM and 22h A-HM). A slightly increase of the J_{sc} value for A-HM cell can be observed, while similar V_{oc} and FF values were measured. The IPCE measurement of the devices was performed both with and without bias light (bias light is used to simulate the actual operating condition for the device during IPCE measurements). The IPCE measured under bias light

revealed significantly lower values despite the fact that only intensities corresponding to 0.5 Sun were used to simulate biasing (Figure 5.5b). This is ascribed to the presence of a poor conducting layer or interface in the device, which results in space charge limitation causing device saturation and hence, the decrease of IPCE during illumination.[47, 48] The limiting layer (low conductivity) could be the interface between ZnO NR and the organic blend due to the problems encounter during infiltration of the active layer. This effect is reflected by the low fill factors presented in these cells. Figure 5.5b represents the IPCE spectra with and without bias light for two cells with similar NR length and aspect ratio from both hydrothermal methods (6h L-HM and 22h A-HM) where the decrease under bias light can be observed.

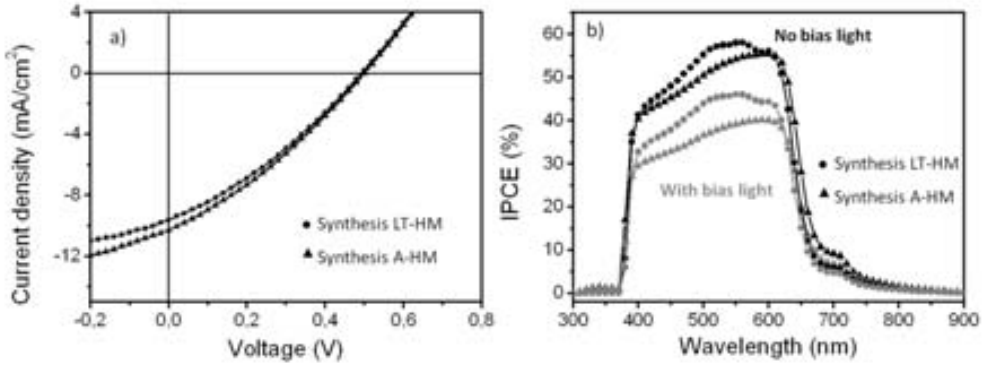

Figure 5.5 a) JV-curves and b) IPCE spectra of the two cells with similar ZnO NR lengths between 1.1-1.6 μm grown by the LT-HM (6h) and the A-HM (22h) syntheses.

5.2.3 Core-shell ZnO/In_xS_y electrodes obtained by the two synthesis methods: application in PSCs

The application of core-shell ZnO NRs/In_xS_y electrodes on PSCs was more challenging. ZnO NR electrodes with a core-shell layer prepared by the SILAR technique with precursor concentrations of 0.1 M of $InCl_3$ and 0.03 M of Na_2S (see chapter 4 for details) and different number of deposition cycles (3, 5 and 10) were applied in PSCs. All the obtained PSCs efficiencies were lower than using bare ZnO NR electrodes. We observed that the PSC performance increased when a lower concentration of the SILAR precursors was applied (25 mM of $InCl_3$ and 7.5 mM of Na_2S). Therefore, these PSCs were optimized with the core-shell ZnO/ In_xS_y electrodes prepared by the LT-HM and the A-HM synthesis methods (grown for 6h, 12h, 22h and 28h) using the SILAR reaction with low concentration. The organic blend

deposition, P3HT:PCBM, was optimized at spin coating velocities of 800 rpm, 400 rpm, and 2 depositions at 400 rpm for each ZnO electrode. Table 5.4 represents the best PSCs results obtained. Almost all the electrodes presented higher efficiencies when thin shell layers were deposited (3 cycles), only one cell presented a better performance for 5 SILAR cycles. The A-HM-1 electrodes improved with deposition speeds at 800 rpm while the LT-HM electrodes presented higher results with two depositions at 400 rpm.

Table 5.4 Best PSCs performance obtained applying core-shell ZnO/ In_xS_y NRs electrodes prepared by the LT-HM and the A-HM synthesis methods and different growth times. The P3HT:PCBM solution concentration was 40:40 mg/mL in chlorobenzene. Cell measured at start. Measurements at start (0h) and AM1.5 light irradiation of 1000 $W \cdot m^{-2}$.

Hydrothermal growth synthesis	ZnO NR growth time (h)	Average NR length (μm)	SILAR cycles	Deposition speed (rpm)	V_{oc} (V)	J_{sc} (mA/cm^2)	FF (%)	PCE (%)
LT-HM	6	1.6 ± 0.2	3	400 + 400	0.54	10.91	31	1.83
	12	3.2 ± 0.5	3	400 + 400	0.52	10.66	29	1.60
	22	5.2 ± 0.2	5	400 + 400	0.39	9.85	34	1.31
	28	5.1 ± 0.4	3	400 + 400	0.43	10.48	28	1.25
A-HM	6	1.6 ± 0.2	3	800	0.55	10.37	31	2.14
	12	3.1 ± 0.5	3	800	0.54	11.68	33	2.06
	22	5.2 ± 0.2	3	800	0.54	10.93	33	1.94
	28	5.1 ± 0.4	3	800	0.54	11.37	32	1.98

The performance comparison between PSCs applying bare ZnO NRs and core-shell ZnO /In_xS_y NRs is presented in Figure 5.6a. Power conversion efficiency enhancement was observed for the core-shell ZnO/In_xS_y NRs electrodes due to the increase of the V_{oc}, from ~0.47 V to ~0.54 V (Table 5.3 and Table 5.4). Only the ~5 μm length NRs electrodes had exactly the same power conversion efficiencies and present the same V_{oc} values (Table 5.4 and Figure 5.6a). The latter V_{oc} improvement was attributed to the application of In_xS_y shell thickness, which acts as electron blocking layer (as commented in chapter 4, section 4.3.3). Moreover, ZnO nanotrees with the core-shell ZnO/In_xS_y structure presented a higher performance than bare nanotrees, due to the V_{oc} and J_{sc} increase. Figure 5.6b represents the shunt resistances (R_{sh}) and series resistances (R_s) for the different core-shell ZnO/ In_xS_y NR electrode thickness. The values of R_{sh} for core-shell PSCs were similar than the values for the bare NRs based PSCs (around 60 and 110 $\Omega \cdot cm^2$). In this case, however, the decrease in efficiency when increasing NR length, was not observed. Furthermore, the R_s values were slightly lower and hence, the performance of core-shell PSCs improved. This response is probably due to the modification

of the surface defects of the ZnO NRs when a shell of In_xS_y is deposited on its surface. The latter can also improve the bonding with the active organic blend, as already reported for dyes when applied in DSCs (see chapter 3 and chapter 4). On the other hand, most of these core-shell PSCs measured and kept in the dark showed a performance decrease after the preparation and first measurement. The same effect was also observed in core-shell ZnO NRs/In_xS_y applied in DSCs and commented in chapter 4 (section 4.3).

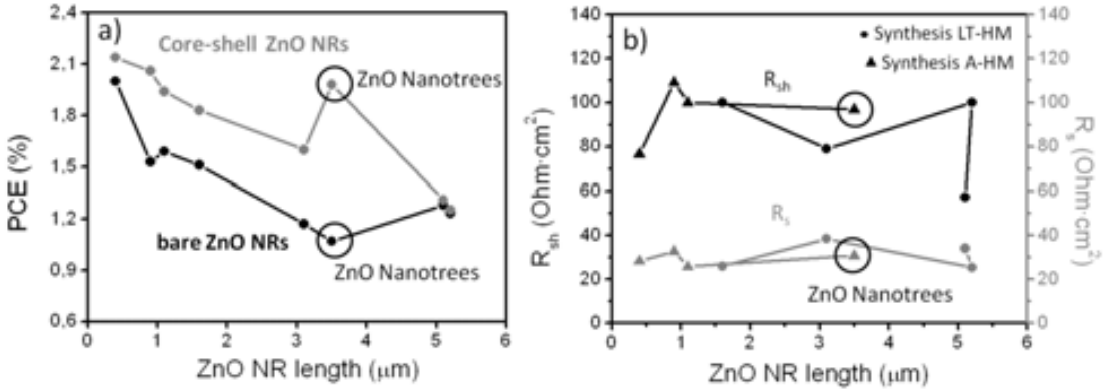

Figure 5.6 a) Performance comparison between bare ZnO NRs (black) and core-shell ZnO/ In_xS_y NRs (grey) in PSCs in function of the NR length and b) representation of the R_{sh} and R_s for PSCs with core-shell structure with different ZnO layer thickness.

Figure 5.7 shows the JV-curves and IPCE spectra of two PSCs applying core-shell ZnO/In_xS_y electrodes with similar NR lengths (between 1.1-1.6 μm) prepared by the LT-HM (6h) and the A-HM-1 (22h). Both JV-curves show the same V_{oc} values and almost the same J_{sc} and FF values, thus, similar power conversion efficiencies were obtained (Table 5.4). The IPCE spectra were surprisingly different for both PSCs. This IPCE difference is probably due to the stability problems of the core-shell structure also observed in DSCs (see section 4.3). Some of the core-shell ZnO/In_xS_y cells showed different degradation behavior, which was more evident when a bias light was applied. The IPCE measured under bias light for both cells presented a decrease as it was observed for bare ZnO NRs PSCs shown in Figure 5.5. However, the decrease was higher for the PSC with core-shell ZnO/In_xS_y prepared by the LT-HM grown for 6h. As indication of the low stability of the core-shell ZnO/In_xS_y electrodes as was also mentioned in chapter 4, see section 4.3.

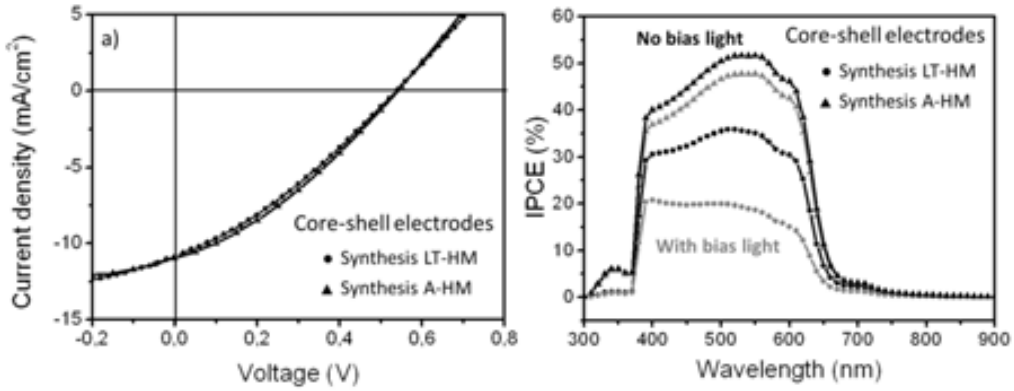

Figure 5.7 a) JV-curves and b) IPCE spectra of PSCs applying core-shell ZnO NRs-Indium sulfide electrodes with similar NR lengths between 1.1-1.6 μm grown by the LT-HM (6h) and the A-HM (22h).

5.2.4 Device characterization by SEM microscopy and EDS analysis

Cross-section SEM images of the PSCs applying different NR lengths and synthesis methods with and without the In_xS_y shell layer were studied. The cross-section SEM images of two PSCs with NRs grown for 12 h by the LT-HM (a) and the A-HM (b) methods are compared in Figure 5.8. Using the backscattered electrons (BSE) we can distinguish the different composition of the layers. Since heavy atoms with high atomic number are stronger scatters than light ones, a back scattering electron (BSE) image can reveal different intensity brightness related to the compositional information of the sample. For example, heavy metals appear brighter in the BSE image than light elements such as organic materials which appear with a dark color. From Figure 5.8 we can see the different NR length obtained for each hydrothermal synthesis at the same growth time (12 h in this case) that corresponds with the already measured length values before the cell preparation (Table 5.3, Figure 3.3). We can also observe that in Figure 5.8-a, the part of the ZnO NRs (bright grey) with the P3HT:PCBM blend (dark grey) has some black parts which means there was no blend infiltration in those points, corroborating the penetration problems commented before. On the other hand, the cell in Figure 5.8-b did not present parts with a dark color in the BSE image pointing out that longer NRs difficult the blend penetration.

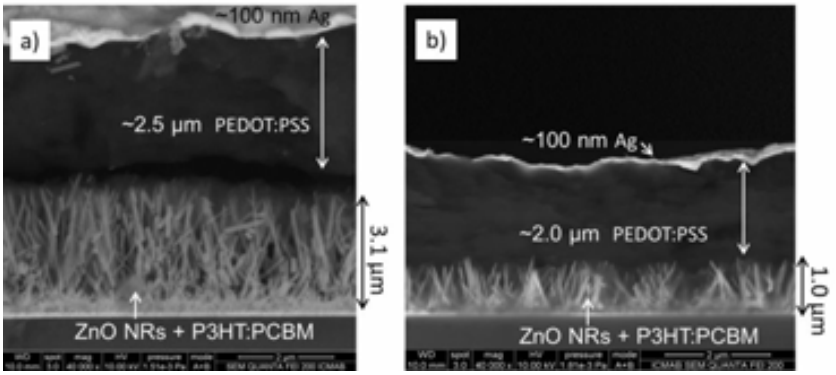

Figure 5.8 Cross section SEM images of two PSCs with bare ZnO NRs grown for 12h by a) the LT-HM and b) the A-HM.

A cross-section SEM comparison between PSCs applying the same bare ZnO NR electrode (LT-HM- 12h growth time) but with different deposition velocities of the organic blend P3HT:PCBM, 800 rpm and 2 x 400 rpm is presented in Figure 5.9. A better blend penetration was observed using two organic blend depositions at 400 rpm (Figure 5.9-b). The spin-coating process of the organic blend solution at 800 rpm, hardened the solution infiltration that only covered the top of the NRs (many black holes can be seen on the bottom of the NRs) (Figure 5.9-a). The latter explains the better PSC performance observed when the organic blend was deposited at 2 x 400 rpm on this electrode (Table 5.3).

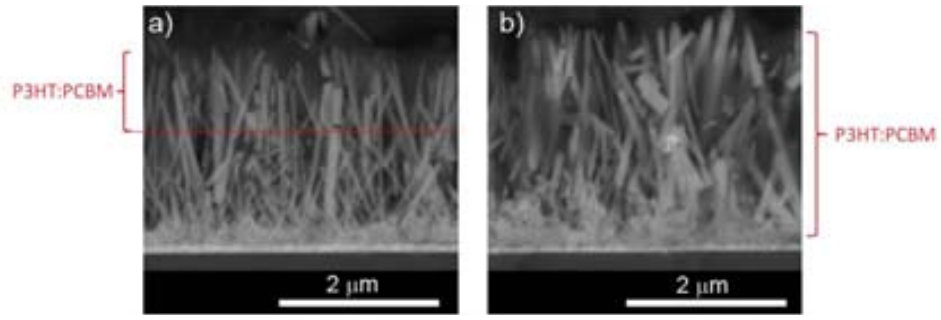

Figure 5.9 Cross section SEM pictures of 2 cells with ZnO NRs prepared by the LT-HM grown for 12h a) blend deposition at 800 rpm and b) 2 x 400 rpm.

Figure 5.10 shows two cross-section SEM images of two PSCs applying bare ZnO NR (a) and core-shell ZnO/In_xS_y NRs (3 cycles) (b) both prepared by the LT-HM grown for 12h. The images of the backscattered electrons detector from the SEM microscope showed organic blend infiltration difficulties within the ZnO NRs for both cells (Figure 5.10). Therefore, the

slightly enhancement in the PSCs applying the core-shell electrodes is due to the V_{oc} values improvement as was commented before.

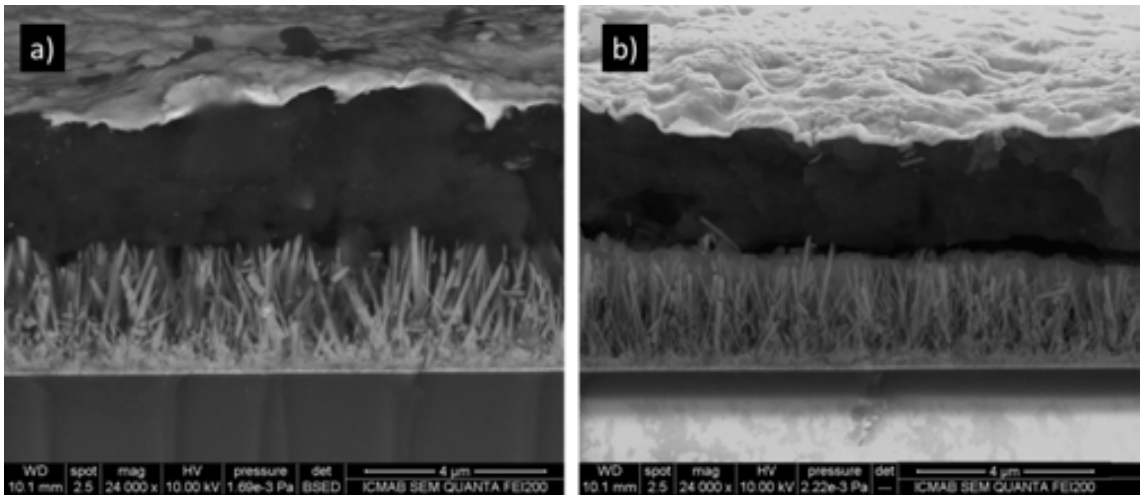

Figure 5.10 Cross section SEM images of two PSCs with a) bare ZnO NRs and b) core-shell (3 cycles) ZnO NRs grown for 12h by the LT-HM. Deposition of the organic solution at 2 x 400 rpm for both cells.

Analyses of energy dispersive X-ray spectroscopy (EDS) along the cross-section area of the cells made in the SEM microscope allowed us to analyze the infiltration properties of the organic active materials within the ZnO NR electrode. Figure 5.11 presents the EDS cross line along several solar cells with ZnO NRs with different thicknesses grown by the LT-HM and the A-HM methods. We can easily observe from the EDS graph the composition of each part from the device, the elements represented are: silver (from counter-electrode), carbon (from PEDOT:PSS and P3HT:PCBM), sulfur (from PEDOT:PSS and P3HT), oxygen (from organic materials and ZnO), zinc (from ZnO) and silicon (from the glass of FTO substrate). The carbon element from organic materials decrease in the ZnO NRs area and did not arrive to the bottom of the NRs showing the low blend penetration for long NRs of 5.0 μm (LT-HM), 3 μm (LT-HM) and 3.4 μm (A-HM-1) shown in Figure 5.11. Only shorter NRs of ~1.3 μm (A-HM) presented a slightly active layer penetration reaching the FTO and hence, the performance achieved for this PSC was higher than the rest of the samples (Figure 5.11-d). The same EDS cross-section experiments were also measured on PSCs with an In_xS_y core-shell layer, but the quantity of indium was too low to be detected by the EDS analyses. The core-shell PSCs presented the same behavior as bare ZnO NRs PSCs, the infiltration of the organic blend was improved for short ZnO NR layers.

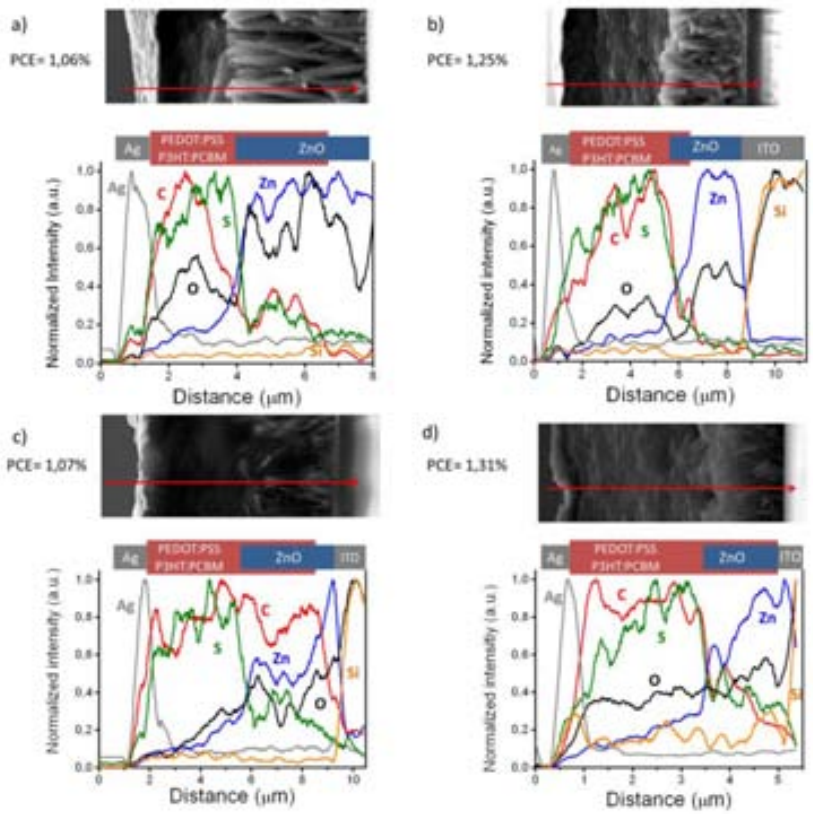

Figure 5.11 Cross-section SEM image and the EDS analysis along the PSCs with different electrodes of ZnO NRs grown by LT-HM method and NR length of a) ~5 μm and b) ~3 μm and grown by A-HM with NR lengths of c) ~3.4 μm and d) ~1.3 μm. Inset graphs: the power conversion efficiencies (PCE) measured for the corresponding PSCs.

5.3 Conclusions

In this chapter polymer solar cells with different ZnO electrodes prepared by the LT-HM and the A-HM-1 methods with and without an indium shell layer were applied in PSCs. An inverted cell configuration was applied: FTO/ZnO NRs/P3HT:PCBM/Ag. First, different parameters of the active layer (concentration, spin coating speed and solvent) were optimized to improve the performance of bare ZnO NRs PSCs. A concentration of 40 mg: 40 mg of P3HT:PCBM in chlorobenzene achieved the best results. The blend deposition speed is dependent on the NR length, longer NR required slower deposition speeds to allow thicker active layers. The best performance obtained was 2.0 % efficiency using short NR length (400 nm) grown by the A-HM synthesis due to the difficulty of the organic blend infiltration. IPCE measurements resulted on a reduction of the performance under bias light showing the presence of a poor interface in the device that corroborates the blend infiltration problems.

Electrodes of ZnO NRs covered with the indium sulfide layer were then applied in the same PSCs. The SILAR deposition of the shell layer was carried out using the precursor concentrations: 25 mM $InCl_3$ and 7.5 mM Na_sS. The latter core-shell structure allowed a slightly increase on power conversion efficiency compared to the bare ZnO NRs based PSCs. This enhancement of the performance was due to the higher V_{oc} obtained since the introduction of the indium sulfide layer modified the energy levels of the cells. The highest power conversion efficiency obtained was 2.14% for the shorter ZnO NR electrode ~400 nm (6h A-HM) with 3 SILAR cycles due to the organic blend infiltration problem.

The active blend solution penetration was studied in more detail using cross section SEM images with backscattered electrons and EDS analysis showing long NRs only covered on top by the active blend solution. Therefore, the highest PSC performance was obtained with short NRs, the increase of the NR length produced a decrease on the cell efficiency.

Degradation studies under continuous solar light irradiation at different atmospheres showed a faster performance decrease under O_2 and N_2 for both types of PSCs, with and without the shell layer. The cells under humid atmospheres of N_2 and air were degraded slower. The latter was attributed to the self-diffusion of oxygen into the ZnO layer that accelerated the degradation of the polymer. Dry N_2 atmospheres allowed the production of oxygen vacancies in the ZnO layer decreasing the performance. The degradation of the core-shell based PSCs was slower under dry N_2 and O_2 but faster under humid N_2 and air compared with bare ZnO NRs PSCs.

5.4 References

1. "Heliatek set new world record efficiency of 10.7% for its organic tandem cell": http://www.heliatek.com/newscenter/latest_news/heliatek-erzielt-mit-107-effizienz-neuen-weltrekord-fur-seine-organische-tandemzelle/?lang=en#.
2. F. C. Krebs, J. Fyenbo and M. Jorgensen, "Product integration of compact roll-to-roll processed polymer solar cell modules: methods and manufacture using flexographic printing, slot-die coating and rotary screen printing", *Journal of Materials Chemistry*, **2010**, 20(41), 8994-9001.
3. S. E. Shaheen, D. S. Ginley, G. E. Jabbour and Ea, "Organic-based photovoltaics. toward lowm-cost power generation", *Mrs Bulletin*, **2005**, 30(1), 10-19.
4. F. C. Krebs, S. A. Gevorgyan and J. Alstrup, "A roll-to-roll process to flexible polymer solar cells: model studies, manufacture and operational stability studies", *Journal of Materials Chemistry*, **2009**, 19(30), 5442-5451.
5. R. A. J. Janssen, J. C. Hummelen, N. S. Saricifti and Ea, "Polymer-fullerene bulk heterojunction solar cells", *Mrs Bulletin*, **2005**, 30(1), 33-36.
6. S. R. Forrest, "The path to ubiquitous and low-cost organic electronic appliances on plastic", *Nature*, **2004**, 428(6986), 911-918.
7. G. Yu, J. Gao, J. C. Hummelen, F. Wudl and A. J. Heeger, "Polymer Photovoltaic Cells - Enhanced efficiencies via a network of internal donor-acceptor heterojunctions", *Science*, **1995**, 270(5243), 1789-1791.
8. K. Takanezawa, K. Hirota, Q. S. Wei, K. Tajima and K. Hashimoto, "Efficient charge collection with ZnO nanorod array in hybrid photovoltaic devices", *Journal of Physical Chemistry C*, **2007**, 111(19), 7218-7223.
9. K. M. Coakley, Y. X. Liu, C. Goh and M. D. McGehee, "Ordered organic-inorganic bulk heterojunction photovoltaic cells", *Mrs Bulletin*, **2005**, 30(1), 37-40.
10. M. Lenes, L. J. A. Koster, V. D. Mihailetchi and P. W. M. Blom, "Thickness dependence of the efficiency of polymer : fullerene bulk heterojunction solar cells", *Applied Physics Letters*, **2006**, 88(24).
11. K. M. Coakley and M. D. McGehee, "Conjugated polymer photovoltaic cells", *Chemistry of Materials*, **2004**, 16, 4533-4542.
12. K. M. Coakley and M. D. McGehee, "Photovoltaic cells made from conjugated polymers infiltrated into mesoporous titania", *Applied Physics Letters*, **2003**, 83(16), 3380-3382.
13. M. Quintana, T. Edvinsson, A. Hagfeldt and G. Boschloo, "Comparison of dye-sensitized ZnO and TiO2 solar cells: Studies of charge transport and carrier lifetime", *Journal of Physical Chemistry C*, **2007**, 111(2), 1035-1041.
14. I. Gonzalez-Valls and M. Lira-Cantu, "Vertically-aligned nanostructures of ZnO for excitonic solar cells: a review", *Energy & Environmental Science*, **2009**, 2(1), 19-34.
15. J. Ajuria, I. Etxebarria, W. Cambarau, U. Munecas, R. Tena-Zaera, J. Carlos Jimeno and R. Pacios, "Inverted ITO-free organic solar cells based on p and n semiconducting oxides. New designs for integration in tandem cells, top or bottom detecting devices, and photovoltaic windows", *Energy & Environmental Science*, **2011**, 4(2), 453-458.
16. K. M. Noone, S. Subramaniyan, Q. Zhang, G. Cao, S. A. Jenekhe and D. S. Ginger, "Photoinduced Charge Transfer and Polaron Dynamics in Polymer and Hybrid Photovoltaic Thin Films: Organic vs Inorganic Acceptors", *Journal of Physical Chemistry C*, **2011**, 115(49), 24403-24410.
17. R. S. Aga, Jr., D. Gunther, A. Ueda, Z. Pan, W. E. Collins, R. Mu and K. D. Singer, "Increased short circuit current in organic photovoltaic using high-surface area electrode based on ZnO nanowires decorated with CdTe quantum dots", *Nanotechnology*, **2009**, 20(46).
18. S. D. Oosterhout, M. M. Wienk, S. S. van Bavel, R. Thiedmann, L. J. A. Koster, J. Gilot, J. Loos, V. Schmidt and R. A. J. Janssen, "The effect of three-dimensional morphology on the efficiency of hybrid polymer solar cells", *Nature Materials*, **2009**, 8(10), 818-824.
19. B. A. Gregg and Ea, "The photoconversion mechanism of excitonic solar cells", *Mrs Bulletin*, **2005**, 30(1), 20-22.
20. I. Gonzalez-Valls and M. Lira-Cantu, "Dye sensitized solar cells based on vertically-aligned ZnO nanorods: effect of UV light on power conversion efficiency and lifetime", *Energy & Environmental Science*, **2010**, 3(6), 789-795.

21. I. Gonzalez-Valls, Y. H. Yu, B. Ballesteros, J. Oro and M. Lira-Cantu, "Synthesis conditions, light intensity and temperature effect on the performance of ZnO nanorods-based dye sensitized solar cells", *Journal of Power Sources*, **2011**, 196(15), 6609-6621.
22. I. Gonzalez-Valls, J. S. Reparaz, F. Güell, M. R. Wagner, G. Callsen, B. Ballesteros, A. Hoffmann and M. Lira-Cantu, "Low temperature growth of vertically-aligned ZnO nanorods for dye sensitized solar cells: unravelling their low power conversion efficiency", *Nano Letters*, **2012**, submitted.
23. Y. Y. Lin, C. W. Chen, T. H. Chu, W. F. Su, C. C. Lin, C. H. Ku, J. J. Wu and C. H. Chen, "Nanostructured metal oxide/conjugated polymer hybrid solar cells by low temperature solution processes", *Journal of Materials Chemistry*, **2007**, 17(43), 4571-4576.
24. C.-T. Chen, F.-C. Hsu, S.-W. Kuan and Y.-F. Chen, "The effect of C(60) on the ZnO-nanorod surface in organic-inorganic hybrid photovoltaics", *Solar Energy Materials and Solar Cells*, **2011**, 95(2), 740-744.
25. N. C. Das, S. Biswas and P. E. Sokol, "The photovoltaic performance of ZnO nanorods in bulk heterojunction solar cells", *Journal of Renewable and Sustainable Energy*, **2011**, 3(3), 033105
26. T. Ichikawa and S. Shiratori, "The Influence of the Organic/Inorganic Interface on the Organic-Inorganic Hybrid Solar Cells", *Journal of Nanoscience and Nanotechnology*, **2012**, 12(5).
27. J.-S. Huang, C.-Y. Chou, M.-Y. Liu, K.-H. Tsai, W.-H. Lin and C.-F. Lin, "Solution-processed vanadium oxide as an anode interlayer for inverted polymer solar cells hybridized with ZnO nanorods", *Organic Electronics*, **2009**, 10(6), 1060-1065.
28. K. Takanezawa, K. Tajima and K. Hashimoto, "Efficiency enhancement of polymer photovoltaic devices hybridized with ZnO nanorod arrays by the introduction of a vanadium oxide buffer layer", *Applied Physics Letters*, **2008**, 93(6).
29. Z. Yuan, J. Yu, N. Wang and Y. Jiang, "Well-aligned ZnO nanorod arrays from diameter-controlled growth and their application in inverted polymer solar cell", *Journal of Materials Science-Materials in Electronics*, **2011**, 22(11), 1730-1735.
30. J.-Y. Chen, F.-C. Hsu, Y.-M. Sung and Y.-F. Chen, "Enhanced charge transport in hybrid polymer/ZnO-nanorod solar cells assisted by conductive small molecules", *Journal of Materials Chemistry*, **2012**, 22(31).
31. Z. Hu, J. Zhang, Y. Liu, Z. Hao, X. Zhang and Y. Zhao, "Influence of ZnO interlayer on the performance of inverted organic photovoltaic device", *Solar Energy Materials and Solar Cells*, **2011**, 95(8), 2126-2130.
32. D. C. Olson, J. Piris, R. T. Collins, S. E. Shaheen and D. S. Ginley, "Hybrid photovoltaic devices of polymer and ZnO nanofiber composites", *Thin Solid Films*, **2006**, 496(1), 26-29.
33. M. Wang, Y. Li, H. Huang, E. D. Peterson, W. Nie, W. Zhou, W. Zeng, W. Huang, G. Fang, N. Sun, X. Zhao and D. L. Carroll, "Thickness dependence of the MoO3 blocking layers on ZnO nanorod-inverted organic photovoltaic devices", *Applied Physics Letters*, **2011**, 98(10).
34. K. H. Lee, B. Kumar, H.-J. Park and S.-W. Kim, "Optimization of an Electron Transport Layer to Enhance the Power Conversion Efficiency of Flexible Inverted Organic Solar Cells", *Nanoscale Research Letters*, **2010**, 5(12), 1908-1912.
35. J. Ajuria, I. Etxebarria, E. Azaceta, R. Tena-Zaera, N. Fernandez-Montcada, E. Palomares and R. Pacios, "Novel ZnO nanostructured electrodes for higher power conversion efficiencies in polymeric solar cells", *Physical Chemistry Chemical Physics*, **2011**, 13(46), 20871-20876.
36. A. Cravino, P. Schilinsky and C. J. Brabec, "Characterization of organic solar cells: the importance of device layout", *Advanced Functional Materials*, **2007**, 17(18).
37. A. Moliton and J. M. Nunzi, "How to model the behaviour of organic photovoltaic cells", *Polymer International*, **2006**, 55(6), 583-600.
38. T. Tromholt, A. Manor, E. A. Katz and F. C. Krebs, "Reversible degradation of inverted organic solar cells by concentrated sunlight", *Nanotechnology*, **2011**, 22(22).
39. F. Verbakel, S. C. J. Meskers and R. A. J. Janssen, "Electronic memory effects in diodes from a zinc oxide nanoparticle-polystyrene hybrid material", *Applied Physics Letters*, **2006**, 89(10).
40. E. A. Parlak, "The blend ratio effect on the photovoltaic performance and stability of poly (3-hexylthiophene): 6,6 -phenyl-C-61 butyric acid methyl ester (PCBM) and poly(3-octylthiophene):PCBM solar cells", *Solar Energy Materials and Solar Cells*, **2012**, 100, 174-184.
41. E. Bundgaard and F. C. Krebs, "Low band gap polymers for organic photovoltaics", *Solar Energy Materials and Solar Cells*, **2007**, 91(11), 954-985.

42. C. J. Murphy and N. R. Jana, "Controlling the aspect ratio of inorganic nanorods and nanowires", *Advanced Materials*, **2002**, 14(1).
43. W. U. Huynh, J. J. Dittmer and A. P. Alivisatos, "Hybrid nanorod-polymer solar cells", *Science*, **2002**, 295(5564), 2425-2427.
44. A. M. Peiro, P. Ravirajan, K. Govender, D. S. Boyle, P. O'Brien, D. D. C. Bradley, J. Nelson and J. R. Durrant, "Hybrid polymer/metal oxide solar cells based on ZnO columnar structures", *Journal of Materials Chemistry*, **2006**, 16(21).
45. S. S. Hegedus and W. N. Shafarman, "Thin-film solar cells: Device measurements and analysis", *Progress in Photovoltaics*, **2004**, 12(2-3), 155-176.
46. K.-i. Ishibashi, Y. Kimura and M. Niwano, "An extensively valid and stable method for derivation of all parameters of a solar cell from a single current-voltage characteristic", *Journal of Applied Physics*, **2008**, 103(9).
47. V. Shrotriya, G. Li, Y. Yao, T. Moriarty, K. Emery and Y. Yang, "Accurate measurement and characterization of organic solar cells", *Advanced Functional Materials*, **2006**, 16(15), 2016-2023.
48. P. Peumans, S. Uchida, S. R. Forrest and Zt, "Efficient bulk heterojunction photovoltaic cells using small-molecular-weight organic thin films", *Nature*, **2003**, 425(6954), 158-162.
49. S. A. Gevorgyan, M. Jorgensen, F. C. Krebs and K. O. Sylvester-Hvid, "A compact multi-chamber setup for degradation and lifetime studies of organic solar cells", *Solar Energy Materials and Solar Cells*, **2011**, 95(5), 1389-1397.
50. M. Lira-Cantu, F. C. Krebs and Dl, "Hybrid solar cells based on MEH-PPV and thin film semiconductor oxides (TiO2, Nb2O5, ZnO, CeO(2)and CeO2-TiO2): Performance improvement during long-time irradiation", *Solar Energy Materials and Solar Cells*, **2006**, 90(14), 2076-2086.
51. M. Lira-Cantu, A. Chafiq, J. Faissat, I. Gonzalez-Valls and Y. H. Yu, "Oxide/polymer interfaces for hybrid and organic solar cells: Anatase vs. Rutile TiO(2)", *Solar Energy Materials and Solar Cells*, **2011**, 95(5), 1362-1374.
52. M. Lira-Cantu and F. C. Krebs, "Hybrid solar cells based on MEH-PPV and thin film semiconductor oxides (TiO2, Nb2O5, ZnO, CeO(2)and CeO2-TiO2): Performance improvement during long-time irradiation", *Solar Energy Materials and Solar Cells*, **2006**, 90(14), 2076-2086.
53. M. Lira-Cantu, F. C. Krebs, P. Gomez-Romero and S. Yanagida, "Conjugated polymers as part of multifunctional organic/inorganic hybrid materials for photovoltaic applications", *Organic/Inorganic Hybrid Materials - 2007*, **2008**, 1007, 249-257.
54. M. Lira-Cantu, K. Norrman, J. W. Andreasen, F. C. Krebs and Nw, "Oxygen release and exchange in niobium oxide MEHPPV hybrid solar cells", *Chemistry of Materials*, **2006**, 18(24), 5684-5690.
55. K. Norrman, M. V. Madsen, S. A. Gevorgyan and F. C. Krebs, "Degradation Patterns in Water and Oxygen of an Inverted Polymer Solar Cell", *Journal of the American Chemical Society*, **2010**, 132(47), 16883-16892.
56. K. Norrman, S. A. Gevorgyan and F. C. Krebs, "Water-Induced Degradation of Polymer Solar Cells Studied by (H2O)-O-18 Labeling", *Acs Applied Materials & Interfaces*, **2009**, 1(1), 102-112.
57. M. Hermenau, M. Riede, K. Leo, S. A. Gevorgyan, F. C. Krebs and K. Norrman, "Water and oxygen induced degradation of small molecule organic solar cells", *Solar Energy Materials and Solar Cells*, **2011**, 95(5), 1268-1277.

Chapter 6
Experimental Section

6.1 Materials

All chemicals were commercially available and used without further purification.

6.1.1 Solvents: Methanol (99.8% Aldrich), ethanol (99.5% Panreac), 2-propanol or isopropanol (99.5% Sigma-Aldrich), acetone (99.5% Panreac), chlorobenzene (99.9% Sigma-Aldrich), 2-(2-methoxyethoxy) acetic acid (MEA) (technical grade Aldrich), chloroform ($CHCl_3$) (≥99% Sigma-Aldrich), *m*-xylol or *m*-xylene (≥99% Sigma-Aldrich), hydrochloric acid fuming (37% Fluka), acetonitrile (ACN, 99.995% Panreac), valeronitrile (99.5%, Sigma-Aldrich), tert-buthyl alcohol (^tBuOH, 99.5% Sigma-Aldrich). All the aqueous solutions were prepared using double distilled and ion-exchange water.

6.1.2 Transparent conductive oxide (TCO) substrates: Indium-tin oxide (ITO) or Fluorinated indium tin-oxide (FTO) slides were purchased from SOLEMS. The ITO properties: R=30-50 ohms, ITO layer produced by sputtering 1000Å, 1.1 mm thick glass. The FTO properties: R=70-100 ohms, FTO layer produced by CVD 800Å, 1.1 mm thick glass. They were cleaned by standard procedures prior to use (sonication for 10 min with H_2O + soap, 2 x H_2O, acetone, and ethanol) and finally cleaned for 20 min in a UV-surface decontamination system (Novascan, PSD-UV) connected to an O_2 gas source.

6.1.3 Materials for the ZnO electrode preparation: Zinc acetate dehydrate (99% Riedel-de Haën), potassium hydroxide (KOH, Na<0.002% Fluka), hexamethylenetetramine (HMT) (99% Aldrich), zinc nitrate hexahydrate ($Zn(NO_3)_2{\cdot}6H_2O$) (98% Sigma–Aldrich), diethanolamine (≥98% Sigma–Aldrich). The reactor for the low-temperature hydrothermal method (LT-HM) was a glass PYREX® Screw Cap bottle (Sigma-Aldrich) and two different autoclave Parr Autodigestion Bombs with PTFE-liner of different capacities were used for the autoclave hydrothermal method (A-HM): 23 mL (model 4749, synthesis A-HM-1) and 45 mL (model 4744, synthesis A-HM-2).

6.1.4 Materials for the In_xS_y shell layer preparation: Indium (III) chloride (98% Aldrich) and sodium thiosulfate (≥98%, Sigma-Aldrich).

6.1.5 Dye-sensitized solar cells (DSC) materials: Iodolyte AN-50 (50 mM tri-iodide in acetonitrile), dye $(Bu_4N)_2Ru$ (debpyH)$_2$(NCS) (Ruthenium 535-bisTBA also known as N-719), Pt-paste Pt-catalyst T/SP and hot melt sealing foil (SX1170) were from Solaronix. The Pt source for the counter electrode preparation by electron beam physical vapor deposition (EBPVD) was 99.95% from Goodfellow (50 nm thickness). Organic dyes used: eosin B and Y (Panreac), D149 (Mitsubishi Paper Mills Limited) and mercury dibromofluorescein disodium salt or also known as mercurochrome (Sigma). The alternative electrolyte for the dye D149 was prepared with: iodine (I_2) (99.8% Sigma-Aldrich), 1-butyl-3-methylimidazolium (BMII) (98 % BASF), guanidine thiocyanate (GuSCN) (99% Sigma).

6.1.6 Polymer solar cells (PSC) materials: Zn powder (≥99%, Aldrich), poly(3,4-ethylenedioxythiophene)-poly(styrenesulfonate) (PEDOT:PSS from Agfa, Orgacon EL-P 5010) diluted with 2-propanol (2:1) with a viscosity around 200 mPa·s, polymer Poly(3-hexylthiophene) (P3HT, Sepiolid P200 from BASF), [60]PCBM (99% purchased from Solenne BV), silver flakes (≥99.9%, Aldrich).

6.2 Preparation and characterization of ZnO buffer-seeds layer

6.2.1 ZnO buffer layer preparation: ZnO electrodes were prepared on FTO and ITO slides (Solems). First, A ZnO buffer layer of about 80-100 nm thick was prepared by spin coating a sol-gel layer of ZnO on top of the clean TCO slides. The sol-gel was prepared using the method previously reported.[1, 2] Briefly, 2.0 g of zinc acetate and 1.07 g of diethanolamine (DEA) were dissolved in 10 mL of isopropanol and heated at 60°C for about 10 min until total dissolution. Then, the solution was diluted with ethanol (1:1) and filtered through a 0.45 μm filter pore (Albet).This sol-gel solution was spin-coated on the TCO substrates and finally the substrates annealed at 450°C for 2 h (heating ramp 3°C/min).

6.2.2 ZnO seed layer preparation: ZnO nanoparticles (NP) were used as seeds to grow the ZnO NRs, and were deposited on top of the buffer layer prepared before. The NPs were synthesized by Pacholski *et. al.* method:[3] a solution of 0.03 M KOH was added dropwise in a refluxing mixture of zinc acetate 0.01 M in methanol at 65°C. After 2 h of reflux, the

solution was allowed to cool down. Then the ZnO NPs were spin spin-coated at 1000 rpm on top of the ZnO buffer layer, between layers the slides were dried at 150ºC for 10 min.[4]

6.2.3 Characterization instruments

Transmission electron microscopy (TEM, 120 kV-JEOL 1210 equipped with Energy dispersive X-rays spectroscopy EDS analyzer LINK QX 2000 X).

6.3 Preparation and characterization of ZnO NRs by the LT-HM

The growth of ZnO NRs by the low temperature hydrothermal method (LT-HM) was carried out in an equimolar aqueous solution of 25 mM zinc nitrate hexahydrate and HMT at 96ºC between 1h and 28h. The aqueous solution was changed every 4-6 hours. A PYREX® Screw Cap bottle was used as the growth reactor. The substrates with the ZnO buffer and seed layer from section 6.2 were placed up-side down, the distance between the substrate and the bottom of the flask was optimized. Handmade plastic supports to place the substrates up-side down in the reactor were made with 3 positions between 6 and 8 cm from the bottom of the flask. Since thermal treatment to the as-synthesized electrodes is known to improve power conversion efficiency, the samples were rinsed with deionized water, dried under N_2 and sintered at 450ºC for 30 min. The ZnO NR synthesis can be made on indium-tin oxide (ITO) or fluorinated indium-tin oxide (FTO) without affecting the final NR dimensions or properties. Nevertheless, since ITO conductivity is well known to be susceptible to temperatures above 450°C, the FTO slides were used to growth the NRs and applied as electrodes in dye-sensitized solar cells (DSC) and polymer solar cells (PSC).[4-6]

6.3.1 Characterization instruments

Scanning electron microscopy (SEM, HITACHI-S-570 and QUANTA FEI 200 FEG-ESEM equipped with Energy dispersive X-rays spectroscopy EDS analyzer detector Oxford INCA).

Transmission electron microscopy (TEM, 120 KV- JEOL 1210 equipped with EDS analyzer LINK QX 2000 X and 200 kV JEM 2011 equipped with EDS detector Oxford Linca).

X-ray powder diffraction (XRD) analyses between 5 and 120 degrees were carried out in a RIGAKU Rotaflex RU200 B instrument, using $CuK\alpha_1$ radiation.

Profilometry measurements were performed with Dektak 3030 from Berkeley basic.

AFM measurements were performed to determine the Pt thickness using the microscope: Agilent 5500 AFM/SPM microscope, formerly Molecular Imaging PicoPlus AFM, from Agilent Technologies. The measurements were carried out with the large scanner. Additionally, Agilent 5500 is equipped with an X-Y nanopositioning stage designed to integrate with Agilent's 5500 microscope (NPXY100E from nPoint, USA) that utilizes closed-loop capacitive feedback to ensure scanning linearity and position accuracy.

Room-temperature photoluminescence (PL) measurements were made with a Kimmon IK Series He-Cd CW laser (325 nm and 40 mW). Fluorescence was dispersed through an Oriel Corner Stone 1/8 74000 monochromator, detected with a Hamamatsu R928 photomultiplier, and amplified through a Stanford Research Systems SR830 DSP Lock-in amplifier.

The time resolved photoluminescence (TRPL) was carried out with a micro-PL setup to ensure that only a couple of nanowires were excited within the laser spot and, thus, to avoid inhomogeneous broadening in the photoluminescence spectra. Up to 10 different spots were investigated in each sample for statistical purposes. The excitation energy was set to 4.66 eV (266 nm) and focused onto the samples using a 20 (NA= 0.4) microscope objective, mounted on a XYZ piezoelectric stage, which allowed minimum steps of 100 nm. The spatial resolution of the system is estimated to be about 1 μm. In this set up, PL and TRPL measurements were performed using the fourth harmonic of a Nd:YAG Coherent laser as excitation source with a quasi-cw power of about 100 μW and pulse widths of 20 ps. A Hamamatsu microchannel- plate (MCP) was employed as detector for the PL and TRPL measurements. For the TR measurements we used the time-correlated single-photon counting technique with a lower time resolution of about 20 ps.

6.4 Preparation and characterization of ZnO electrodes by the A-HM

ZnO nanostructured electrodes were also synthesized by an autoclave hydrothermal method (A-HM). The difference between the LT-HM and the A-HM is the pressure added into the synthesis when an autoclave reactor is used. Two autoclave reactors for the A-HM synthesis were applied, a 4749 (synthesis 1) and another 4744 (synthesis 2) both Parr Autodigestion Bombs with PTFE-liner. The substrates FTO/ZnO buffer-seeds layer (from section 6.2) were placed up-side down inside the PTFE liner reactor using the same 25 mM equimolar solution of $Zn(NO_3)_2$ and HMT at 150°C between 6h and 28h. The pressure during the growth process inside the autoclave reactor was approximately $1.2 \cdot 10^7$ Pa. The distance between the substrate and the bottom of the flask was kept at 1 cm (synthesis A-HM-1) and 2.5 cm (synthesis A-HM-2). After the growth synthesis, the slides were rinsed with deionized water, dried under N_2 and sintered at 450ºC for 30 min.[7]

6.4.1 Characterization instruments.

Scanning electron microscopy (SEM, QUANTA FEI 200 FEG-ESEM equipped with Energy dispersive X-rays spectroscopy EDS analyzer detector Oxford INCA)

Transmission electron microscopy (TEM, 200 kV JEM 2011 equipped with EDS detector Oxford Linca).

X-ray powder diffraction (XRD) analyses between 5 and 120 degrees were carried out in a RIGAKU Rotaflex RU200 B instrument, using $CuK\alpha_1$ radiation.

Profilometry measurements were performed with Dektak 3030 from Berkeley basic.

Room-temperature photoluminescence (PL) measurements were made with a Kimmon IK Series He-Cd CW laser (325 nm and 40 mW). Fluorescence was dispersed through an Oriel Corner Stone 1/8 74000 monochromator, detected with a Hamamatsu R928 photomultiplier, and amplified through a Stanford Research Systems SR830 DSP Lock-in amplifier.

The time resolved photoluminescence (TRPL) was carried out with a micro-PL setup to ensure that only a couple of nanowires were excited within the laser spot and, thus, to avoid inhomogeneous broadening in the photoluminescence spectra. Up to 10 different

spots were investigated in each sample for statistical purposes. The excitation energy was set to 4.66 eV (266 nm) and focused onto the samples using a 20 (NA= 0.4) microscope objective, mounted on a XYZ piezoelectric stage, which allowed minimum steps of 100 nm. The spatial resolution of the system is estimated to be about 1 μm. In this set up, PL and TRPL measurements were performed using the fourth harmonic of a Nd:YAG Coherent laser as excitation source with a quasi-cw power of about 100 μW and pulse widths of 20 ps. A Hamamatsu microchannel- plate (MCP) was employed as detector for the PL and TRPL measurements. For the TR measurements we used the time-correlated single-photon counting technique with a lower time resolution of about 20 ps.

Attenuated total reflectance infrared (ATR-FTIR) spectroscopy of the powder dye N719 and the FTO/ZnO NR-dye N719 substrates were measured using a Perkin Elmer spectrometer, doing 10 min scans for the substrates and 32 scans for the powder dye N719 in the range of 600-4000 cm^{-1}.

6.5 Preparation and characterization of the In_xS_y shell layer

A core-shell structure of ZnO NR/In_xS_y was synthesized. The In_xS_y layer was deposited following the Successive Ion Layer Absorption and Reaction (SILAR) technique reported by T. Dittrich *et. al.*[8] The ZnO electrodes are dipped first in $InCl_3$ aqueous solution then in Na_2S aqueous solution and at the end in distilled water to do a SILAR cycle. The concentration of the $InCl_3$ solution was maintained at 0.1 M and two different Na_2S solution concentrations were used: 0.03 M and 0.15 M. The pH of the Na_2S solution was controlled between 7-8 adjusted with a 0.2 M solution of HCl. Different shell layer thicknesses were prepared by the SILAR method applying 3, 5, 10, 15, 20 and 40 cycles. After the shell deposition, the substrates were dried with N_2 and annealed at 200ºC for 30 min. The ZnO electrodes used for the core-shell fabrication were the following: electrodes grown by the LT-HM (section 6.3) for 6h-electrode A, 12h-electrode B, 22h-electrode C and grown by the A-HM (section 6.4) for 6h-electrode D, 12h-electrode E and 28h-electrode F.[9]

6.5.1 Characterization instruments

Scanning electron microscopy (SEM, QUANTA FEI 200 FEG-ESEM, equipped with EDS detector Oxford INCA)

Transmission electron microscopy (TEM, 200 KV- JEM 2011 equipped with EDS detector Oxford LINCA).

X-ray powder diffraction (XRD) analyses between 5 and 120 degrees in a RIGAKU Rotaflex RU200 B instrument, using CuKα_1 radiation.

Attenuated total reflectance infrared (ATR-FTIR) spectroscopy of the powder scratched ZnO NR and the core-shell ZnO/In_xS_y powder were measured using an instrument Tensor 27 from Brüker. The measures were made with 32 scans, resolution of 4 cm^{-1} in the range of 550-4000 cm^{-1}.

6.6 Dye-sensitized solar cells preparation and characterization

The FTO/ZnO nanostructured electrodes prepared by the LT-HM (section 6.3), the A-HM (section 6.4) and the core-shell ZnO/In_xS_y electrodes (section 6.5) were applied in dye-sensitized solar cells (DSC). First, they were sensitized in a 0.5 mM/L solution of $(Bu_4N)_2Ru(debpyH)_2(NCS)$ (N-719 dye) at different times and temperatures in order to obtain the optimal dye loading conditions. Platinized FTO counter electrode was prepared with the Pt-catalyst by doctor blade and annealed at 450ºC/30 min (2 thicknesses, 50 nm and 60 nm). The doctor blade technique or also known as tape casting is a widely used technique to prepare thin films on large areas. This technique consists of coating a paste on a substrate fixed by tape. The film thickness depends on the thickness of the tape. When 1 tape was used a Pt layer of 50 nm was obtained and for 2 tapes, the Pt thickness was 60 nm. Another platinized FTO counter electrode was applied in DSCs, the Pt was evaporated on the FTO substrates by electron beam physical vapor deposition (EBPVD) (thicknesses: 20 nm, 50 nm, 100 nm and 150 nm). Then, the ZnO electrodes and the Pt counter electrodes were bounded thermally together using a hot melt sealing foil. The liquid electrolyte was introduced through a small hole on the Pt counter-electrode by capillary forces applying vacuum. Finally, the DSCs were hermetically sealed with a small piece of glass to close the filling hole.[4-6, 9] Different organic dyes were used. All the dye concentrations were 0.5 mM in ethanol for Eosin Y and Eosin B, methanol for Mercurochrome and acetonitrile (ACN)/tert-buthyl alcohol (^{t}BuOH) 1:1 for D149. The dye D149 was applied in DSC using another electrolyte that was prepared with 0.6 M BMII, 0.03 M I_2 and 0.1 M GuSCN in a solvent mixture of ACN/valeronitrile (85:15).[10]

6.6.1 Characterization instruments

The solar simulation at CIN2 was carried out with a Steuernagel Solarkonstant KHS1200 equipped with an AM1.5 filter for all characterisation (1000 W/m^2, AM1.5G, 72ºC). The calibration was made according to ASTM G173. IV-curves were measured using a Keithley 2601 multimeter. Light intensity was 1000W/m^2 calibrated, a Zipp & Konen CM-4 pyrometer is used constantly during measurements to set light intensity and a calibrated S1227-1010BQ photodiode from Hamamatsu is also applied for calibration before each measurement.

IPCE analyses were carried out with a QE/IPCE measurement System from Oriel at 10 nm intervals between 300 and 700 nm. The results were not corrected for intensity losses due to light absorption and reflection by the glass support.

Measurements at different conditions were carried out in a home-made solar cell holder as described in reference.[11] The solar cell holder is a two-piece glass reactor with a cooling jacket for temperature control, with a home-designed o-ring sealed cap. It has ports for thermocouple, inlet and outlets for low pressure gas flow, quartz window (5 cm diameter) and cable connections (see Figure 6.1). An UV Filter can be placed on top of the quartz window. The holder can analyze up to two 1 cm by 2.5 cm solar cells, but larger reactors, with 15 cm diameter quartz window, can hold larger solar cells.[11] The temperature of the experiments was monitored with a digital thermo hygrometer (HD2301/01, Afora). Measurements were carried at temperatures between 25º to 75º C with incident power light variation from 800 to 1800 W/m^2. Moreover, measurements with and without a UV-light filter (< 400 nm, Thorlabs) were also carried out. Before measurements, cells were allowed to stabilize at the desired temperature for 10 min and for 5 min more at each incident light. All the DSCs were carefully sealed to avoid electrolyte losses and device degradation.

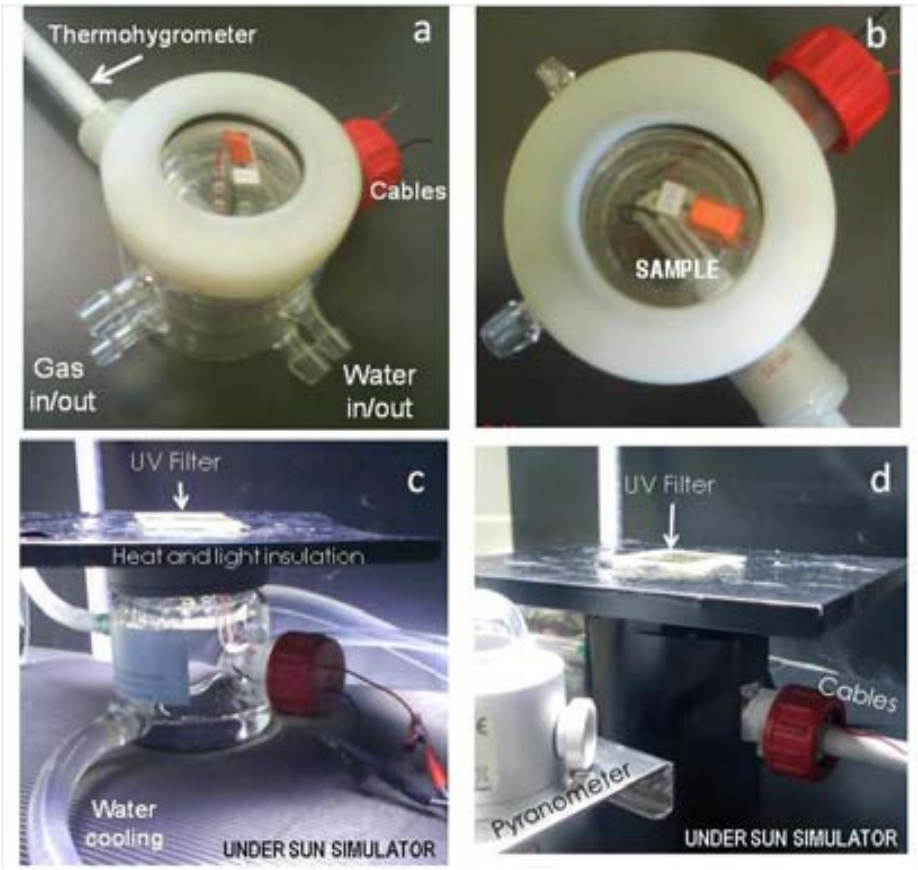

Figure 6.1 Home-made glass reactor with a cooling jacket for water cooling, thermo hygrometer and UV Filter included. a) Side View, b) Top view, c) and d) different configurations mounted under the sun simulator.[11]

UV-Visible analyses of solutions and thin films were made in a Shimadzu 1800 spectrophotometer. Desorption of the dye from the ZnO electrode was performed after DSC fabrication and characterization. The two electrodes were separated by applying heat and then the ZnO electrode was immersed in a basic 1 mM KOH aqueous solution until total dye desorption. The indication of the effective dye desorption is when the ZnO electrode appeared colourless and the solution presented a pink colour from the dye. Then, the solution was measured by UV-vis absorption. The quantity of dye adsorbed on the surface of the ZnO electrode was measured.[12]

6.7 Polymer solar cells preparation and characterization

Two third parts of the FTO conductive layer were covered with tape to be protected and the other third part was etched with Zn powder and a 2M HCl solution. Then, the substrates were rinsed with water and cleaned by standard procedures prior to use (sonication for 10 min with H_2O + soap, 2 x H_2O, acetone and ethanol). The electrodes were then covered with a ZnO buffer layer prepared by sol-gel solution and the ZnO seeds layer as described in section 6.2. Then the ZnO NR and NTr were prepared with and without In_xS_y layer (see section 6.3, 6.4 and 6.5). The ZnO electrodes were annealed at 140°C for 5 minutes before the active layer solution P3HT:PCBM was spin-coated on top (some drops of chlorobenzene were added on the ZnO electrode to improve the adherence). The concentrations of the P3HT:PCBM blends were, 24:24 mg/mL, 40:24 mg/mL and 40:40 mg/mL using different solvents (chlorobenzene, chloroform or *m*-xylol). The active layer solution was placed on top of the FTO/ZnO substrate before the spin coater was started. The spinning speeds used for blend deposition were 1500 rpm, 800 rpm, 400 rpm and 2 x 400 rpm. The following step was the deposition of the hole transport layer, PEDOT:PSS. The solution was spin coated at 1000 rpm after a pretreatment of the surface with isopropanol to improve adhesion. The substrate was then annealed at 140°C for 5 minutes. The silver counter-electrode was deposited by vacuum evaporation at a $\sim 10^{-6}$ Torr pressure. The extra active area from outside the silver deposited counter-electrode was scratched and cleaned with chlorobenzene and 2-propanol to remove the organic components. Active areas were around ~0.25-0.3 cm^2 (after scratch).[13]

6.7.1 Characterization instruments

Cross-section images of the PSCs were carried out in a scanning electron microscopy (SEM) (QUANTA FEI 200 FEG-ESEM equipped with and Oxford Inca Energy Dispersive X-ray spectroscopy (EDS) analyzer).

A solar simulator KHS 575 providing AM1.5G illumination (1000 $W \cdot m^{-2}$, 49°C) from Steuernagel Lichttechnik GmbH was used for the solar cell characterization. The intensity was calibrated using a reference diode. A Keithley 2400 source-measure unit was used for the IV-characteristics.

IPCE measurements were recorded using a solar cell spectral response measurement system model QEX10 from PV measurements, Inc. The instrument uses a xenon arc lamp source, monochromator, filters and reflective optics to provide stable monochromatic light to a photovoltaic test device. A broadband bias light also illuminates the test device to simulate end-use conditions. The system uses a detection circuit designed to maximize measurement speed and accuracy in solar cell research.

6.8 References

1. M. Lira-Cantu, F. C. Krebs and Dl, "Hybrid solar cells based on MEH-PPV and thin film semiconductor oxides (TiO2, Nb2O5, ZnO, CeO(2)and CeO2-TiO2): Performance improvement during long-time irradiation". *Solar Energy Materials and Solar Cells* **2006,** 90 (14), 2076-2086.
2. M. H. Aslan, A. Y. Oral, E. Mensur, A. Gul, E. Basaran and Ap, "Preparation of c-axis-oriented zinc-oxide thin films and the study of their microstructure and optical properties". *Solar Energy Materials and Solar Cells* **2004,** 82 (4), 543-552.
3. C. Pacholski, A. Kornowski and H. Weller, "Self-assembly of ZnO: From nanodots, to nanorods". *Angewandte Chemie-International Edition* **2002,** 41 (7), 1188-1191.
4. I. Gonzalez-Valls, Y. Yu, B. Ballesteros, J. Oro and M. Lira-Cantu, "Synthesis conditions, light intensity and temperature effect on the performance of ZnO nanorods-based Dye sensitized solar cells". *Journal of Power Sources* **2011,** 196, 6609–6621.
5. I. Gonzalez-Valls and M. Lira-Cantu, "Dye sensitized solar cells based on vertically-aligned ZnO nanorods: effect of UV light on power conversion efficiency and lifetime". *Energy & Environmental Science* **2010,** 3 (6), 789-795.
6. I. Gonzalez-Valls and M. Lira-Cantu, "Effect of testing conditions on the photovoltaic performance of ZnO-based dye sensitized solar cells". In *Vi Encuentro Franco-Espanol De Quimica Y Fisica Del Estado Solido - Vi Rencontre Franco-Espagnole Sur La Chimie Et La Physique De L Etat Solide*, J. J. Carvajal,M. AguiloandF. Diaz, Eds. **2010**; Vol. 8, pp 28-32.
7. I. Gonzalez-Valls, J. S. Reparaz, F. Güell, M. R. Wagner, G. Callsen, B. Ballesteros, A. Hoffmann and M. Lira-Cantu, "Low temperature growth of vertically-aligned ZnO nanorods for dye sensitized solar cells: unravelling their low power conversion efficiency". *Nano Letters* **2012**, submitted.
8. C. Herzog, A. Belaidi, A. Ogacho and T. Dittrich, "Inorganic solid state solar cell with ultra-thin nanocomposite absorber based on nanoporous TiO(2) and In(2)S(3)". *Energy & Environmental Science* **2009,** 2 (9), 962-964.
9. I. Gonzalez-Valls, B. Ballesteros and M. Lira-Cantu, "Innovative vertically-aligned ZnO Nanorods – Indium sulfide core-shell with enhanced performance in Dye-sensitized Solar Cells". **2012,** In preparation.
10. Y. Xie, P. Joshi, S. B. Darling, Q. L. Chen, T. Zhang, D. Galipeau and Q. Q. Qiao, "Electrolyte Effects On Electron Transport and Recombination at ZnO Nanorods for Dye-Sensitized Solar Cells". *Journal of Physical Chemistry C* **2010,** 114 (41), 17880-17888.
11. M. Lira-Cantu, A. Chafiq, J. Faissat, I. Gonzalez-Valls and Y. H. Yu, "Oxide/polymer interfaces for hybrid and organic solar cells: Anatase vs. Rutile TiO(2)". *Solar Energy Materials and Solar Cells* **2011,** 95 (5), 1362-1374.
12. N. R. Neale, N. Kopidakis, J. van de Lagemaat, M. Gratzel and A. J. Frank, "Effect of a coadsorbent on the performance of dye-sensitized TiO2 solar cells: Shielding versus band-edge movement". *Journal of Physical Chemistry B* **2005,** 109 (49), 23183-23189.
13. I. Gonzalez-Valls, D. Angmo, S. A. Gevorgyan, J. S. Reparaz, F. C. Krebs and M. Lira-Cantu, "Comparison of two types of vertically-aligned ZnO NRs for highly efficient polymer solar cells". *Journal of Polymer Science Part B: Polymer Physics* **2012,** submitted.

Chapter 7

General Overview and Conclusions

The thesis work described in this manuscript encompasses partial conclusions and results about different nanostructured materials based on vertically-aligned ZnO nanorods and their application in Dye sensitized solar cells and Organic solar cells. This chapter summarizes the general conclusions for each chapter, and gives a brief discussion on the most significant results obtained. We also present the future work that can lead to more significant and interesting results or that could support the work presented here.

7.1 Solution processed water-based ZnO Nanorods

The initial aim of this work was focused on the synthesis of ZnO NR. We chose this material due to the need for photoactive electrodes for excitonic solar cells able to be obtained by low-temperature, water-based and solution processable methods. These characteristics are highly compatible with high speed fabrication; large area and low-cost production of excitonic solar cells (Dye sensitized solar cells and organic solar cells). Moreover, the possibility to obtain ZnO as nanorods (NRs) in a vertically-aligned architecture, added up to the requirements of high power conversion efficiency, since NRs were known for their good electron transport (in comparison with other nanostructures, like nanoparticles). Throughout the experimental work developed in this thesis, we found out that many are the parameters required for the optimization of the synthesis of the ZnO NRs and that it is critical the careful optimization of the synthesis methods for reproducibility. Surface quality of the ZnO NRs (as will be explained below) is observed to be highly important for good power conversion efficiency.

7.2 Surface quality of ZnO Nanorods and its effect on Dye sensitized solar cells

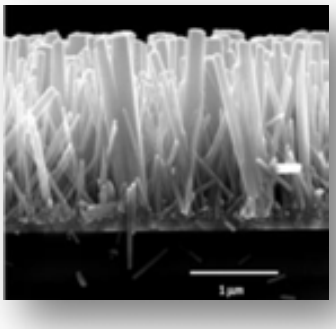

Only after a careful analysis of the literature on the photovoltaic properties of ZnO NRs obtained by the low-temperature hydrothermal method, we were able to realize that the synthesis methodology is an important factor in order to obtain high power conversion efficiency in DSCs. Surprisingly, our findings revealed that the lowest power conversion efficiency in DSC are obtained when the ZnO NRs are synthesized by the method employed in this work, the low temperature hydrothermal method (LT-HM), in comparison with other techniques like electrochemistry, vapor deposition, etc. A slight modification of the synthesis method, this is, the application of a pressurized autoclave during synthesis resulted in the modification of the final ZnO NR quality improving the power conversion efficiency of the final DSC. PL and TRPL analysis showed that many are the possible parameters that affect the final quality of the NRs during synthesis, but low crystal quality is in all cases observed. The surface of the ZnO NRs obtain by the LT-HM are characterized by high amount of surface defects, like oxygen vacancies or similar resulting in low power conversion efficiency. Unfortunately, the later means that this method is probably not the best choice for the fabrication of vertically aligned ZnO NRs for excitonic solar cells. The high amount of surface defects are recombination centers, thus the obtained electrodes could probably be more suitable for other optoelectronic applications like OLEDS.

7.3 New ZnO Nanostructure: Nanotrees

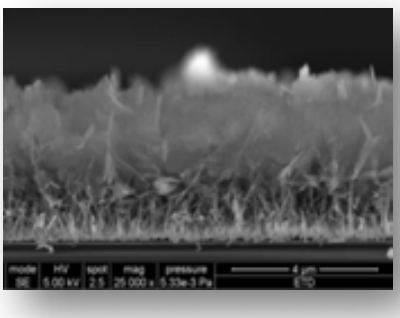

A different strategy was employed in order to improve the power conversion efficiency of the DSC applying vertically aligned ZnO NRs: the surface area of the electrode was increase. To do this, the opening of the top of the NR by a modification of the synthesis method was possible and a true enhancement of the power conversion efficiency was achieved. We called the new nanostructure “nanotree” due to its physical similarity with a real tree. The new

nanostructure was observed to be beneficial for the enhancement of the power conversion efficiency of excitonic solar cells where a liquid electrolyte was used like in a Dye sensitized solar cells. Yet, it was a disadvantage for solar cells where a viscous active layer is used, like in an organic solar cell, due to infiltration problems of the active polymeric layer.

7.4 Core-shell inorganic nanostructures for ZnO Nanorods: Oxide vs. hydroxide shells

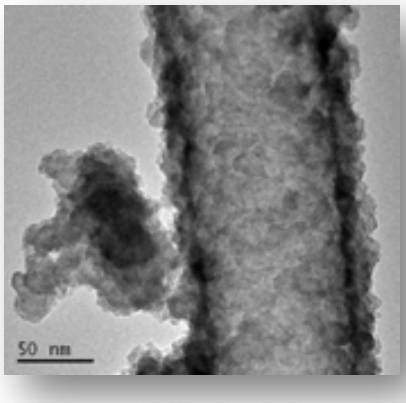

The best power conversion efficiency was obtained when a thin shell layer of an inorganic material based on Indium Sulfide was applied on the ZnO NR surface. The composition of the shell layer was tuned by the variation of the reactants used during synthesis. Thus, the inorganic shell composition was varied from high S content, In_2S_3, to its low S-content and hydroxide form, $In(OH)_xS_y$. The composition with higher amount of –OH and low -S content resulted in the highest power conversion efficiency of 2.3 % for a 3 μm NR length. The good response was attributed to two main factors:

1) The thin shell layer of a few nm, together with the wide band gap value of the hydroxide of more than 5 eV, are two characteristics that permit the shell layer to act as an insulating layer, similar to the application of oxide barrier layers in Dye sensitized solar cells, probably reducing the recombination rate.
2) The higher amount of –OH sites available in the shell layer of the ZnO can be used as linkers between the oxide and the N719 Dye, increasing the amount of dye adsorbed.

7.5 Future work

This thesis work has been focused on the synthesis of different ZnO nanostructures and their application in excitonic solar cells. The work for the future must be focused on more specialized characterization of the electrodes applying well-known physical or physicochemical techniques such as impedance spectroscopy, electron lifetime, transient spectroscopy, XPS, UPS, etc. Especially for the electrodes made by core-shell materials, that resulted in the highest power conversion efficiency. We expect that these analyses, together with the results obtained with these techniques, will permit to prove the idea of the application of the electrodes in different optoelectronic devices like OLEDS, or small molecule Organic solar cells. Moreover, there is much to be done with respect to the application of these electrodes with different dyes in Dye sensitized solar cells or their possible application in solid state dye sensitized solar cells.

7.6 Conclusions

The objectives of this thesis: study of vertically-aligned ZnO nanostructures and their application in excitonic solar cells (XSC) have been achieved. The syntheses of the different ZnO nanostructures: two types of nanorods (NR), nanotrees (NTr) and core-shell ZnO/In_xS_y (CS) structures have been studied, together with their full characterization:

- The low-temperature hydrothermal method (LT-HM) was used to prepare ZnO NR electrodes. The effect of different synthesis conditions were studied on the obtained NRs. The NR length and diameter were controlled modifying the synthesis growth time.

- A modified synthesis method, autoclave hydrothermal method (A-HM), was introduced. The NRs obtained with the A-HM had different morphologies than by the LT-HM, they were shorter for the same growth time and had a needle top shape. A new nanostructure was obtained after 28h growth time, ZnO nanotrees (NTr).

- A shell layer of In_xS_y was deposited on top of the ZnO NRs and NTrs. These core-shell In_xS_y layers were prepared by a low-cost synthesis method: the successive ion layer adsorption and reaction (SILAR) method. Two different Na_2S concentrations and SILAR cycles were applied on the vertically-aligned ZnO nanostructures.

- All these ZnO nanostructures were characterized by SEM, TEM, XRD, UV-vis, ATR-FTIR, PL and TRPL measurements. The ZnO nanostructures had a wurtzite hexagonal crystalline structure. Different surface properties were observed for the LT-HM and the A-HM. Lower surface defects were measured and longer free exciton lifetimes for the A-HM electrodes on the A-HM electrodes.

The vertically-aligned ZnO nanostructures were applied in Dye-sensitized solar cells (DSC) and Polymer solar cells (PSC). The solar cells parameters were optimized in order to enhance the power conversion efficiency. **Error! Reference source not found.** shows the highest power conversion efficiencies obtained in DSC and PSC applying the different ZnO nanostructures.

- In both types of XSCs, the CS electrodes achieved the highest performance, 2.1% in PSC and 2.3% in DSC. The CS structures acted as blocking electron barrier, helping the electron transport and avoiding the electron recombination.

- The application of the modified NRs using the A-HM improved the solar cell performance for both XSCs even though these NR lengths were shorter than the obtained by the LT-HM (see Figure 7.1).

- The effect of several testing parameters such as temperature was analyzed on the ZnO NRs based DSCs prepared by the LT-HM. The application of UV-light irradiation showed a large dependence on the power conversion efficiency due to the surface defects present on the ZnO structure that modified the ZnO-dye interaction.

- The NTrs enhanced the DSC performance but decreased the PSC performance. The latter was attributed to the top structure that avoided the polymer blend infiltration in PSCs and thus, reduced the power conversion efficiency.

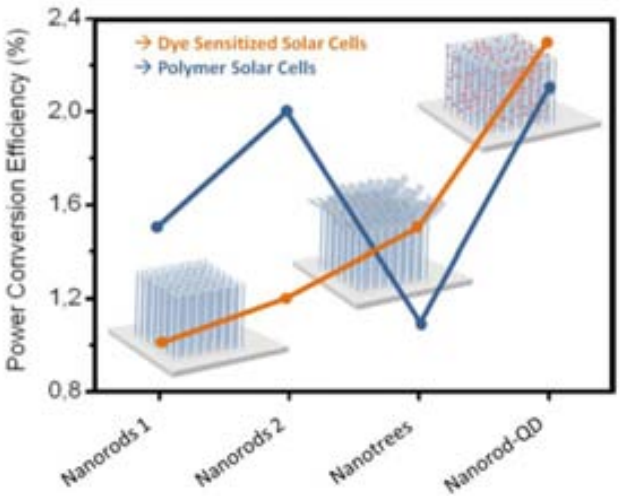

Figure 7.1 DSC and PSC power conversion efficiency vs. the ZnO nanostructure.

List of Publications/Awards

Journal articles:

1- Vertically-aligned nanostructures of ZnO for excitonic solar cells: a review

I. Gonzalez-Valls and M. Lira-Cantu

Energy Environ. Sci., **2009**, 2, 19-34.

2- Dye-sensitized solar cells based on vertically-aligned ZnO nanorods: effect of UV light on power conversion efficiency and lifetime

I. Gonzalez-Valls and M. Lira-Cantu

Energy Environ. Sci., **2010**, 3, 789-795.

3- Synthesis conditions, light intensity and temperature effect on the performance of ZnO nanorods-based Dye sensitized solar cells

I. Gonzalez-Valls, Y. Yu, B. Ballesteros, J. Oro and M. Lira-Cantu

J. Power Sources, **2011**, 196, 6609-6621.

4- Aligned TiO_2 nanocolumnar layers prepared by PVD-GLAD for transparent dye sensitized solar cells

L. González-García, I. Gonzalez-Valls, M. Lira-Cantu, A. Barranco and A. R. González-Elipe

Energy Environ. Sci., **2011**, 4, 3426-3435.

5- A clean Low-Temperature ZnO Deposition Method for Multipourpose Applications

M. Estruca, I. Gonzalez-Valls, C. Domingo, M. Lira-Cantu and J. A. Ayllón

Eur. J. Inorg. Chem., **2011**, 281-285.

6- Oxide/polymer interfaces for hybrid and organic solar cells: Anatase vs. Rutile TiO_2

M. Lira-Cantu, A. Chafiq, J.Faissat, I.Gonzalez-Valls and Y. Yu

Solar Energ. Mater. & Solar Cells, **2011**, 95, 1362-1374.

7- Comparison of two types of vertically-aligned ZnO NRs for highly efficient Polymer Solar Cells

I. Gonzalez-Valls, D. Angmo, S. A. Gevorgyan, J.S Reparaz, F. C. Krebs and M. Lira-Cantu. *J. Pol. Sci. Part B: Physics,* **2013**, Volume 51, Issue 4, pages 272–280, 15 February 2013

8- An evaluation of low-cost upscaling compatibility of five different ITO-free architectures for polymer solar cells: a comparative study based on photovoltaic properties, stability, and processing

D. Angmo, I. Gonzalez-Valls, S. Veenstra, W. Verhees, S. Sapkota, S. Schiefer, B. Zimmermann, Y. Galagan, J. Sweelssen, M. Lira-Cantu, R. Adriessen, J. M. Kroon and F. C. Krebs

J. App. Pol. Sci., **2013**, DOI: 10.1002/APP.39200. On line.

9- Low temperature hydrothermal growth of Vertically-aligned ZnO Nanorods for Dye sensitized solar cells: unraveling their low power conversion efficiency

I. Gonzalez-Valls, J. S. Reparaz, F. Güell, M. R. Wagner, G. Callsen, B. Ballesteros, A. Hoffmann and M. Lira-Cantu

Submitted, **2013**.

10- Innovative vertically-aligned ZnO Nanorods/In_xS_y core-shell with enhanced performance in Dye-sensitized Solar Cells

I. Gonzalez-Valls, B. Ballesteros and M. Lira-Cantu

In preparation

11- A novel ZnO nanostructure with an improved performance in Dye-sensitized solar cells: ZnO Nanotrees

I. Gonzalez-Valls, B. Ballesteros, F. Güell and M. Lira-Cantu

In preparation

Book Chapter:

12- Nanomaterials for Solar Cells

M. Lira-Cantu and I. Gonzalez-Valls

Encyclopedia of Nanotechnology, **2012**, Editorial Springer, B. Bhushan (editor), volume 1, in press. DOI 10.1007/978-90-481-9751-4.

Proceedings:

13- Effect of testing conditions on the photovoltaic performance of ZnO-based dye sensitized solar cells

I. Gonzalez-Valls and M. Lira-Cantu

Physics Procedia, **2010**, 8, 28-32.

14- Comparison of different vertically aligned ZnO nanostructures in excitonic solar cells: nanorods, nanocore-shells and nanotrees

I. Gonzalez-Valls and M. Lira-Cantu

Proc. SPIE 8471, Next Generation (Nano) Photonic and Cell Technologies for Solar Energy Conversion III, 84710X, **2012**, doi:10.1117/12.929678.

Awards:

1- 2013 –Fundación Iberdrola Research award.

Project: Flexible Small Molecule Organic Solar Cells

2- 2012 – Materials Today. Online Poster award competition. Best poster award.

Modification of surface defects in vertically-aligned ZnO nanostructures to improve power conversion efficiency of excitonic solar cells.

Irene Gonzalez-Valls, Juan S. Reparaz, Frank Güell, Markus R. Wagner, Gordon Callsen, Belen Ballesteros, Axel Hoffmann, Monica Lira-Cantu

3- 2008 –Nanosmat 2008, Barcelona (Spain). Best Poster Award.

Sol-gel and Hydrothermal Synthesis of Thin Film Nanostructured Oxides for Emerging Photovoltaics.

Monica Lira-Cantu, Irene Gonzalez-Valls, et.al.

http://www.cin2.es/english/news-room-news.php?noticia=55&ano=2008&mes=All

4- 2012 Scholarship to assist at the conference Nanospain, Santander, España.

5- 2010 Scholarship to assist at the conference Hybrid and Organic Photovoltaics (HOPV), Assisi, Italia.

Other publication unrelated to this thesis:

1- "Helter-Skelter-Like" Perylene Polyisocyanopeptides

E. Schwartz, V. Palermo, C. E. Finlayson, Y. S. Huang, M. B. L. Otten, A. Liscio, S. Trapani, I. Gonzalez-Valls, P. Brocorens, J. Cornelissen, K. Peneva, K. Mullen, F. C. Spano, A. Yartsev, S. Westenhoff, R. H. Friend, D. Beljonne, R. J. M. Nolte, P. Samori and A. E. Rowan

Chem. -Eur. J., **2009**, 15, 2536-2547.

Acknowledgements

The work presented in this thesis wouldn't have been possible without the help of many people. A PhD thesis is a road which we never walk alone. Sometimes it has many difficult obstacles or we need to be strong enough to climb high mountains. Other times, the way goes down with a wonderful landscape. In all those moments there is always someone by your side to support you on the hard times and someone you can share the happy moments with. Doing this PhD thesis was a wonderful experience for me and, although I sometimes wanted to quit, I'm glad now that I didn't do it. The PhD provided me with many different kinds of knowledge, not only about chemistry and science materials but also about how to deal with problems, how to present my work to others and something very important: it gave me the opportunity of meeting new people from other countries and of travelling to new places for conferences or experiments.

Primero quiero agradecer a mi directora de mi tesis, Mónica Lira Cantú, por darme la oportunidad de hacer esta tesis, por enseñarme tanto estos años y estar siempre disponible para solucionar los problemas. Hemos compartido muchos momentos importantes juntas, como montar el laboratorio en la ETSE o desmontarlo y trasladarlo al nuevo edificio, la llegada de nuevos estudiantes, conferencias…etc. Todos estos momentos los guardo en mi memoria como buenos recuerdos y experiencias vividas durante el doctorado. Uno de esos momentos que aprecio más es la dedicación con la que me ayudaste a preparar mi primera charla, gracias! Eres una persona a la que admiro por tener tantas buenas ideas y tanta energía para hacer nuevos proyectos. Gracias por todo, Mónica.

I gràcies també a la tutora de Tesis Maria Muñóz Tapia per avalar aquesta tesis.

This thesis was funded by the PhD scholarship BES-2009-028996 and the projects ENE2008-04373 (Nanostructured Materials for Organic Solar Cells) and Consolider NANOSELECT CSD2007-0041 from the Spanish Ministry of Science and Innovation, MICINN. Also other projects contributed: the Spanish National Research Council, CSIC, for the PIE-200860I134 (Synthesis and Characterization of Doped Oxides for Nanocrystalline Solar Cells) and XaRMAE of the Catalonia Government (Reference Center for Advanced Materials).

Durante estos años de doctorado he conocido mucha gente muy especial en el CIN2 (tanto del CSIC como del ICN) que me han ayudado mucho de diferentes formas.

Compañeros del grupo de los que muchos ya se han ido. A Roger, gràcies per compartir amb mi el primer any de doctorat, em vas ajudar molt en els primers passos de la tesis. A part de la feina també vam compartir molts bons moments amb la gent del ICMAB que guardo en la meva memoria con un tresor. A Natalia I. González, fuiste una buena compañera de trabajo y también una muy buena amiga y lo sigues siendo aunque estés tan lejos. Hecho de menos las risas en el laboratorio y más las risas fuera, eres una persona alegre y optimista a la que aprecio mucho. Siddiki, I remember you having always a smile on your face. With you, I've learnt a lot of things from your country and also your culture. I would specially like to thank Youhai Yu, you taught me many important things for my PhD. Your great experience was very helpful for all my work, thanks! I wish you a great success in your future job and life as well. A Gerardo que al hacer el doctorado en el mismo tiempo nos hemos ayudado mutuamente muchas veces y nos hemos turnado todos los equipos del laboratorio. Gerardo, gracias por ser tan paciente con todas mis preguntas y por pasar tanto tiempo discutiendo cosas del trabajo, ya te queda poco a ti también y seguro que todo te sale muy bien! A Roque, llegastes justo en el peor memento de mi tesis, cuando toca escribir y no morir en el intento, gracias por hacerme reir tantas veces y por ayudarme en todos los aspectos de la física que yo no sabía. Siempre tienes tiempo para escuchar y ayudar a los amigos y eso es algo que valoro mucho en una persona. Espero que sigamos en contacto y me vayas contando todas las novedades, y sobretodo espero que todo te salga bien, en lo profesional y personal. A Natalia Martínez, estuviste poco tiempo de visita pero fue suficiente para que nos hiciéramos amigas, ánimos en esta etapa de buscar trabajo! I would like to thank also all the French visiting students from ENSICAEN university: Jeremy Faissat, Amine Chafiq, Thomas Blevin, Löic Gros, David Beltrand and Aurelie Vanwaelscappel. I hope you had a good experience working in the laboratory with us. Also, I want to thank Jonas Pampel, I hope your PhD is going well in Dresden!

A los **colaboradores del grupo**. A José A. Ayllon y sus estudiantes Marc Estruga y también Pau Bosch de la Universitat Autonoma de Barcelona. Al grupo del Instituto de Materiales de Sevilla, Lola González, Ángel Barranco y Agustín R. Gonzalez-Elipe. Gracias Lola por todos los emails comentando cosas del trabajo y las medidas que hicimos juntas, al final salió una buena publicación! A Frank Güell de la Universitat de Barcelona per les mesures de photoluminiscencia, gràcies per explicarme el funcionament i fer-me entendre el significat del que obteniem. A Sebas Reparaz del CIN2, por las medidas de Time-Resolved

PL. Gracias por todas tus explicaciones, estas medidas han sido muy útiles para entender la diferencia entre los dos tipos de síntesis de los nanorods.

Los amigos del Máster de Nanotecnología: Maria Guix, Joan Comenge, Lorena García, Míriam Varón, Carlos Carbonell, Cornelius Krull y Alfonso Alarcón. Empezamos juntos este camino del doctorado y hemos seguido compartiéndolo a lo largo de los años. Ahora algunos ya han acabado y otros estamos al final del trayecto pero espero que aunque después nuestros caminos se separen, sigamos en contacto y quizá compartamos otro tramo de camino en otro momento.

Al empezar el doctorado estuve unos meses en el **ICMAB**, cuando aún no teníamos laboratorio y allí conocí personas muy especiales que aunque después no estuvimos en el mismo edificio seguimos en contacto y siendo amig@s. Una de estas personas tan especial es Ana Lopez Periago, hemos compartido grandes experiencias juntas y siempre has estado a mi lado en los buenos y malos momentos, gracias! A Francesc, Costana, Ana Milena, Belencita, Nina, Javi, Laura, David, Jullieth, Nerea, Corina, Omar y a todos los que me olvido. Gracias por las cenas y la buena compañía! También agradecer a Trini y a toda la gente de administración por la ayuda en papeleos. En el primer año de doctorado en el ICMAB empecé a cantar en la coral, quiero agradecer al director de la coral Raúl y a todos los integrantes que compartimos un buen rato cantando, lástima que me faltara tiempo y lo dejara.

No puedo dejar de agradecer a los **amigos del CIN2** que compartimos cada día comidas y cafés durante el trabajo y más actividades fuera. A Sandra García, gracias por ser tan alegre y optimista, siempre tienes un buen plan o propuesta cultural, espero que todo te vaya muy bien en Francia. A Marta Gonzalez, tu energía y simpatía hacía las comidas muy divertidas, aunque ahora cada vez te vemos menos, gracias por todo! A Miguel Angel, la amistad y estima que te tengo no lo romperá la distancia, tenemos que ir a visitarte eh, gracias por estar siempre ahí escuchando y dando consejos. Carlos Sanz, con tus comentarios y bromas nos reímos en la comida muchos años, y me has ayudado mucho con tus consejos, disfruta mucho de esta etapa como papa. Raquel Castillo, aunque no eres del CIN2 te incluyo aquí porque eres una más de nuestro grupo de comidas. Gracias por todos estos años de amistad (15? Son tantos que ya no me acuerdo), me alegró mucho que después de compartir la adolescencia (instituto-universidad) nos reunamos otra vez en el doctorado, espero que todo te salga igual de bien que hasta ahora. Rafael, otro de mis amigos mexicanos, a todos os tengo mucho cariño y todos sois muy especiales. A Jose

Angel Silva, con tu seguridad y optimismo seguro que te sale un buen doctorado, ánimos que ya falta poco! To Desanka, thanks for your smiles! Miguel Pruneda, el veterano de las comidas, siempre con sabios consejos. A Roberto Robles, por tener siempre tanto conocimiento sobre muchas cosas variadas y aclararnos muchas dudas. To Mickaël Kepenekian, congratulations for you new job! I wish you a happy life in the new city. A Alberto Castaño por la compañía en los cafés. También quiero agradecer a los compañeros de despacho en la ETSE que han sido muchos porque cambié 2 veces de despacho. Del grupo de Arben Merkoçi: Marisa, Briza, Ana, Marisol, Eden, Claudio, Miquel, Mariana, Sandrine, Helena, Flavio y todos sus estudiantes visitantes. Del grupo de Dani Ruiz: Nuria, Javi, Elena, Juliane y Pablo (Pablo, gracias por ayudarme con las medidas de AFM de mis sustratos). Del grupo de Víctor Puntes: Neus, Cecilia, Sofia, Jordi, Eudald, Martí, Ngoc, Vincent, Isaac, Zoë, y todos sus estudiantes visitantes. Del grupo de Lara Lechuga: Ana Belén, Stefania, Borja, Mar, Daphne, Mari Carmen, Bert, Iraís, Sam, César y Maria.
Quiero agradecer también a la gente de **administración y mantenimiento del CIN2.** Al director del CIN2, Albert Figueres, a Xavi Ros, Carlos Domínguez y Astrid Francesh, también a Dulce Tienda, Mireia Collados y Ángela Zarate. Y a todos los del departamento de IT.

Haig d'agraïr també els **serveis de microscopia de la de la UAB** a Onofre Castell, Emma Rossinyol, Francesc Bohils. Gràcies per ajudar-me en els primers passos de la microscopia electrònica amb el SEM i TEM. Agraïr també al **grup d'òptica de la UAB**, gràcies Francesc Pi per totes les evaporacion de platí.

Als **serveis de microscopia del ICMAB**, vull agraïr a Judith Oró per totes les hores que m'ha ajudat en el SEM i TEM, gràcies per la teva paciència i companyia! Sempre m'ha agradat mesurar al ICMAB quan tu hi eres i poder parlar de moltes coses diferents, també m'has ajudat amb tots els dubtes teòrics dels instruments, gràcies! Haig d'agraïr també a Ana Esther que també m'ha ajudat molt amb el SEM. Al **X-ray Diffraction lab del ICMAB**, gràcies Jordi Rius per totes les mesures de raigs X.

Als **serveis de microscopia del CIN2**. Els últims mesos de la tesis m'ha ajudat a fer mesures de TEM el Marcos Rosado. Una altra persona molt important en aquesta tesis és Belén Ballesteros, que ha passat moltes hores ajudant-me amb el TEM d'alta ressolució dels serveis de microscopia de la Universitat Autònoma de Barcelona. Moltes gràcies Belén per totes les mesures que han sortit tan bé, després de passar tantes hores juntes ja et considero una amiga més igual que a la Judith Oró, les dues heu contribuït molt en aquesta

tesis. A Daniel Ruiz Molina, Pablo Gonzalez, Elena Bellido y Alberto Martínez por ayudarme con **medidas de AFM** y a Julianne Simmchen y Javi Sáiz por ayudarme con **medidas de IR**. A todo el grupo de Víctor Puntes por dejarme utilizar cuando lo necesitaba la **centrifugadora**. A Daniel Maspoch y todo su grupo por enseñarme a utilizar el Dip-pen, aunque después no lo pude incluir en la tesis, es una experiencia más.

During the PhD I did a short stay for 4 month in the RISØ-DTU University, Roskilde (Denmark). I would like to thank Professor Frederick C. Krebs for letting me work in his group (Solar Energy Programm, SOL) and teach me so many new things about organic solar cells and the roll-to-roll process. It was a very fruitful experience! I'd like to thank all the people from Frederick's group, they were very friendly to me and helped me with everything I needed: Dechan (thanks for everything!), Suren, Bente, Hanne, Eva, Birgitta, Martin, Jon, Thomas R. A., Thomas T., Thue, Kion, Mikkel, Roar, Markus, Birgit, Henrik, Morten. And also the people I met outside work: Phuong, Jaime, Alicia, Kasper, Anna, Helge.

Before the PhD I started doing research in the University of Nijmegen (Holand), doing an Experimental Master in Organic Chemistry. This was a rewarding experience that convinced me to follow the research career. I would like to thank Professor Roeland Nolte, Dr. Jeroen Cornelissen and Dr. Joan Farrera for the opportunity they gave me to do this research in the University of Nijmegen. Also I really thank Erik and Matthijs, who supervised my work all that year, for all their help, the good moments we shared, their patience and their optimism that helped me so much in difficult situations. You were great supervisors! And I'm really happy we are still in contact. Erik, I'm sure you will be soon a great Group Leader and Matthijs, thanks for sending me postcards and pictures from your family. Thanks to Heather as well, you are a very good friend! I'm really looking forward seeing you and do a trip with you this summer. All the people from Nolte's group have been everyday a big support. When I needed help or I had questions, everybody tried to help me or answered them. People like Nico, Pili, Andrés, Marco, Kasper, Michal, Rosalyne, Cyrille, Richard, Paul Thomassen, Marta (la meva segona mare, gràcies per tot!), Isa, Maria, Laura, Silvia, Arend, Michiel, Paul van Gerven, Dani, Alexander, Sanders (two of them), David, Ton, Irene, Joost, Friso, Joris, Mark, Paul Kouwer, Marta (Madrid), Carol and especially a very important person, thanks to everyone! And also I want to thank other people I met in Niijemgen who are not chemists, for their friendship: Bea, Paula, Giorgia, Claudio, Virginia, Feli, Marta (rubia), Alejandra, Benedita, Paco and Laura.

Haig d'agraïr també als amics de tota la vida i als que he anat fent durant aquest camí del doctorat per tot el suport moral i distreure'm de la feina. Especialment a Eva, Guillem, Lili, Hana, Pepi, Mariona, Cris, Victor, Ana, Sonia, Maria, Joana, Mariam, Lourdes, al ekipa del raval: Maria, David, Fede, Vio, Lluís, Raquel, Carles, Sigfrid, Claire, Adri i Joan. També a la Raquel, Albert i Aran i Elo i Javi. Gràcies a tots!

I per últim vull agraïr a la meva família que sempre ha estat al meu costat ajudant-me de totes les maneres possibles, tant la familia de Lleida-Barcelona com la de Murcia. I sobretot agraïr els meus pares i germà per tot, sense vosaltres no hauria pogut fer la tesis, us estimo molt! També vull agraïr a una persona molt important, Albert, que cada dia ha estat al meu costat recolzant-me i m'ha fet riure en moments difícils. I al Isi per cantar-me mentre escrivia la tesis.